Department of Physics
Indian Institute of Technology Guwahati
Ph.D. Thesis

Insights into the half-metallicity in Heusler compounds with $3d$ and $4d$ transition metal elements

Srikrishna Ghosh

Supervisor: Prof. Subhradip Ghosh

April, 2019.

Insights into the half-metallicity in Heusler compounds with $3d$ and $4d$ transition metal elements

A thesis submitted by

Srikrishna Ghosh

to

Indian Institute of Technology Guwahati
in partial fulfillment of the requirements
for the award of the degree of
Doctor of Philosophy in Physics

Department of Physics
Indian Institute of Technology Guwahati
Guwahati - 781039, Assam, India

Statement

The work contained in the thesis, entitled "*Insights into the half-metallicity in Heusler compounds with 3d and 4d transition metal elements*", has been carried out at the Department of Physics, Indian Institute of Technology Guwahati, India by me under the supervision of Prof. Subhradip Ghosh. The material of this thesis has not been submitted elsewhere for any other degree. Works presented in the thesis are all my own unless referenced to the contrary in the text.

(Srikrishna Ghosh) Date:
Roll No. - 136121006
Department of Physics
Indian Institute of Technology Guwahati
Guwahati - 781039, India

Disclaimer

The bibliography included in this thesis is, by no means complete but contains the ones which are consulted thoroughly by me. I apologize for inadvertently missing out some of the research papers, review articles and other scientific documents pertaining to the focus of this thesis which should also have been cited. For illustration purpose some of the figures in this thesis are taken from other sources and properly cited.

Certificate

It is certified that the work contained in the thesis entitled "*Insights into the half-metallicity in Heusler compounds with 3d and 4d transition metal elements*" by Mr. Srikrishna Ghosh, a Ph.D. student of the Department of Physics, Indian Institute of Technology Guwahati is carried out under my supervision and has not been submitted elsewhere for the award of any other degree.

(Prof. Subhradip Ghosh) Date:
Department of Physics
Indian Institute of Technology Guwahati
Guwahati - 781039, India

Dedicated to

my parents, my sister Jolly

and

Barsa

Acknowledgement

My thesis supervisor Prof. Subhradip Ghosh deserves sincere thanks for his valuable guidance, scholarly inputs and consistent encouragement through out this work and beyond. I have been highly influenced by his immense patience, insightful comments and constructive criticisms at different stages of my research. I also thank him for giving me the opportunity to be involved in different problems and collaborations that helped me a lot to increase my experience and knowledge. I'll always cherish the memory of working with a great teacher and a person like him for the rest of my life.

I thank Dr. Biplab Sanyal, my collaborator for helping me in learning many theoretical aspects of the subject.

I heartily acknowledge my doctoral committee members - Prof. Ananthakrishnan Srinivasan, Prof. Charudatt Y Kadolkar and Prof. Aditya Narayan Panda for helping me with their useful discussions during the annual assessments of my research work. My sincere thanks go to all the former and present heads of the department (Prof. Saurabh Basu, Prof. Poulose Poulose and Prof. Subhradip Ghosh) during my Ph.D study. All the technical assistants, the academic and non-academic staffs of the department who helped me in various ways during my research period are deeply appreciated. Basab-da owes many thanks for his support in resolving different computer related issues. I am also thankful to all other faculty members for their help and guidance whenever I needed. I am thankful to the department of Physics IIT Guwahati for allowing me to utilize Newton cluster, funded under the FIST programme by DST, India and Param Ishan, IIT Guwahati for the supercomputer facility.

This thesis would not have been completed without the scholarly interactions of my senior group members, Dr. Souvik Paul, Dr. Debashish Das and Dr. Ashis Kundu. I gained a lot specially from Debashishs-da and Ashis at various points of my research programme through their extensive support in learning different concepts and making me familiar with different electronic structure packages. I also thank

my junior Sheuly for sharing research experiences.

Staying happily for a long time in this beautiful institute would have not been possible without a great friend circle, seniors and juniors across different departments. All of them are very close to my heart. I am thankful to my seniors Arnab-da (Kaka), Ramiz-da, Kallol-da and Sudin-da for their support. In this opportunity, I specially appreciate the brotherly guidance of Sourav-da and Kartik-da who helped and inspired me a lot to learn different computer programming related issues. I feel very fortunate to have friends like Sanjib and Debashish (DK) for their ever extending help and support since I met them. I thank my friends, batch-mates and lab-mates Noor, Kajwal, Arun, Pulak, Rajkumar, Susmita, Eshita, Camelia, Arun, Krishnanjan and my juniors Sumit, Karuna and Sayandeep for their various help during my Ph.D study. I will always miss our stroll with my dear friend Pankaj after dinner. I would also like to thank Gourab, Subhankar, Arindam-da, Arnab-da (Barreto) and other teammates from the ground for the unforgettable memories we had together while playing football in the field. I acknowledge the help of Sujoy da and Pakhi da.

In this opportunity, I specially thank Sabarni-di for enriching me with her music lessons. I express my sincere gratitude to Deepnwita Basu madam and her family for their affections.

I would like to thank my younger sister Jolly for her unconditional love and constant support during tough times. I am thankful to my uncle Kartik Chandra Das and aunt Sumitra Das for financial support to my family and study from class X to my M.Sc. I would have not come so far without them. My special thanks go to my brother in law Late Uttam Pal for his support and motivation in many ways. I would also like to thank my teachers from my schooldays Amar Babu, Haradhan Babu, Srimanta Babu, Sadhan Babu, Sisir Babu, Balaram Babu, Shanti Babu, Utpal Babu and Sadhana Madam for their immense affection and scolding which make me what I am today. I am also thankful to my childhood friends Tuna and Subha for their constant support. I thank Barsa for being my inspiration since I met her.

I would also like to express my gratitude to Lionel Messi and Pandit Hariprasd Chourasia for their beautiful and heart touching playing in their respective field which has always inspired me to go ahead in life with joy.

Most importantly, I would like to thank my mother for her blessings, unconditional love, support, and sacrifices for me. I owe everything to her.

Abstract

Experimental synthesis and theoretical prediction of half-metals in Heusler family have been the driving force in searching new materials for spintronics applications. So far, in most of the studies all the magnetic constituents of the half-metallic magnetic Heuslers are $3d$ transition metal atoms. Investigations into compounds with one or more than one constituents with $4d$ electrons are fewer in number and not systematic either. Mn, Fe and Co based Heusler compounds are well known for their unique magnetic properties and practical applications. In order to understand the physics of half-metals in a systematic way and without being material specific, in this thesis, we have explored, in detail 54 ternary compounds (six ternary series) $X_2X'Z$ and 36 quaternary compounds (four quaternary series) $CoX'Y'Z$ as the daughter compounds of these ternary compounds, where X = Mn, Fe, Co; X′ = $4d$ transition metal atoms across the $4d$ row of the periodic table; Y′ = Mn, Fe and Z = Al, Si. The major motivation for this work was to explore the compounds across several series by changing one or two of the constituents to get insights into the roles of the different magnetic constituents along with that of the main group elements. A comprehensive overview of these compounds, addressing the trends in structural, electronic and magnetic properties has been presented here along with the prediction of new half-metals. A simple picture of hybridization of the d orbitals of the neighbouring atoms is used to explain the origin of the half-metallic gap in these compounds. We have shown that the arrangements of the magnetic atoms in different Heusler lattices are largely responsible for the interatomic exchange interactions that are correlated with the features in their electronic structures as well as with the possibility of occurrence of half-metallicity. To find out the role of $4d$ elements, we have made one to one comparison between the isoelectronic pairs of ternary (quaternary) compounds where in one case the magnetic constituents are all $3d$ transition metal atoms and in the other one of them is a $4d$ transition metal atom. We found that the major features in the electronic structures remain intact if a $3d$ X′ constituent is replaced with an isoelectronic $4d$ element as long as the crystal structure of the pair of compounds are same, implying that the total number of valence electrons can be used as a predictor of half-metallic nature in compounds from Heusler family. We have also explored the phenomenon of site-dependent substitution affecting half-metallic behaviour and the possibility of half-metallic behaviour in chemically disordered Heusler compounds. In a nutshell, the results presented in this thesis provide important insights into the evolution of half-metallicity in

magnetic Heusler compounds.

Contents

List of abbreviations and acronyms

DFT	Density functional theory
DMRAM	Dynamic magnetoresistive random access memory
DOS	Density of states
FP	Full potential
GGA	Generalized gradient approximation
GMR	Giant magnetoresistance
HM	Half-metal
HMF	Half-metallic ferromagnets
KKR	Korringa-Kohn-Rostoker
LAPW	Linearized augmented plane wave
LDA	Local density approximation
MCE	Magnetocaloric effect
MFA	Mean field approximation
MR	Magnetoresistance
MRAM	Magnetoresistive random access memory
MTJ	Magnetic tunnel junction
NCPP	Norm conserving pseudopotential
PAW	Projector augmented wave
PP	Pseudopotential
SC	Semiconductor
SGS	Spingapless semiconductor
SPRKKR	Spin-Polarized-Relativistic Korringa-Kohn-Rostoker
STT	Spin-transfer-torque
USPP	Ultrasoft pseudopotential
VASP	Vienna Ab initio Simulation Package

Chapter 1

Introduction

Materials have always been an integral part of the development of human civilization for ages. Even several historical ages have been named on the basis of the most important material of that era like stone, bronze or iron ages. Together with the scientific and technological advancements in last few centuries we have seen a colossal jump in the progress of our civilization mainly due to inventions of semiconductor based electronic devices, used for scientific investigations as well as in our daily lives. Demand for functional materials, with specific target properties, has led extensive experimental and theoretical investigation of different classes of materials such as metals, semiconductors, insulators, ceramics, polymers and composites, to name a few. With modern theoretical and experimental techniques it has been possible to understand and correlate different physical properties of these materials and consequently engineer them according to the requirements. Heusler compounds are one of the most explored group of materials due to their versatile functional properties observed over the decades.

1.1 Heusler Compounds

Heusler compounds, named after F. Heusler, attracted much attention due to their ferromagnetic nature even though none of its constituents, copper-manganese bronze [2] and a main group element like aluminium and tin was magnetic. Since the discovery in 1903, Heusler compounds have been extensively studied in search of new interesting properties. A variety of diverse magnetic phenomena like half-metallicity,

An useful concise discussion about Heusler compounds can be found in *Heusler Compounds: properties, Growth, Applications*, by Felser, Claudia and Hirohata, Atsufumi, Springer, 2015 [1].

magnetic shape-memory effect, giant magnetocaloric effect and magnetic recording have been observed in some of the Heusler compounds [3–9]. Interestingly most of the properties of Heusler compounds are comprehended from its rather simple crystal structure and total valance electron count of the particular compounds.

1.2 Crystal structures of Heusler Compounds

In the early years, Heusler compounds were thought to be possessing Cu_2MnAl prototype structure *i.e.* a structure with $X_2Y'Z$ composition with the ratio of elements X, Y′ and Z 2:1:1. Later ternary compounds were discovered with the same crystal structure but having a vacancy in one of the sites for X elements. Ternary compounds with 1:1:1 atomic proportion (XY′Z) are called 'half-Heusler' and have their unique interesting properties. Improved computational facilities and increasing research interest led to investigation of Heusler compounds by varying the elements and their ratios to explore different possibilities of crystal structures on the basis of predictive calculations. Heusler compounds are generally considered to consist of four interpenetrating *fcc* sub-lattices. In Fig. 1.1 we have schematically represented all the possible ordered crystal structures of Heusler compounds with different possible arrangements of the constituent elements. A, B, C and D are the 4 crystallographic sites with co-ordinates (0, 0, 0), (1/4, 1/4, 1/4), (1/2, 1/2, 1/2) and (3/4, 3/4, 3/4) respectively. In the full-Heusler or $L2_1$ structure (Space group no. 225; $Fm\bar{3}m$) the sites A and C are called $4a$(0, 0, 0) and $4b$(1/2, 1/2, 1/2) Wyckoff positions which are symmetric. The equivalent B and D sites are called $8c$((1/4, 1/4, 1/4). If B and D sites are occupied with two different atoms then the resulting structure is called an inverse-Heusler structure (space group no. 216;$F\bar{4}3m$) and these sites are called $4c$(1/4, 1/4, 1/4) and $4d$(3/4, 3/4, 3/4) Wyckoff positions.

Throughout this dissertation the element Z stands for a main-group (*sp*) element (like Al, Si *etc.*) and X, Y′ and X′ are all transition metal elements. As seen from the Fig. 1.1, in case of 'half-Heusler'(XY′Z) and 'full-Heusler' ($X_2Y'Z$) compounds, Z and Y′ atoms are located at the crystallographically symmetric positions $4a$ and $4b$ sites, so as to form a rock-salt structure, with Z and Y′ being the most and least electronegative elements respectively. For a 'full-Heusler' ($L2_1$) structure both of the $8c$ sites are occupied by X atoms. The prototype for $L2_1$ structure is Cu_2MnAl [10, 11]. Now if one of the remaining two $8c$ sites is kept vacant then the resulting structure is called a 'half-Heusler' structure resulting in a non-centrosymmetric cubic structure (space group no. 216;$F\bar{4}3m$, $C1_b$) with the

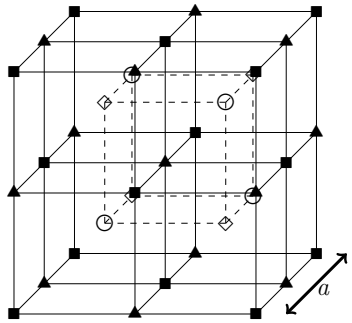

	■ A	○ B	▲ C	◇ D
Semi-Heusler ($C1_b$): XY′Z	Z	X	Y′	
Full-Heusler ($L2_1$): X_2Y′Z	Z	X	Y′	X
Inverse Heusler (XA): X_2Y′Z	Z	Y′	X	X
Quaternary Heusler : (XX′)Y′Z	Z	X	Y′	X′

Figure 1.1: Representation of various possible crystal structures of the Heusler compounds schematically. Heusler structures can be assumed to be made of 4 interpenetrating *fcc* lattices making it a b.c.c lattice if all the atoms in the crystal was alike.

prototype structure being MgAgAs [12]. After the discovery of half-metallic ferromagnet NiMnSb in 1983 by de Groot *et al.* [13] half-Heuslers have drawn considerable attention. An inverse-Heusler structure is generated if two of the X atoms of X_2Y′Z compounds occupy crystallographically different sites, say 4*b* and 4*d*. The prototype structure for these compounds is $CuHg_2Ti$ [14] or $AgLi_2Sb$ [15, 16]. Inverse-Heusler (XA) structure is found very often when the number of valance electrons of X is less than that of Y′, in X_2Y′Z compounds; Mn_2CoSn being an well known example [17, 18]. If all the sublattices in the Heusler compound are occupied by different atoms then we get a quaternary-Heusler (XX′Y′Z) compound. LiMgPdSn [19, 20] is the prototype structure for quaternary Heusler compounds. However, by keeping the position of Z atom fixed at 4*a* site, the remaining three transition metal atoms of quaternary-Heusler structure can be combined in 3 ways, leading to three possible crystal structures for a quaternary-Heusler compound [21]. Apart from these structures with cubic symmetry, other structural phases like various tetragonal variants, Cu_3Au-like structure and hexagonal structures have also been reported [22–25]. In this dissertation, we have not considered those structural phases.

In this thesis we have explored all possible structural variants of *fcc* symmetry (Fig. 1.1) in Heusler X_2Y′Z and XX′Y′Z compounds to find the optimized structure of each of the compounds in our study. The arrangement of the atoms in a particular crystallographic structure is explained using standard empirical rules, based on simple valance electron count of the transition metal elements and the relative electronegativities of the transition metal elements. These will be discussed in details

during discussions on the compounds explored in this thesis.

1.3 Magnetic properties of Heusler compounds

As mentioned earlier, Heusler compounds gained much of its fame due to its unique varieties of magnetic properties in spite of their rather simple crystal structures. The origin of different kinds of magnetism in Heusler compounds is strictly dependent on the presence of unfilled *d*-orbitals of the transition metal elements and the interaction between the constituent elements. Most of the magnetic Heusler compounds found are ferromagnets saturating in an weak external magnetic field. For Mn based X_2MnZ systems it is generally found that the magnetic moment of Mn atom is localised and may be as high as $4\mu_B$. These compounds are well studied to explore the effects on magnetism of these compounds due to the changes in the electron concentration and atomic disorder. Quaternary Heusler compounds are explored extensively to understand the role of the $3d$ (X) and *sp* (Z) atoms in magnetic properties of Heusler compounds. The *sp* electron concentrations are found to influence the magnetic properties through both the moment formation and the type of magnetic order of the systems [26]. Antiferromagnetic order is experimentally found in some of the semi-Heusler ($C1_b$) and full-Heusler ($L2_1$) compounds. The antiferromagnetic order is observed mostly in compounds where Mn atoms occupy lattice sites crystallographically equivalent to those occupied by the Z elements. Full-Heusler compounds with B2-type disorder are energetically favorable for antiferromagnetic ordering as the interatomic Mn-Mn distance is smaller [27]. Some of the B2-type disordered X_2MnZ (X=Ni, Pd; Z=Al, In) Heusler compounds are reported to have antiferromagnetic behavior [26]. In case of semi-Heusler compounds with $C1_b$ structure the Mn-Mn distance is larger and the antiferromagnetic interaction is supposed to be mediated by intermediate X or Z atoms. Ferrimagnetism is not observed very often in Heusler compounds in comparison with ferromagnetic and antiferromagnetic orders. A handful of Heusler compounds like CoMnSb, Mn_2VAl and Mn_2VGa [26] have been identified as Ferrimagnets. Recently compensated ferrimagnetic materials have aroused interest as it could limit the stray magnetic field like that in antiferromagnetic materials but at the same time can be spin polarized, an essential criteria for using them in spintronics devices. Mn_3Ga in DO_{22} phase is claimed to be a ferrimagnetic material [28]. DO_3 Mn_3Al has been theoretically and experimentally verified to exhibit compensated ferrimagnetism [29].

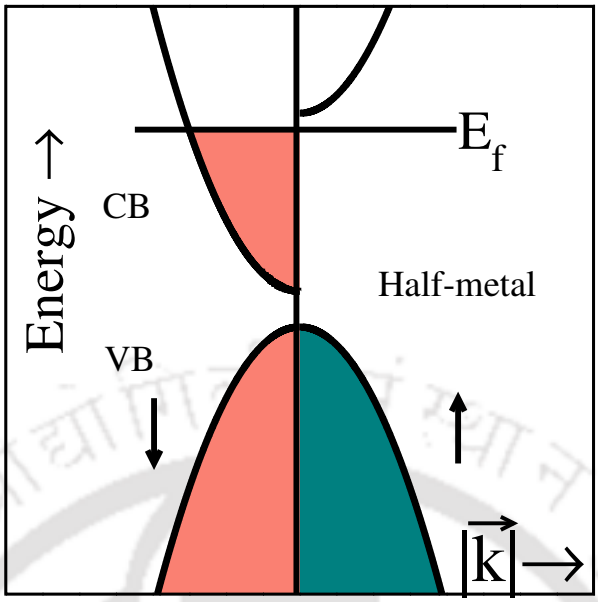

Figure 1.2: Schematic band structure of half-metals. CB and VB stand for conduction and valance bands respectively.

1.4 Spintronics

Spintronics is the portmanteau of three words "Spin Transfer Electronics". As the name suggests spintronics can be thought of as an extension of usual semiconductor based electronics where both the charge and spin of the electrons are considered [30]. An external magnetic field polarizes the electrons by orienting their spins in spintronics devices to generate spin dependent electric current or spin current [31–33]. Spintronics materials are nowadays successfully used in devices related to magnetic memory (data storage) [34, 35] and magnetic recording (read, write head) [36] though potentially these materials can be used in many other applications. Magnetoresistance (MR) [37], a change in the resistance of the material due to change in the applied magnetic field, is the basic property, exploited in these devices. After the discovery of the "giant magnetoresistance (GMR)" [38–41] in late 1980s, research in spintronics materials have seen a gigantic leap. In GMR devices, also named as 'spin valve', different layers of ferromagnetic materials are separated by a non-magnetic material and a large change in resistance is achieved by applying an external magnetic field which aligns the spins of the used materials. Depending on the orientations of the ferromagnetic layers the resistance is varied. When the

The details of spintronics are given in *Spintronics: from materials to devices*, by Felser, Claudia, and Gerhard H. Fecher, Springer Science & Business Media, 2013. [30]

ferromagnetic layers are aligned along the direction of the applied field, lower electronic resistance is observed. The resistance becomes higher if the layers are aligned otherwise. Two variants of GMR are used in the devices: (1) current-in-plane (CIP), where the electric current flows parallel to the layers and (2) current-perpendicular-to-plane (CPP), where the electric current flows in a direction perpendicular to the layers.

Combining the phenomena of spin-dependent tunneling and spin-valve engineering concepts, highly sensitive magnetic read heads have been developed recently. GMR based sensors have entirely been replaced by the Magnetic tunnel junction (MTJ) [42, 43] read heads. With new materials having inter-dependent multiple properties, spintronic materials are the suitable candidates for engineering further advances in the field of MTJs. Interestingly MTJs can be upgraded to non-volatile magnetoresistive random access memory (MRAM) [44, 45], first demonstrated by IBM in 1999. Since then, active research for MRAM is going on due to its high-density applications [46]. The MRAM devices would replace the conventional charge-based memory devices such as Dynamic-RAM(DRAM), Embedded-DRAM and even Static-RAM. An interesting fact about MRAM is, the possibility of using spin-transfer-torque (STT) along with its high tunneling magnetoresistance [47, 48]. The effect which is used to adjust the orientation of the magnetic layers in the MTJ by using a spin-polarized current, is called STT. The current becomes spin-polarized current which consists of mainly one type of spin (spin-up or spin-down), while passing through a thick magnetic layer or the fixed layer. When this spin-polarized current is passed through a second thinner layer, called free layer, the angular moment is transferred to this layer by changing its orientation. This oscillates the orientation of the magnet. With the advantage of low power consumption, more scalability, and unlimited endurance compared to MTJ now STT-MRAM, the STT along with MRAM, is used [49].

1.5 Half-metallic ferromagnetic Heusler compounds for spintronics applications

The demand for new potential materials to use in spintronics applications led to exploration of the Heusler compounds for new magnetic materials called half-metallic ferromagnets (HMF). HMF are desirable for spintronics applications due to their unique electronic structure. As seen in Fig. 1.2, the band structure of HMF shows

a metallic behavior in the majority spin channel whereas the minority spin channel shows a clear semiconducting gap. The inception of HMF property in $C1_b$ NiMnSn and PtMnSb, based on band structure calculations [13] spearheaded the research in the field of half-metallicity. Electronic structure calculations by Kübler *et al.* found similar feature in $L2_1$-type Co_2MnAl [50]. Ishida *et al.* proposed Co_2MnZ, (Z = Si, Ge) as half-metals [51]. Half-metallicity has been predicted in many other materials like metal-filled carbon nanotubes [52], binary magnetic oxides (CrO_2 and Fe_3O_4), colossal magnetoresistance materials (Sr_2FeMoO_6 and $La_{0.7}Sr_{0.3}MnO_3$) [53], diluted magnetic semiconductors ($Ga_{1-x}Mn_xAs$) and zinc-blende compounds MnAs and CrAs [54–56].

For half-metallicity, a semiconducting gap at one of the spin channels is necessary. For half-metals, as the band structure (Fig. 1.2) suggests, there is higher density of states (DOS) at the Fermi level along one spin channel, the majority band, than the other, the minority band. The spin polarization (P), that decides the applicability of a material in spintronics, is defined as

$$P = \frac{N^{\uparrow}_{E_F} - N^{\downarrow}_{E_F}}{N^{\uparrow}_{E_F} + N^{\downarrow}_{E_F}} \times 100 \quad \% \tag{1.1}$$

where the $\uparrow$ and $\downarrow$ represent the spin directions and $N^{\uparrow}_{E_F}$ or $N^{\downarrow}_{E_F}$ are the density of states at the Fermi energy along the respective directions. For ideal half-metals either $N^{\uparrow}_{E_F}$ or $N^{\downarrow}_{E_F}$ is zero making them 100% spin polarized. A spin polarization greater than 90% together with a pseudo gap (a gap, close to Fermi level) is considered to be 'nearly half-metallic', implying a good potential of spintronics applicability.

1.5.1 Origin of the half-metallic gap

The origin of half-metallic gap in Heusler compounds can be understood in terms of the hybridizations of the *d*-bands of the transition metal constituents. A generalised picture of the hybridization [7, 57–63] provides enough insights into the half-metallic property and is consistent with the Slater-Pauling rule [57, 58], to be discussed in the next subsection.

The hybridization patterns of *d*-orbitals are dependent on the structure type of the particular material. In all cases very low lying $s - p$ bands stabilize the structure by accommodating the charges from the transition metal atoms, with *d*-

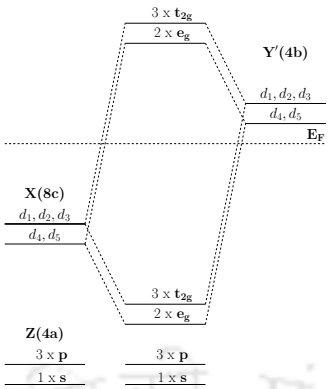

Figure 1.3: Schematic representation of possible hybridization between spin-down orbitals associated with different sites in semi-Heusler (XY′Z) compounds. Energetically lower lying bonding hybridized orbitals are occupied and separated from antibonding hybridized orbitals by a gap. Here d_1, d_2 and d_3 represents the d_{xy}, d_{yz} and d_{zx} orbitals, respectively, and d_4, d_5 is shown by d_{z^2}, $d_{x^2-y^2}$ orbitals

electrons [5]. In case of half-Heusler compounds (XY′Z) with the $C1_b$ structure Y′ and Z atoms are located at the symmetric sites but the $s-p$ orbitals of Z atoms lie well below the Fermi level. Thus the hybridization of d-orbitals of X and Y′ atoms takes place according to the symmetry of the d-orbitals, creating (i) 5 bonding d-hybrids (2 doubly-degenerate e_g and 3 triply degenerate t_{2g} hybrid orbitals) (ii) five non bonding hybrid d-orbitals (2 doubly-degenerate e_g and 3 triply degenerate t_{2g} hybrid orbitals) as shown in Fig. 1.3. The Fermi level is pinned in the gap between the bonding t_{2g} and antibonding e_g minority spin states for half-metallic Heusler compounds with $C1_b$ structure, leading to 100% spin polarization.

In Fig. 1.4 we show a schematic representation of probable hybridization between spin-down orbitals associated with different sites in $X_2X'Z$ Heusler compounds. First the d orbitals of the atoms on symmetric sites ($8c$ in the space group 225, $4c$ and $4d$ in space group-216) hybridize creating (i) 5 bonding d-hybrids (2 doubly-degenerate e_g and 3 triply degenerate t_{2g} hybrid orbitals) (ii) five non bonding hybrid d-orbitals (2 doubly-degenerate e_u and 3 triply degenerate t_{1u} hybrid orbitals)(Fig. 1.4.(a)). The bonding e_g and t_{2g} orbitals, having tetrahedral symmetry, can only hybridize with d-orbitals of the remaining transition metal atoms. Thus, ultimately we are left with five bonding and five anti-bonding states which are non-transforming with the u representation [7, 64] and can not couple with d-orbitals of the remaining transition metal atom (1.4.(b)). In case of a half-metal there is an energy gap in one spin-channel, where the Fermi-energy is pinned in. It's worth mentioning the same hybridization scheme is also used to explain half-metallicity of quaternary Heusler compounds [63] as replacing one of the two X atoms of $X_2X'Z$ by a different

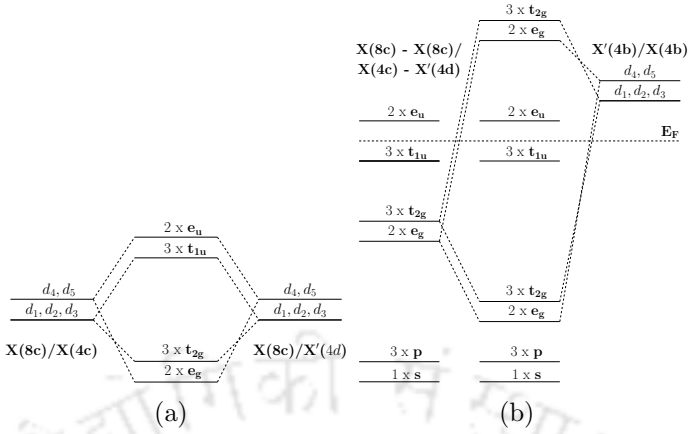

Figure 1.4: Schematic representation of possible hybridization between spin-down orbitals associated with different sites in $X_2X'Z$ compounds. (**a**) The hybridization between the transition metal atoms at symmetric positions 8*c*-8*c*(4*c*-4*d*)for Heusler(Inverse Heusler) compounds) (**b**) The hybridization with the remaining transition metal atom. It is to be noted that same hybridization scheme works for quaternary Heusler compounds as well, where one of the two X atoms is replaced by a different transition metal atom Y′.

transition metal atom Y′ produces XX′Y′Z compounds.

1.5.2 Slater-Pauling rule

Even though there is no unique way to identify potential half-metals among Heusler compounds, there does exist a guiding rule, known as Slater-Pauling (SP) rule, to predict possible half-metals. Though the well-known Slater-Pauling behavior was derived for binary transition metal compounds [57–60, 65] it is applicable to all half-metallic ferromagnetic Heusler compounds. SP rule simply connects the total spin-magnetic moment per formula unit (M) with the total number of valance electrons per formula unit (N_V) [59, 60] with a linear equation, $M = |N - 2N_\downarrow|$, where $N_\downarrow$ is the number of available valance states per formula unit below the Fermi level in the spin-channel where the half-metallic gap is situated . As mentioned in the earlier section, the half-metallic gap originates due to the hybridization of the d-orbital of the transition metals in such a way that the Fermi level lies in the gap bordering two hybrid orbitals in that particular spin-channel. Conventionally the half-metallic gap is assumed to be associated with the minority spin-channel. The position of the Fermi-level in the minority or spin-down channel, determines which Slater-Pauling rule the material follows as the number of states in this particular spin-channel below the Fermi-level is always fixed and any extra electron would be placed in unoccupied states of other spin-channel. The value of $N_\downarrow$ depends on where the Fermi-level

lies in the system according to the standard hybridization model [7, 66, 67]. For ordered compounds this rule implies that if the total spin-magnetic moment of the systems deviates slightly from an integer value the half-metallicity is lost entirely. For compounds with non-integer site occupancies the scenario is different and M might have non-integer values [60, 68].

From Fig. 1.3 we can see the E_F is situated between bonding t_{2g} and antibonding e_g states implying that the half-Heuslers would follow $M = |\mathrm{N_V} - 18|$ rule. For full-Heuslers the situation is different. Since presence of one extra transition metal element leads to increase in total valance electrons count as well as in the number of d-orbitals, there are a number of possible SP rules half-metallic compounds would follow depending upon the position of the Fermi level E_F as seen in Fig. 1.4.(b). If E_F is situated between t_{1u} and t_{2g} states, it would follow $M = |\mathrm{N_V} - 18|$ rule. $M = |\mathrm{N_V} - 24|$ rule is followed when E_F lies between t_{1u} and e_u states. Likewise $M = |\mathrm{N_V} - 28|$ rule is followed when E_F is situated between the antibonding e_g and non bonding e_u states. Normally $M = |\mathrm{N_V} - 18|$ rule is valid for compounds with early transition metals like Sc, Ti *etc.* However compounds with 21 valance electrons can obey both $M = |\mathrm{N_V} - 18|$ and $M = |\mathrm{N_V} - 24|$ SP rules. Similarly compounds with 26 valance electrons can follow $M = |\mathrm{N_V} - 24|$ and $M = |\mathrm{N_V} - 28|$ SP rules. Detailed studies on full Heusler [69] and inverse Heusler compounds [67] confirm the above mentioned connection between $\mathrm{N_V}$ and a particular SP rule.

1.6 Ternary and quaternary Heusler compounds for spintronics applications

With more than thousand possible combinations between the $3d$ transition metal elements, there has been extensive studies on mainly ternary [70, 71] and quaternary [72–74] Heusler compounds. We are mainly concerned about the ternary and quaternary Heusler compounds with magnetic properties and potential applicability in spintronics or magnetoelectronics.

Among the magnetic Heusler compounds with all magnetic components from $3d$-element series, Mn based ones are well known for their unique magnetic properties while Co based Heusler compounds are well known for having intrinsic high Curie temperature and high spin polarization [75–78] making them possible to use in actual spintronics devices. Fe-based Heusler compounds are known to be soft ferromagnets with Curie temperature as high as 900 K making them suitable for

potential magnetic applications [79]. In the next few subsections we review briefly the available results on Mn, Co and Fe based Heusler compounds.

1.6.1 Mn-based Ternary compounds

$Mn_2X'Z$ Heusler compounds have drawn considerable interest for their possible implementation as free magnetic layers in spin-transfer torque devices such as spin-transfer torque random-access memory (STT-MRAM) [80]. Experimental realization of inverse Heusler compound Mn_2CoAl as spingapless semiconductor (SGS) [81–83] has increased more attention towards this family of Heuslers as new materials for spintronics.

Mn_2NiGa is a well studied compound as it is directly related with Ni_2MnGa [84], a well known magnetic shape memory alloy. During the ongoing process of functionality improvement of Ni_2MnGa by varying the composition of Ni and Mn, Mn_2NiGa was synthesized first by Liu *et al.*. It was found to crystallize in inverse Heusler structure at high temperatures [85]. In Mn_2NiGa, the Mn atoms are ferrimagnetically coupled, which is seen in most of the Mn_2-based inverse Heusler compounds, resulting in a low saturation magnetization compared to Ni_2MnGa [86, 87]. In spite of low magnetization, the ferrimagnetic coupling between two Mn atoms gives rise to a plethora of interesting physical properties in Mn_2NiGa [87] as well as in other Mn-based inverse Heuslers. Singh *et al.* reported spin-valve-like magnetoresistance in Mn_2NiGa at room temperature [88]. Recently, a notable inverse magnetocaloric effect (MCE) was reported in Mn_2NiGa [89].

Tetragonal Mn_3Ga is another famous compensated ferrimagnet with a high Curie temperature of more than 700 K [28, 90, 91]. Different experiments [22, 23, 92, 93] show that Mn_3Ga crystallizes in cubic, tetragonal and hexagonal structures. Mn_3Ga is a promising material for STT-MRAM [92] and magnetic tunnel junction [23] applications. Among others, Mn_2FeGa has been synthesized in similar crystallographic phases like Mn_3Ga [24, 25, 94] and is useful in magnetic storage technology. Mn_2CoGa, a high spin-polarized material, has been studied in bulk and thin films and its possible applications have been explored [95, 96]. Mn_2NiAl, Mn_2NiSn and Mn_2NiIn are predicted to be magnetic shape memory materials [97–100] from DFT calculations. Like Mn_3Ga, compensated ferrimagnetic Mn_3Al thin films are synthesized and found to have high Curie temperature (650 K) and nominal zero or low net magnetic moment [29].

1.6.2 Co-based Ternary compounds

Co_2-based Heusler compounds ($Co_2X'Z$) form an important subset of Heusler compounds as a large number of compounds in these series are predicted to be half-metallic ferromagnets from *ab initio* calculations [7, 50, 68, 101–105]. These materials posses a gap around the Fermi energy in their minority spin-channel and have high Curie temperatures making them advantageous for spintronic devices. For actual applications, half-metals with high-Curie temperature is required as the band gap shrinks with increasing temperature, and the depolarization effects are relative to the Curie temperature (T/T_C) [3]. $Co_2Cr_{0.6}Fe_{0.4}Al$ [102] is significant due to its large negative magnetoresistance effects (TMR ratio 317% at 4 K) [106]. $Co_2FeAl_{0.5}Si_{0.5}$ was also reported for magnetoresistance effects (TMR ratio 175% at room temperature) [107]. Highest Curie temperatures in the range of 1100-1200 K were found in $Co_2FeAl_xSi_{1-x}$ systems with 100% spin polarization [75]. Co_2MnSi is a promising candidate for half-metal with a Curie temperature as high as 985 K [108]. Co_2MnSn [109], Co_2MnX (X = Si, Ge) [51] are also reported to be half-metals. Ishida *et al.* [51] hinted a possible correlation between the valance electrons and the band-gap. They also pointed that the half-metallicity in these Co-based Heusler compounds might be tunable. Even the Curie temperatures of Co_2 based compounds are known to be associated with valance electron count [110].

1.6.3 Fe-based Ternary compounds

The main reason behind the search for new Fe-based Heusler compounds [70, 111] is to find potential candidate to use in rare-earth free hard magnets as well as to understand the instabilities in Heusler compounds. Fe_2CoGe, Fe_2NiGe, Fe_2NiGa, Fe_2CuGa and Fe_2CuAl have been synthesized and have high Curie temperatures up to about 900 K [79]. Though predicted to adopt a tetragonal structure these materials were found to crystallize in the cubic inverse Heusler structure with differing degrees of atomic disorder. $Fe_{1+x}Co_{2-x}Si$ ($0 \leq x \leq 1$) [112] thin films are ideal materials for STT-MRAM. Fe based Heusler compounds are also used for thermoelectric applications [113, 114].

1.6.4 Quaternary Heusler compounds

Quaternary compounds XX′Y′Z with 1:1:1:1 stoichiometry provide a good playground for searching and understanding interesting new materials. The three possible variants in the lattice occupancies make these systems very interesting with

the intricate interactions between three different constituent transition metal element atoms. After finding half-metallicity in ternary compounds in 1980s, search for half-metallicity or for that matter for any other functional properties in quaternary compounds were started. Large negative magnetoresistance was observed for a large range of temperature in $Ni_{50}Mn_8Fe_{17}Ga_{25}$ melt-spun ribbons[115]. Though equiatomic quaternary Heusler compounds were expected to have several interesting properties, not much combinatorial studies were done untill the theoretical prediction of SGS properties in several quaternary Heuslers. The experimental success in justifying the theoretical claim of quaternary Heusler compound CoFeMnSi as SGS [116] indicated that members of quaternary Heusler family might be potential candidates as materials for spintronics applications. In search of new SGS compounds, quaternary Heuslers are investigated by several groups [61, 63]. Based upon calculations by first-principles Plane Wave-Pseudo-potential method Xu *et. al* [63] predicted that CoFeMnSi, CoFeCrAl, CoMnCrSi, CoFeVSi and FeMnCrSb are SGS . However, a first-principles Full-Potential Local orbital calculations, claimed that only CoFeCrAl and CoMnCrSi are SGS while CoFeVSi and CoFeMnSi are half-metals [61] , contradicting the results of Xu *et. al.* Recently CoFeMnSi and CoFeCrGa have been experimentally been shown to be SGS [116, 117] whereas CoFeCrAl has been claimed to be half-metal [118] by the same experimental-group even though the main features of DOS and band structures of these systems are strikingly similar. Recent search for half-metals and other functionalities has predicted a number of compounds with quaternary Heusler structure to be promising though inadequate experimental evidences has made it difficult to justify all of those claims and same is true for ternary Heusler compounds as well [49, 63, 73, 83, 116, 119]. For instance CoFeMnSi was predicted to be SGS but was claimed to be half-metallic previously while it has been confirmed as SGS later [116] with better experimental testimonials.

Apart from quaternary compounds like antiferromagnetic semiconductor CrVTiAl [61] most of the potential quaternary Heusler compounds contain at least one of Mn, Fe and Co atoms if not two or all of them. This is because quaternary Heusler compounds are supposed to be the daughter compounds of suitable ternary compounds and most of the magnetic Heusler compounds, related to spintronics applications, are either Mn, Fe and Co based. It is also to be noted that the constituent transition metal elements of the Heusler compounds mostly studied so far are from $3d$ row of the periodic table. Compared to this, the investigations into compounds with either both X and Y′ or X, X′ and Y′ are elements with $4d$ electrons or one of them a $4d$ element are only a handful. Presence of both $3d$ and

$4d$ magnetic elements in the same compound with Heusler structure is expected to provide interesting perspectives. Such investigations too, are not systematic, in the sense that they do not explore compounds across various series by changing one or two of the constituents. Such investigations are necessary as they can provide useful insights into the roles of various magnetic constituents along with that of the main group elements. A thorough comparison between materials with all $3d$ constituents and ones with both $3d$ and $4d$ too would have had a comprehensive picture of the physics of the origin of half-metallic behaviour, its sustainability under various situations, and possible tunibility, all necessary for quick and intelligent search of new materials.

1.7 Materials-simulation by first-principles electronic structure calculations

The discussions in the previous subsections clearly demonstrate that $X_2X'Z$ and $XX'Y'Z$ compounds make a playground where the fundamental picture behind the fascinating structural, electronic and magnetic properties of these Heusler compounds can be explored. The natural way to do this theoretically is to obtain the solution of Schrödinger equation for electrons in real solids, where their quantum mechanical behaviour is determined by the presence of other electrons and atomic nuclei. Exact solution of the Schrödinger equation is not possible for many body systems, a well known problem. Hence we need appropriate approximations. The Density Functional Theory (DFT) [120, 121] which projects the many body interacting system onto a non-interacting single particle one; where the many body interactions are taken care of in an average way through a single term, has made the required breakthrough to arrive at parameter-free, first principles methods so that robust and accurate results on materials properties can be obtained. Integration of DFT based first-principles methods with advanced softwares made tackling of complex problems accurately within reasonable time period [122–128]. Over the years, application of these methods in calculating the electronic structures of collinear and complex noncollinear magnetic ground states [129–132], dynamical properties of materials [133, 134] and simultaneous comparison of these results with experimental observations confirmed the accuracy of these methods. Various problems related to sub-lattice disordered compounds [135, 136] have also been encountered with these sophisticated tools. Over the years, these methods are widely accepted to predict

properties of new materials where experimental evidence is not present. Therefore, the DFT based first-principles methods are the essential tool for fundamental understanding of materials that I have worked with during my doctoral research.

1.8 Outline of the thesis

In this thesis we have made attempts in the unexplored directions mentioned in the last paragraph of section 1.6. Using Density functional theory (DFT) based electronic structure calculations we have tried to explore systematically six ternary ($X_2X'Z$) with X = Mn, Fe, Co and four quaternary Heusler CoX′Y′Z series with Y′ = Mn, Fe; X′, the nine elements along the row of 4*d* elements in the periodic table and Z = Al, Si. As mentioned in section 1.6, Co, Mn and Fe based Heusler compounds have variety of magnetism driven applications. Thus, we find it intriguing to explore specifically Mn_2 , Fe_2 and Co_2 based ternary compounds for the search of new materials for spintronics applications with one magnetic element being one with 4*d* electrons. It is worth mentioning here that quaternary structures can be regarded as a combination of the suitable full Heusler compounds. Considering these ternaries as parent compounds, quaternary daughters with Co, Mn and Fe can be derived. This was the reason for choosing the above mentioned quaternary series. The motivations behind the work were the following:

1. To search for possible new half-metals with 4*d* transition metals.

2. To understand the effects and their origin, of the presence of an element with 4*d* electrons on the structure, electronic and magnetic properties of ternary and quaternary compounds where the other magnetic elements are from 3*d* transition metal series. A systematic study spanning across several Heusler series would help understand the comparative roles of 4*d* and 3*d* elements.

3. To understand the effects and their origin, of replacing an element with 3*d* electrons by an element with 4*d* electrons on the electronic and magnetic properties in the context of half-metallicity.

4. To understand the impacts and their origin, of replacing the main group element Si with Al in case of ternary and quaternary compounds having both 3*d* and 4*d* elements as magnetic components.

5. To understand the role of site dependent substitution of a 3*d* element and the consequent half-metallic behaviour in Heusler compounds.

In this dissertation we have primarily focused on the structural, electronic and magnetic properties of six ternary and four quaternary Heusler series to understand the physics behind half-metallic properties in some of the compounds. Trends in Curie temperatures and exchange interactions for all these compounds were investigated to find the possibility of actual realisation of interesting compounds coming out of our study. We provided a general framework of hybridizations between various constituents and demonstrated that along with crystal structure, and the number of valence electrons, the details of electronic structures are the key behind the trends of various physical properties obtained in our work. The work, very importantly, pinpoints the crucial differences between materials with all magnetic constituents from $3d$ transition metal series and ones with both $3d$ and $4d$ transitions metals, and attempts at microscopic explanations of the same.

Chapter 2 contains a brief description of theoretical methods, used for material simulations. Starting with a description of Density functional theory (DFT), the most popular and successful method for the quantum mechanical description of complex many-body problem in a computationally tractable way. Then various implementations of the DFT which are used in this work are described. We have used two different techniques: the projected augmented wave method (PAW) [137] and the Korringa Kohn Rostokaer-Green's function method [123, 124] as implemented in Vienna Ab initio Simulation Package (VASP) [138, 139] and Munich Spin-Polarized-Relativistic Korringa-Kohn-Rostoker (SPRKKR) [140] band structure program package, respectively.

In **Chapter 3**, we discuss the outcomes of our intensive study of 54 $X_2X'Z$ ternary Heusler compounds where X = Mn, Fe or Co; Z = Al or Si; and X′ a $4d$ element. We present our findings on the trends in structural, electronic, magnetic properties and on the possible half-metals and near half-metals. A simple picture of hybridization of the d orbitals of the neighboring atoms is used to explain the origin of the half-metallic gap in all the compounds. We find that the crystal structure, the number of valence electrons and the positions of the d states of the $3d$ elements in a compound are the deciders of the physical properties addressed here. We report seven half-metallic magnets with 100% spin polarization and a few with high spin polarization (greater than 90%), the"near half-metals", which could be of potential use in applications as well. We find that the major features in the electronic structures remain intact if a $3d$ X′ constituent is replaced with an isoelectronic $4d$,

implying that the total number of valence electrons can be used as a predictor of half-metallic nature in compounds from Heusler family.

In **Chapter 4** we present our investigations of the structural, electronic and magnetic properties of 36 quaternary Heusler compounds having the chemical formula CoX′Y′Z, where Y′ = Mn, Fe; X′ a 4*d* element and Z = Al, Si. From Z = Al series we did find two true half-metals with 100% spin polarization though the Curie temperatures are very low for them. Z = Si series has been an interesting one as we could identify five new half-metallic ferromagnets of spin polarization nearly 100% alongwith very High Curie temperatures. In both series, we could identify a few "near half metals" which possibly can be tuned to exhibit half-metallic behaviour. We demonstrate that like the ternary series, the electronic structures by and large remain same for isoelectronic compounds irrespective of whether all magnetic elements are 3*d* elements, as long as the crystal structures remain same. We have reported some observations regarding fewer number of half-metals in the quaternary series with 4*d* elements as compared to the ones with all magnetic constituents being 3*d* transition metals. This warrants further deep, extensive investigations into the microscopic picture governing half-metallic behaviour in Heuslers.

The work presented in Chapter 4 demonstrates that half-metallicity is not straightforwardly transferrable from ternary parent compounds to the daughter quaternary compounds. In **Chapter 5** this aspect of site-dependence of substitution affecting half-metallic behaviour is addressed. A case study involving Mn_2RhSi, Co_2RhSi and CoMnRhSi is done to examine this. We find an intricate relationship between substituting site, substituting element, sustainability of spin magnetic moments of magnetic elements involved, composition and half-metallicity. The observations are explained in terms of the trends in the electronic structures and connections are made to the trends in the variations of magnetic exchange parameters and Curie temperatures. Overall, this case study provides important insights into the tunibility of half-metallic behaviour in compounds with 4*d* transition metal elements.

Chapter 6 concludes with the summary of the important outcomes from the thesis. We also describe the possible extensions of our work.

Chapter 2

Methods for material simulations

In this chapter, we provide a brief discussion of the theoretical methods, used in this thesis for material simulation. The calculations in this thesis are carried out using density functional theory (DFT). For obtaining the results furnished in this thesis, we have used two different implementations of DFT calculations. We have provided descriptions of how the ground-state total energies, densities of states and band structures as well as the magnetic exchange interactions and the transition temperatures are calculated using DFT based formalisms.

2.1 The many-body Hamiltonian

In principle any quantum mechanical description of matter is done by finding solutions of the Schrödinger equation, though in most cases it is too complex to solve. The electronic structures of materials are calculated by solving the time-independent, nonrelativistic many-body Schrödinger equation 2.1 for the many-body wave function ψ with suitable approximations.

$$\mathcal{H}\Psi = E\Psi \tag{2.1}$$

$\mathcal{H}$ is the Hamiltonian and E is the total electronic energy of the system. The many body wave function Ψ is expressed as,

$$\Psi = \Psi(\mathbf{r}_1, \mathbf{r}_2, ..., \mathbf{r}_i, ..., \mathbf{R}_1, \mathbf{R}_2, ..., \mathbf{R}_I, ...) \tag{2.2}$$

$\mathbf{r}_i$ and $\mathbf{R}_I$ are the positions of electrons and atomic nuclei respectively with i

and I as indices for electrons and ions, respectively. The Hamiltonian $\mathcal{H}$ describing the motion of each individual electron and nuclei for every atom in the system can be written as

$$\mathcal{H} = -\frac{\hbar^2}{2}\sum_I \frac{\nabla_I^2}{M_I} - \frac{\hbar^2}{2}\sum_i \frac{\nabla_i^2}{m_i} + \frac{1}{2}\sum_{I\neq J}\frac{Z_I Z_J e^2}{|\mathbf{R}_I - \mathbf{R}_J|} + \frac{1}{2}\sum_{i\neq j}\frac{e^2}{|\mathbf{r}_i - \mathbf{r}_j|} - \sum_{i,I}\frac{Z_I e^2}{|\mathbf{r}_i - \mathbf{R}_I|} \tag{2.3}$$

M_I and m_i represent the mass of the nucleus and electron respectively, Z_I is the charge of nucleus. The first two terms in the Hamiltonian are kinetic energies of nuclei and electrons, respectively. Other three terms are Coulomb interactions between nuclei and nuclei, electrons and electrons and electrons and nuclei respectively. In practice, due to innumerable degrees of freedom associated with this equation, the exact solution for the many body Hamiltonian (Eq. 2.3) for real systems like molecules and solids is not possible. Several additional approximations are essential at different levels to obtain feasible solutions. They are discussed in the next subsections.

2.2 The Born-Oppenheimer approximation

The mass of a nucleus is much larger than the mass of the electrons implying that the electronic time scale is orders of magnitude less than that of the nuclear time scale. This simply means that the ions can be considered as stationary while studying the electronic degrees of freedom. This leads to the first step to reduce the degrees of freedom in Eq. 2.3, known as Born-Oppenheimer approximation [141] which decouples the dynamics of electrons and nuclei. Now, the total wave function can be approximated as a product of the electron wave function and the ionic or nuclear wave function as shown below.

$$\Psi(\mathbf{r}_1, \mathbf{r}_2, ...; \mathbf{R}_1, \mathbf{R}_2, ...) = \psi(\mathbf{r}_1, \mathbf{r}_2, ...; \mathbf{R}_1, \mathbf{R}_2, ...) \cdot \chi_{nuc}(\mathbf{R}_1, \mathbf{R}_2, ...) \tag{2.4}$$

The ionic positions are now parameters only in the electronic wave functions. With Born-Oppenheimer approximation, the electronic structure problem can be reformulated as solving a quantum many-body Schrödinger equation for electronic degrees of freedom only. Within this approximation, the Hamiltonian reduces to

$$\begin{aligned}\mathcal{H}_e &= -\frac{\hbar^2}{2}\sum_i \frac{\nabla_i^2}{m_i} + \frac{1}{2}\sum_{i\neq j}\frac{e^2}{|\mathbf{r}_i - \mathbf{r}_j|} - \sum_{i,I}\frac{Z_I e^2}{|\mathbf{r}_i - \mathbf{R}_I|} \\ &= T_e + V_{ee} + V_{ext}\end{aligned} \tag{2.5}$$

T_e is the kinetic energy of the electrons, V_{ee} is the Coulomb energy due to electron-electron interaction and V_{ext} is the interaction with external potential.

2.3 Density Functional Theory (DFT)

Even with the simplification of Born-Oppenheimer approximation, Eq. 2.1 is a complicated many-electron eigenvalue problem and finding a tractable solution is quite impossible even with modern day computers. W. Kohn in his Nobel lecture [142] mentioned that "traditional wave-function methods, which provided "required" chemical accuracy, are generally limited to molecules with a small total number of chemically active electrons". The Density Functional theory (DFT) offers an excellent way to evade this problem. Instead of considering an intricate many-electron wave function based formalism, dealing with numerous degrees of freedom due to all electrons in the system, DFT disentangles the many-body problem by constructing the ground state properties as functionals of a single particle electronic charge density. Considering electronic energy in terms of electron density distribution, $n(r)$ was not new. Thomas [143] and Fermi [144] developed a useful theory considering the interacting electrons moving in an external potential $V(r)$, and provided a simplified one -to-one implicit relation between $V(r)$ and the density distribution $n(r)$. Like the wave function based Hartree [145] and Hartree-Fock [146] methods, the all important electron-electron interactions were incorporated by a mean field approximation. Subsequent refinements to the theory (with different exchange and correlation) could not increase its accuracy in calculating properties of real materials. Nevertheless, the Thomas-Fermi (TF) theory did point out the importance of one electron density $n(r)$ providing an approximate solution of the many body Schrödinger equation. P. Hohenberg and W. Kohn established required connection between the one electron density function, $n(r)$ with the wave function $\Psi(r_1, r_2, ..., r_N)$ to describe the electronic structure of matter in their pioneering work in 1964 [120]. Nowadays DFT is one of the most popular, successful and essential tool for electronic structure calculation due to its phenomenal success in describing the ground state properties of large number of materials in different forms like bulk, surfaces, interfaces, nanostructures

etc. The heart of the DFT is summarized in the following two theorems:

Theorem I : For any system of interacting electrons in an external potential $V_{ext}(\mathbf{r})$, the ground state density $n_0(\mathbf{r})$ uniquely, except for a constant, determines this potential [122].

Theorem II : The exact ground state energy of a system in an external potential $V_{ext}(\mathbf{r})$, is the global minimum value of a universal functional for the energy $E[n]$, associated with the density $n(r)$, and the density that minimizes the functional is the exact ground state density $n_0(\mathbf{r})$ [122] .

The first theorem simply implies that in an external potential $V_{ext}(\mathbf{r})$, the electron density determines the ground state energy represented by a universal functional

$$E_{HK}[n] = F_{HK}[n] + \int V_{ext}(\mathbf{r})n(\mathbf{r})\, d^3\mathbf{r} \tag{2.6}$$

The universal functional $F_{HK}[n]$ includes all kinetic and potential internal energies of the system and the interaction energy with the external potential is represented by the second term. The second theorem basically shows the way to find the ground state total energy by minimizing the energy functional $E[n]$.

Thus, compared to the conventional wave function based approaches, which is practically a bit of hassle, DFT offers a different outlook by considering that the ground state properties of an interacting electronic system, theoretically are determined by the ground state density. However, the energy functional $E[n]$ of Hohenberg-Kohn theorems, is not known and it makes these theorem inappropriate for practical applications. The Kohn-Sham formalism [121] along with the Hohenberg-Kohn theorems makes DFT a success. Kohn-Sham approach maps the many-body problem onto a single-body problem by introducing an auxiliary noninteracting electronic system where the electrons are exposed to an effective external potential $V_{ext}(\mathbf{r})$, constrained to the fact that the resulting density of the noninteracting system is equal to that of the density of the true interacting system. Together with the variational principle, Kohn-Sham formalism leads to the famous Schrödinger-like eigenvalue equation:

$$(\mathcal{H}_{KS} - \epsilon_i)\phi_i(\mathbf{r}) = 0 \tag{2.7}$$

where $\mathcal{H}_{KS}$ is the effective Hamiltonian, ϵ_is are the eigenvalues and $\phi_i(\mathbf{r})$ is the single particle orbital. The Hamiltonian, in the independent electron approximation

of Kohn-Sham scheme can be expressed as

$$\mathcal{H}_{KS} = -\frac{1}{2}\nabla^2 + V_{eff} \quad (in\ Hartree\ units) \tag{2.8}$$

with,

$$V_{eff} = V_{ext}(\mathbf{r}) + V_{Hartree}(\mathbf{r}) + V_{XC}(\mathbf{r}) \tag{2.9}$$

The Hartree energy, $V_{Hartree}$ is is given by

$$V_{Hartree} = \frac{1}{2}\int \frac{n(\mathbf{r})n(\mathbf{r'})}{|\mathbf{r}-\mathbf{r'}|}\, d^3\mathbf{r} d^3\mathbf{r'} \tag{2.10}$$

The *exchange and correlation* potential, $V_{XC}(\mathbf{r})$ is defined as,

$$V_{XC} = \frac{\delta E_{xc}[n]}{\delta n(\mathbf{r})} \tag{2.11}$$

The contribution of all known potentials due to effective independent electrons approximation along with the unknown contribution, the exchange-correlation, constitutes the effective potential of Eq. 2.9. This, in turn, determines the required energy functional E_{HK} (Eq. 2.6). Once we know the exchange-correlation energy $E_{xc}[n]$, the total energy of the system in its ground state can be calculated in terms of electron density $n(\mathbf{r})$ [147].

The single-electron orbitals $\phi_i(\mathbf{r})$ are used to calculate the density as

$$n(\mathbf{r}) = \sum_{i=1}^{N} |\phi_i(\mathbf{r})|^2 \tag{2.12}$$

The total number of electron is given by

$$\mathcal{N} = \int n(\mathbf{r})\, d^3\mathbf{r} \tag{2.13}$$

In Kohn-Sham self-consistent approach, equations (2.6-2.13) are used to compute the ground state energy of an electronic system with

$$E_{KS} = T_s[n] + \int V_{ext}(\mathbf{r})n(\mathbf{r})\, d^3r + E_{Hartree}[n] + E_{xc}[n] \tag{2.14}$$

with single particle kinetic energy T_s as

$$T_s = \frac{1}{2}\sum_{i=1}^{N}\nabla^2\phi_i(\mathbf{r}) \tag{2.15}$$

Thus with the above single particle non-spinpolarized formulae we can find the electron density from the potential self-consistently. Now for the spin-density functional formalism, two spin-densities $n^{\uparrow}(r)$ and $n^{\downarrow}(r)$ are introduced as the solutions of the very starting Kohn-Sham equation 2.7 for the same effective potential as above. Only the exchange-correlation part is modified and the spin-dependent exchange-correlation potential can be written as

$$V^{\sigma}_{XC}([n^{\uparrow}, n^{\downarrow}; r]) = \frac{\delta E_{xc}[n^{\uparrow}, n^{\downarrow}]}{\delta n^{\sigma}(\mathbf{r})} \tag{2.16}$$

where $\sigma = \uparrow or \downarrow$.

It is to be noted that the functional, $E_{xc}[n^{\uparrow}, n^{\downarrow}]$ is of great interest in the fundamental development of DFT and its origin is rooted into the very basic approximation of Hartree-Fock, used to treat a many-body (many-electron) system. $E_{xc}[n^{\uparrow}, n^{\downarrow}]$ defined as the difference between the the kinetic energy plus true internal energies of the actual many body interacting system and those of the auxiliary single particle system with electron-electron interactions replaced by the Hartree energy. So, E_{xc} is simply the sum of the errors comes in to the picture due to the use of non-interacting kinetic energy and classical electron-electron interaction. The exchange part of $E_{xc}[n^{\uparrow}, n^{\downarrow}]$ takes care of fact that the presence of an electrons at the point $\mathbf{r}$ reduces the total energy (density) of the other electrons at the point $\mathbf{r}'$; and the linear response function, $\chi(\mathbf{r}, \mathbf{r}'; \omega)$, describing the change of total density at the point $\mathbf{r}$ due to perturbing potential (arises due to the kinetic energy or movement of the electron) at the point $\mathbf{r}'$, with frequency ω.

In a notion of Eq. 2.12, the electronic charge density, ρ of the one-electron orbitals $\phi_j(\mathbf{r})$ may be defined as

$$\rho(\mathbf{r}) = \sum_{j=1}^{N}|\phi_j(\mathbf{r})|^2 \tag{2.17}$$

and an orbital dependent "*exchange-chargedensity*", ρ_i^{HF} for the i^{th} orbital and involving a spin dependent factor, coupling with only states (i, j) with the same

spin coordinates (s_i, s_j) can be expressed as

$$\rho_i^{HF}(\mathbf{r}, \mathbf{r}') = \sum_{j=1}^{\mathbf{N}} \frac{\phi_j^*(\mathbf{r}')\phi_i(\mathbf{r}')\phi_i^*(\mathbf{r})\phi_j(\mathbf{r})}{\phi_j^*(\mathbf{r})\phi_i(\mathbf{r})} \delta_{s_i,s_j} \tag{2.18}$$

With the defined charge densities we can define the corresponding *Coulomb* or *Hartree* potential density as

$$\mathcal{V}_H(\mathbf{r}) = \int \frac{\rho(\mathbf{r})}{|\mathbf{r} - \mathbf{r}'|} d^3\mathbf{r}' \tag{2.19}$$

and similarly the *exchange* potential density as

$$\mathcal{V}_X^i(\mathbf{r}) = -\int \frac{\rho_i^{HF}(\mathbf{r}, \mathbf{r}')}{|\mathbf{r} - \mathbf{r}'|} d^3\mathbf{r}'. \tag{2.20}$$

The *correlation* part of the E_{xc} contains rest of the terms which are excluded in calculating the total energy in Hartree-Fock method. Calculating the *correlation energy* (E_c) for a complex system is very difficult and one way to calculate E_{corr} is to find the difference between the exact energy of a many-body electronic system, (E_{exact}), and the energy of the system calculated using the Hartree-Fock approximation, E_{HF}: $E_{corr} = E_{exact} - E_{HF}$.

In Kohn-Sham approach the exact ground-state energy and density is calculated, in principle only if the functional $E_{xc}[n]$ is known. Search for useful approximations to construct accurate $E_{xc}[n]$ has been a major area of research. Proper approximations are required to construct the exchange and correlation term in solids. The Local Density Approximation (LDA) [121] is the simplest yet very popular and effective approximation. The basic assumptions of LDA is that the local exchange-correlation energy density per electron is dependent only on the local density and in a solid it is assumed to be the same as that of the homogeneous electron gas. Within LDA the E_{xc}, can be expressed as

$$E_{xc}^{LDA}[n] = \int n(\mathbf{r})\varepsilon_{xc}^{hom}(n(\mathbf{r}))d^3r \tag{2.21}$$

where ε_{xc}^{hom} is the sum of the exchange and correlation energies of the homogeneous electron gas of density $n(\mathbf{r})$.

As expected homogeneous electron gas approach is not a suitable approximation where the electron densities vary rapidly as is the case of many atoms or molecules. Even with its drawback in producing the correct electronic ground states in some

important cases, LDA is widely used due the fact that it is successful in cases of simple systems.

Along with the electron density, the gradient corrections on the electron density was included to take care of the problems in the LDA. Such approximations are called Generalized Gradient Approximation (GGA) [148–150]. The GGA functional can be expressed as

$$E_{xc}^{GGA}[n] = \int d^3r\, n(\mathbf{r})\, \varepsilon_{xc}^{GGA}(n(\mathbf{r}), |\nabla n(\mathbf{r})|) \tag{2.22}$$

There exist a number of forms for the GGA energy density per electron, ε_{xc}^{GGA}. Extensive development has been made to find other approximations for exchange-correlation apart from GGA functional. Only GGA functionals have been used for the calculations presented in this thesis.

It is worth mentioning here that to construct the *exchange-correlation* functional, E_{xc}, out of several approximations, LDA and GGA functionals refer only to the exchange part of E_{xc}. In all cases the *correlation* part is treated by the early parametrization of the group of Perdew [151].

The possibility of opting different basis sets to express the solution of equation 2.7, gives rise to different electronic structure methods, implementing DFT. This makes it a challenge to develop simultaneously accurate and time efficient numerical methods, depending on the nature of the problem addressed, in modern day computational material science. Three major groups of methodologies are used nowadays: the Pseudopotential (PP) methods, the full potential (FP) methods and the Green's function based methods. In this work we have used Pseudopotential and Green's function based methods. In the next section we briefly discuss them.

2.4 Pseudopotential method

The wave function of an electron in a periodic potential is represented by a discrete set of plane waves according to Bloch's theorem. We need large number of plane waves to express the strong core potential, characterised by the tightly bound core orbitals and the wiggles in the wave functions of the valance electrons in the core, arising due to orthogonality of core and valance states. In PP method, instead of a strong core potential, a pseudopotential corresponding to a "Pseudo-Hamiltonian" is considered, such that outside a cut-off radius the ground state wave functions calculated in this approach resemble that of the all electron wavefuction. This method

basically removes the wiggles by a smooth pseudo-wavefuction represented by a reasonable number of plane waves, in the core region, making the method computationally tractable. The evolution of plane wave based pseudopotential methods which are widely used in the electronic structure calculations are briefly described in the next subsections.

2.4.1 Norm-Conserving Pseudopotentials (NCPP)

While developing the pseudopotentials the main focuses were to (*i*) make it as soft as possible ensuring the usage of fewer planewaves (*ii*) make it as transferable as possible so that a pseudopotential for a given element can easily be applicable in different environments and (*iii*) produce a pseudo-charge density mimicking the valance charge density as accurate as possible [125]. The first computationally tractable pseudopotentials were the norm conserving pseudopotentials (NCPP). The NCPPs are constructed such that the pseudo-wavefuctions (and potential) imitate the actual valance wavefuctions (and potentials) outside of some cut-off radius, equivalent to the core radius, r_c. Within the cut-off radius, the pseudo-wavefuctions and the actual wavefuctions are different but are constrained to conserve the norm, *i.e.*,

$$\int_0^{\mathbf{r}_c} \varphi^{PS*}(r)\varphi^{PS}(r)r^2\, dr = \int_0^{\mathbf{r}_c} \varphi^{AE*}(r)\varphi^{AE}(r)r^2\, dr \tag{2.23}$$

φ^{PS} and φ^{AE} are the pseudo and all electron wavefunctions respectively. This approach works well for *sp* elements but the transition metals and rare earth elements with localized d and f states need a very large plane wave basis set, and NCPP becomes rather intractable.

2.4.2 Ultrasoft Pseudopotentials (USPP)

The pseudo-wavefuctions generated in NCCP approach are constrained to match well with the all-electron wavefuction outside the $\mathbf{r}_c$. The norm-conservation inside $\mathbf{r}_c$ demands a large plane wave basis set which is against the criteria for fast conservation in planewave based calculations. Vanderbilt and co-workers [152–154] eluded this issue by proposing a new and radical approach by allowing the pseudo-wavefuctions to be as soft as possible inside $\mathbf{r}_c$, though outside $\mathbf{r}_c$, the NCPP approach was maintained. This approach considerably reduces the number of plane waves required to construct the basis set with the cost of introducing some compli-

cations. Three innate complications in the construction of ultrasoft pseudopotential are: (i) since the wavefunctions are not necessarily been normalized, they introduce a non-trivial overlap term in the secular equation, (ii) the pseudo charge density cannot simply be obtained with calculations $\sum \varphi^* \varphi$ as done with norm-conserving pseudopotentials, rather, a term is needed to be added in the core region, (iii) relaxation of the norm conservation results in less transferable pseudopotentials. However, Vanderbilt pseudopotentials have been used over the years in large-scale calculations and proved their reliability in condensed matter calculations. Most importantly, the cost of generating these kinds of pseudopotentials is negligible compared to the cost of calculations where they are used.

2.5 Projector Augmented Wave (PAW) method

The pseudopotential method is very useful in term of speed and memory, yet the loss of information of the full wave function close to the nucleus was a major drawback. Calculation of certain properties like hyperfine parameters and electric field gradients are very much sensitive to these information. Also due to many adjustable parameters and degrees of freedom used in the construction of pseudopotentials, it is not always possible to yield reliable results in the real material environment using a particular pseudopotential with fixed parameters. The Projector Augmented Wave (PAW) is a more general approach, introduced by Peter Blöchl [137] in 1994, which is a combination of ideas from all-electron Linearized Augmented Plane Wave (LAPW) methods [125–128, 155] and pseudopotential methods. The main idea of PAW method was to retain the all-electron character, by dividing the wave function into two parts: partial wave expansion in a sphere around the atom (augmentation region) and envelope functions outside the spheres (interstitial region). At the sphere edge this true and pseudo wavefuctions are connected by a linear transformation. A brief description of this formalism is presented in this section.

The practically relevant all-electron wavefuctions $|\psi_n\rangle$ are mapped from computationally convenient smooth wavefuctions $\left|\tilde{\psi}_n\right\rangle$ by a linear transformation operator $\hat{\mathcal{T}}$ in PAW method.

$$|\psi_n\rangle = \hat{\mathcal{T}} \left|\tilde{\psi}\right\rangle \tag{2.24}$$

The true wave functions are already smooth at a certain distance from the core (r_c^a). This implies that the transformation must be unitary beyond the augmentation cut-

off ($|\mathbf{r} - \mathbf{R}^a| > r_c^a$) and a sum of atom-centered contribution inside the augmented sphere.

$$\hat{\mathcal{T}} = 1 + \sum_a \hat{\mathcal{T}}^a \tag{2.25}$$

where a is an atom index and $\hat{\mathcal{T}}^a = \hat{\mathcal{T}}^a(\mathbf{r} - \mathbf{R^a}) = \mathbf{0}$ for $|\mathbf{r} - \mathbf{R}^a| > r_c^a$. The cut-off radii r_c^a are chosen carefully to avoid overlap between augmented spheres. The smooth wavefunction, inside the augmentation region, can be expanded into smooth partial waves $\tilde{\phi}^a$

$$\left|\tilde{\psi}_n\right\rangle = \sum_{i,a} c_{ni}^a \left|\tilde{\phi}_i^a\right\rangle \tag{2.26}$$

The all-electron wavefunction is expressed likewise as

$$|\psi_n\rangle = \sum_{i,a} c_{ni}^a |\phi_i^a\rangle \tag{2.27}$$

The linear transformation operation in terms of smooth partial waves is expressed as

$$|\phi_i^a\rangle = (1 + \hat{\mathcal{T}}^a)\left|\tilde{\phi}_i^a\right\rangle \implies \hat{\mathcal{T}}^a \left|\tilde{\phi}_i^a\right\rangle = |\phi_i^a\rangle - \left|\tilde{\phi}_i^a\right\rangle \tag{2.28}$$

Combining equations from 2.24-2.28 the true wave function can be expressed as

$$|\psi_n\rangle = \left|\tilde{\psi}_n\right\rangle - \sum_{i,a} c_{ni}^a \left|\tilde{\phi}_i^a\right\rangle + \sum_{i,a} c_{ni}^a |\phi_i^a\rangle \tag{2.29}$$

The coefficients (c_{ni}^a) must be linear functional of the smooth wavefuction, as the transformation operator $\hat{\mathcal{T}}$ is linear. With some smooth projector functions $\tilde{p}_i^a$, c_{ni}^a can be expressed as

$$c_{ni}^a = \left\langle \tilde{p}_i^a \middle| \tilde{\psi}_n \right\rangle \equiv \mathcal{P}_{ni}^a \tag{2.30}$$

As mentioned earlier, the condition of non-overlapping of the augmented sphere forces the one-center expansion of smooth wavefuctions $\sum_i \left\langle \tilde{p}_i^a \middle| \tilde{\psi}_n \right\rangle \left|\tilde{\phi}_i^a\right\rangle$ to be

identical with $\left|\tilde{\phi}_i^a\right\rangle$. Thus the completeness condition is given by

$$\sum_i \left|\tilde{\phi}_i^a\right\rangle\left\langle\tilde{p}_i^a\right| = 1 \tag{2.31}$$

This in turn implies that the smooth projector functions and partial waves are mutually orthogonal within the augmentation sphere *i.e.*

$$\left\langle\tilde{p}_{i_1}^a\middle|\tilde{\phi}_{i_2}^a\right\rangle = \delta_{i_1,i_2} \tag{2.32}$$

Now, using Eq. 2.28 and Eq. 2.31 the transformation operator $\hat{\mathcal{T}}^a$ can be written in a closed form

$$\mathcal{T} = \sum_a \sum_i \left(|\phi_i^a\rangle - \left|\tilde{\phi}_i^a\right\rangle \right) \langle\tilde{p}_i^a| \tag{2.33}$$

The all-electron, Kohn-Sham wavefuction $\psi_n(\mathbf{r}) = \langle\mathbf{r}|\psi_n\rangle$ now can be written as, (using Eq. 2.29 and Eq. 2.30)

$$\psi_n(\mathbf{r}) = \tilde{\psi}_n(\mathbf{r}) + \sum_a \sum_i \left(\phi_i^a(\mathbf{r}) - \tilde{\phi}_i^a(\mathbf{r})\right) \left\langle\tilde{p}_i^a\middle|\tilde{\psi}_n\right\rangle \tag{2.34}$$

or

$$\begin{aligned} |\psi_n(\mathbf{r})\rangle &= \left|\tilde{\psi}_n\right\rangle + \sum_a \sum_i \left(|\phi_i^a\rangle - \left|\tilde{\phi}_i^a\right\rangle \right) \left\langle\tilde{p}_i^a\middle|\tilde{\psi}_n\right\rangle \\ &= \left|\tilde{\psi}_n\right\rangle + \sum_a \left(\sum_i \left(|\phi_i^a\rangle \left\langle\tilde{p}_i^a\middle|\tilde{\psi}_n\right\rangle - \left|\tilde{\phi}_i^a\right\rangle \left\langle\tilde{p}_i^a\middle|\tilde{\psi}_n\right\rangle \right) \right) \end{aligned} \tag{2.35}$$

From Eq. 2.35, we find that the all-electron wavefunction is decomposed in to two explicitly separated extended-space and atom-centered contributions. This is the basic idea in PAW method, that is, to write the all-electron wavefunction as the sum of the smooth pseudo-wavefunction (smooth everywhere) and sum over the subtraction of one-centered all electron contribution and one-centered pseudo part. Exploiting Eq. 2.35 compact expression for various quantities in PAW method [138, 156–158] can be obtained. The PAW method as implemented in the VASP code [159], is used throughout this thesis.

2.6 Green's Function method of Korringa, Kohn and Rostoker (KKR)

Green's function based Korringa-Kohn-Rostoker (KKR) electronic structure method was introduced independently by Korringa [123] in 1947 and by Kohn and Rostoker [124] in 1954 respectively. In this method, multiple scattering approach is used to find the solution of Schrödinger equation. The multiple scattering approach leads to the determination of the scattering properties of each atom center or single site by a scattering matrix. Multiple-scattering theory is then applied for solving the equation of one electron scattered at many different potentials (all atomic sites in the lattice). This separation of the single scattering and the multiple scattering problems are connected by the condition that the incident wave at each scattering center has to be equal to the sum of the outgoing waves from all the other scattering centers. This splitting, yields the most important feature of these KKR Green's function based formalism, that is, the separation of the structural part and the potential part.

KKR method provides a natural approach to a localized description of electronic properties, response functions and susceptibility that can be applied to alloys and other disordered systems and systems with impurity. The important extension of the KKR approach is dependent on the construction of the Green function. The Green function of free space (the ideal periodic potential) is efficiently used to produce the crystal Green function (locally confined impurity potentials) via a Dyson equation. This approach is particularly a very efficient technique for solving the impurity problem without construction of the huge supercells, as done in wavefunction based methods.

The key steps in the KKR Green's Function formalism are as described below. The system is approximated to be composed of an assembly of non-overlapping spherical muffin-tin (MT) potentials centered on each lattice site of a crystal. Within MT the spherically symmetric potential is defined by the MT radius (R_{MT}) while in the remaining interstitial part it is assumed to be constant and accordingly can be set to zero [160]. Then, the crystal Green's function $G(\mathbf{r}, \mathbf{r}^{'}; E)$ can be evaluated from the free space Green's function $g(\mathbf{r}, \mathbf{r}^{'}; E)$ by

$$G(\mathbf{r}, \mathbf{r}^{'}; E) = g(\mathbf{r}, \mathbf{r}^{'}; E) + \int dr^{''} g(\mathbf{r}, \mathbf{r}^{''}; E) V(\mathbf{r}^{''}) G(\mathbf{r}^{''}, \mathbf{r}^{'}; E) \tag{2.36}$$

where $V(\mathbf{r}^{'})$ denotes the assembly of muffin-tin potentials. The above equation is

not used for practical calculations due to convergence problem. Instead, a cell-centered angular momentum based representation is introduced. The cell-centered representation of $g(\mathbf{r}, \mathbf{r}^{'}; E)$ is expressed by

$$\begin{aligned} g(\mathbf{r}+\mathbf{R_m}, \mathbf{r}^{'}+\mathbf{R_n}; E) &= g(\mathbf{r}, \mathbf{r}^{'}+\mathbf{R_n}-\mathbf{R_m}; E) \\ &= -i\sqrt{E}\sum_{L} J_L(\mathbf{r}) H_L(\mathbf{r}^{'}+\mathbf{R_n}-\mathbf{R_m}) \end{aligned} \tag{2.37}$$

where H_Ls are the Hankel functions and J_Ls are the spherical Bessel functions. With our assumption of periodic MT potentials, centered at lattice sites R_m, each outgoing wave from site R_m can be expanded in a basis of incoming waves at site R_n using an addition theorem of Hankel functions [161]:

$$H_L(\mathbf{r}^{'}+\mathbf{R_n}-\mathbf{R_m}; E) = \frac{i}{\sqrt{E}}\sum_{L^{'}} g^{mn}_{LL^{'}}(E) J_{L^{'}}(\mathbf{r}; E) \tag{2.38}$$

and making use of the following relations.

$$\begin{aligned} J_L(\mathbf{r}; E) &= j_\ell(\sqrt{E}r) Y_L(\mathbf{r}) \\ H_L(\mathbf{r}; E) &= h_\ell(\sqrt{E}r) Y_L(\mathbf{r}) \end{aligned} \tag{2.39}$$

Where Y_Ls are spherical harmonics. Now, the free electron Green's function can be expressed as

$$\begin{aligned} g(\mathbf{r}+\mathbf{R_m}, \mathbf{r}^{'}+\mathbf{R_n}; E) = -i\sqrt{E}\delta_{mn}\sum_{L} J_L(r_<; E) H_L(r_>; E) \\ + \sum_{LL^{'}} J_L(\mathbf{r}; E) g^{mn}_{LL^{'}} J_L(\mathbf{r}^{'}; E) \end{aligned} \tag{2.40}$$

The structure constants are defined by

$$g^{mn}_{LL^{'}}(E) = -4\pi i\sqrt{E}(1-\delta_{mn})\sum_{L^{''}} i^{\ell-\ell^{'}+\ell^{''}} C^{L^{''}}_{LL^{'}} H_{L^{''}}(R_m - R_n; E) \tag{2.41}$$

with the Gaunt coefficients

$$C^{L^{''}}_{LL^{'}} = \int d\Omega Y_{L^{''}}(\mathbf{r}) Y_{L^{'}}(\mathbf{r}) Y_L(\mathbf{r}) \tag{2.42}$$

Similarly, the crystal Green's function has the cell-centered mixed site-angular mo-

mentum representation as follows,

$$G(\mathbf{r}+\mathbf{R_m},\mathbf{r}^{'}+\mathbf{R_n};E) = -i\sqrt{E}\delta_{mn}\sum_{L}\mathcal{J}_L(r_<;E)\mathcal{H}_L(r_>;E) + \sum_{LL'}\mathcal{J}_L(\mathbf{r};E)G^{mn}_{LL'}\mathcal{J}_L(\mathbf{r}^{'};E) \tag{2.43}$$

with the following relations.

$$\begin{aligned}\mathcal{J}_L(\mathbf{r};E) &= P_\ell(\sqrt{E}r)Y_L(\mathbf{r})\\ \mathcal{H}_L(\mathbf{r};E) &= Q_\ell(\sqrt{E}r)Y_L(\mathbf{r})\end{aligned} \tag{2.44}$$

The contribution of the multiple scattering or back scattering to the Green's function is represented by the second term, in equation 2.40, which is also used to produce the band structure. The relation between $G^{mn}_{LL'}(E)$ and $g^{mn}_{LL'}(E)$ can be obtained by inserting the above expressions for the Green's function into the integral equation

$$G^{mn}_{LL'}(E) = g^{mn}_{LL'}(E) + \sum_{L''m,} g^{mm^{'}}_{LL'}(E)t^{m^{'}}_{L''}G^{m^{'}n}_{L''L'}(E) \tag{2.45}$$

where t-matrix $t^{m^{'}}_{L''}$ is defined as

$$t^{m^{'}}_{L''} = \int\int d\mathbf{r_m}d\mathbf{r}^{'}_{\mathbf{m}}J_L(\mathbf{r}_{m'};E)t^{m^{'}}(\mathbf{r}_{m'},\mathbf{r}^{'}{}_{m'};E)J_{L'}(\mathbf{r}^{'}{}_{m'};E) \tag{2.46}$$

When the scattering centers are aligned periodically in the crystal, $G^{mn}_{LL'}$ and $g^{mn}_{LL'}$ can be Fourier transformed as,

$$G^{mn}_{LL'}(\mathbf{R}_m-\mathbf{R}_n;E) = \frac{1}{\tau}\int_\tau G_{LL'}(\mathbf{k},E)e^{i\mathbf{k}(\mathbf{R_m}-\mathbf{R_n})}d\mathbf{k} \tag{2.47}$$

$$g^{mn}_{LL'}(\mathbf{R}_m-\mathbf{R}_n;E) = \frac{1}{\tau}\int_\tau g_{LL'}(\mathbf{k},E)e^{i\mathbf{k}(\mathbf{R_m}-\mathbf{R_n})}d\mathbf{k} \tag{2.48}$$

where τ is the volume of the first Brillouin zone. Substituting them into equation 2.45, one gets

$$G_{LL'}(\mathbf{k},E) = g_{LL'}(\mathbf{k},E) + \sum_{L''}g_{LL'}(\mathbf{k},E)t_{L''}G_{L''L'}(\mathbf{k},E) \tag{2.49}$$

Finally,

$$G_{LL'}(\mathbf{k}, E) = \sum_{L''}[\delta_{L''L} - g_{L''L}(\mathbf{k}, E)t_L]g_{L''L}(\mathbf{k}, E) \tag{2.50}$$

Then, the crystal Green's function is given by

$$\begin{aligned} &G(\mathbf{r} + \mathbf{R_m}, \mathbf{r}' + \mathbf{R_n}; E) = -i\sqrt{E}\delta_{mn}\sum_L \mathcal{J}_L(r_<; E)\mathcal{H}_L(r_>; E) \\ &+\mathcal{J}_{Lm}(\mathbf{r})\int \tfrac{d\mathbf{k}}{\tau} exp(i\mathbf{k}.(\mathbf{R_m} - \mathbf{R_n}))\sum_{L''} g_{LL''}(\mathbf{k}, E)[1 - tg(\mathbf{k}, E)]^{-1}_{L''L'}\mathcal{J}_{L'n}(\mathbf{r}') \end{aligned} \tag{2.51}$$

The band structure is then calculated by finding the zeros of the determinant of the matrix from the equation 2.50 for each $\mathbf{k}$

$$det|\delta_{LL'} - t_L(E)g_{LL'}(\mathbf{k}; E)| = 0 \tag{2.52}$$

The energy eigenvalues are determined as a function of $\mathbf{k}$ in this procedure and hence, an energy dispersion relation $E(\mathbf{k})$ is yielded. The zeros of the KKR matrix gives the poles of the Green's function; each pole corresponds to the eigenstate of the Hamiltonian.

In this thesis we have used the Munich group's implementation of the Green's function formalism as done in SPRKKR package [162] mainly to compare our results from the PAW based VASP package as well as to calculate the magnetic exchange interactions and the Curie temperatures, discussed in the following section.

2.7 Calculations of the magnetic exchange interactions and the magnetic transition temperatures

All the materials studied here have 3 transition metals with d electrons, two $3d$ and a $4d$ element. Magnetism in transition metals is known to depend on the atomic character of d electrons and inter-atomic exchange interactions. Hence, together with the electronic structures (density of states (DOS) and band structures), we have computed the magnetic exchange interactions J_{ij} as well as the magnetic transition temperatures or Curie temperatures (T_c) of all compounds, studied here, to comprehend the magnetism for these materials better. The methods, used in this thesis to compute the magnetic exchange interactions and the Curie temperatures (T_c) are presented in this section.

2.7.1 The magnetic exchange interactions (J^{ij})

With multiple scattering Green function formalism as implemented in SPRKKR code [140], we have calculated the magnetic pair exchange parameters. Here, the spin part of the Hamiltonian is mapped to an effective Heisenberg model for the spin interaction of sites using the following formula

$$H = -\sum_{\mu,\nu}\sum_{i,j} J^{ij}_{\mu\nu}\mathbf{e}^{i}_{\mu}.\mathbf{e}^{j}_{\nu} \tag{2.53}$$

where μ, ν represent different sub-lattices; i, j indices are used to denote the atomic positions and $\mathbf{e}^{i}_{\mu}$ is the directional unit vector along the direction of magnetic moments at site i belonging to sub-lattice μ. The magnetic exchange interactions $J^{ij}_{\mu\nu}$s, calculated from the energy differences due to infinitesimally small orientations of a pair of spins resulting a perturbation in spin-density, within the formulation of Liechtenstein *et. al.* [163], based on magnetic force theorem [164], takes the following form.

$$J^{ij} = \frac{1}{4\pi}\int_{-\infty}^{E_F} dE\ \mathrm{Im\ Tr}(\Delta_{\mathrm{i}}\hat{\mathrm{T}}^{\mathrm{ij}}_{\sigma}\Delta_{\mathrm{j}}\hat{\mathrm{T}}^{\mathrm{ji}}_{\sigma\prime}) \tag{2.54}$$

here σ is the spin index, $\hat{T}$ is the scattering path operator related to the off-diagonal elements of the Green's function and $\Delta_i = (\hat{t}^{-1}_{i\sigma}\text{-}\hat{t}^{-1}_{i\sigma\prime})$, $\hat{t}$ is the single scattering matrix. The trace, Tr is over the orbital indices of the scatting matrix. Once $J^{ij}_{\mu\nu}$s are calculated using the first-principle calculations we can find the nature of the coupling of the i and j atoms and the Curie temperatures. A positive (negative) values for J^{ij} indicate ferromagnetic (antiferromagnetic) coupling between atoms i and j.

2.7.2 Curie temperature (T_c) calculation with mean field approximation (MFA)

In this thesis we have used mean field approximation (MFA) [165] to calculate the Curie temperature (T_c), estimated using the J^{ij}. Since we are mainly concerned about the trends in the T_cs across the particular series and the relation between the T_cs and the J^{ij}s, overestimation of T_c by MFA is not going to be our concern for the time being.

For a multi-sublattice material, within the mean field approximation the Curie

temperature is obtained by solving the system of coupled equations [165–167]

$$\langle \mathbf{e}^{\mu} \rangle = \frac{2}{3k_B T} \sum_{\nu} J^0_{\mu\nu} \langle \mathbf{e}^{\nu} \rangle \tag{2.55}$$

where $\langle \mathbf{e}^{\nu} \rangle$ is the average Z component of $\mathbf{e}^{\nu}_i$ and $J^0_{\mu\nu} \equiv \sum_i J^{0i}_{\mu\nu}$. Eq. 2.55 can be expressed in the form of an eigenvalue matrix problem

$$(\mathbf{\Theta} - T\mathbf{I})\mathbf{E} = 0, \tag{2.56}$$

where $\Theta_{\mu\nu} = (2/3k_B)J^0_{\mu\nu}$, $\mathbf{I}$ is a unit matrix and $\mathbf{E}$ is the vector of $\langle \mathbf{e}^{\nu} \rangle$. The largest eigenvalue of matrix $\mathbf{\Theta}$ determines the value of the Curie temperature [165].

2.8 Summary

In this chapter, we have briefly described the state-of-the-art computational techniques used in condensed matter physics, i.e., DFT based methods, for obtaining the results used in this dissertation. To retrieve useful information from the materials which I have investigated, two different implementations of DFT have been extensively used; (i) PAW method as implemented in the VASP, mainly for structural and electronic structure calculations (ii) Full potential KKR method as implemented in the SPRKKR package, primarily to calculate exchange interaction parameters and Curie temperatures. The reason behind choosing VASP over SPRKKR to calculate the electronic structure is mainly due to its easy usage and speed while relaxing the structure.

Chapter 3

Exploration of half-metallicity in ternary Heusler compounds $X_2X'Z$ (X = Co, Fe, Mn, X′ = $4d$ elements and Z = Al, Si)

3.1 Introduction

In the introductory chapter, we have discussed, in somewhat detail, that the highest number of magnetic half-metals are found in ternary Heusler compounds $X_2X'Z$. Overwhelmingly large number of half-metals have X and X′ as transition metal elements with $3d$ electrons. Comparatively, exploration with either both or one of the two transition metal constituents being elements with $4d$ electrons are very few [169–171].

In this chapter we present our results on structural, electronic and magnetic properties of six ternary series $X_2X'Z$, with X = Mn, Fe, Co , Z = Al, Si while X′ is varied from Y to Ag down the series in the periodic table, by Density functional theory (DFT) based electronic structure calculations. The reasons for choosing Co_2, Mn_2 and Fe_2 based compounds have been discussed in section 1.8. The motivations behind the work are as follows:

1. search for new half-metallic magnets.

The contents of this chapter are from [168], Accepted in Physscripta

2. understanding of the impacts on properties related with half-metallic behaviour and magnetism in materials having both 3d and 4d elements.

3. comparative study of isoelectronic compounds with same X and Z but different X′; in one case X′ a 3d transition metal while in the other case it's 4d transition metal, to understand the origin of their electronic properties in the context of half-metallic behaviour.

The chapter is organised as follows: Computational details and the methods, used in this work are given in the next section. In the subsequent section (Section 5.3) we present the discussions of the calculated results on structural, electronic and magnetic properties of the ternary compounds mentioned above along with a comparative understanding with compounds having only 3d elements as the magnetic components. The conclusions and future outlook are presented at the end.

3.2 Computational Details

We have used spin-polarized DFT based projector augmented wave methods as implemented in Vienna Ab-initio Simulation Package (VASP) [137–139] with Generalized Gradient Approximation (GGA) [172] for calculating electronic structure. An energy cut-off of 450 eV and a Monkhorst-Pack [173] 25 x 25 x 25 k-mesh was used for self-consistent calculations while a larger 31 x 31 x 31 k-mesh was used for calculating densities of sates. We set the energy and the force convergence criteria to 10^{-6} eV and 10^{-2} eV/Å respectively.

With multiple scattering Green function formalism as implemented in SPRKKR code[140] we have calculated the magnetic pair exchange parameters as discussed in chapter 2. Full potential spin polarized scalar relativistic Hamiltonian with angular momentum cut-off $l_{max} = 3$ is used to calculate the energy differences by the SPRKKR code. We have use a uniform k-mesh of $22 \times 22 \times 22$ for Brillouin zone integrations. The Green's functions were calculated for 32 complex energy points distributed on a semiconductor contour. For the self-consistence cycles, the energy convergence criterion was set to 10^{-6} Ry . The calculated $J^{ij}_{\mu\nu}$ were used further to compute the Curie temperatures within the mean field approximation[167].

3.3 Results and Discussions

3.3.1 Structural Properties

As mentioned in section 1.2, $X_2X'Z$ ternary Heusler compounds crystallise in two prototype structures: the"regular" Heusler or $L2_1$ with the space group $Fm\bar{3}m$ (space group number 225) or, the "inverse" Heusler, with the space group $F\bar{4}3m$ (space group number 216). The structures are schematically shown in Fig 3.1.

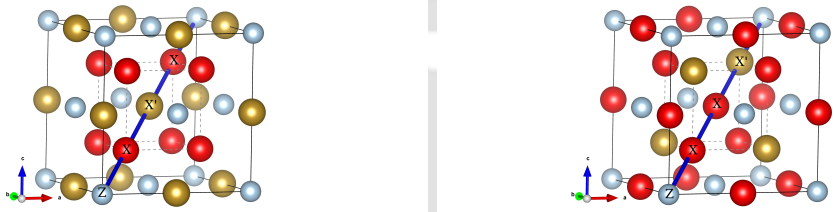

(a) (b)

Figure 3.1: Crystal structure of ternary Heusler compounds $X_2X'Z$ in (**a**) T_I (Heusler *i.e* two X atoms are in symmetric positions) (**b**) T_{II} (Inverse Heusler *i.e* X and X′ are in symmetric positions).

In Table 3.1 we present the structural properties (the crystal structure type and the lattice constant) of the lowest energy Heusler phases, obtained by our calculations, for the compounds considered here. The trends in the structure types can be understood from the following empirical rule based on the electronegativities of the constituents which has been successful in explaining the structural preferences for a number of Heusler intermetallics[101, 116–119, 179–186]: if the main group element is fixed at 4*a* site, the 4*b* site should be occupied by the least electronegative element of the remaining three transition metal atoms [187]. From our results, we find that except Mn_2NbZ, $X_2Mo'Z$ (X = Mn, Fe, Co) and Co_2TcAl this rule explains the structure types for all other compounds. The computed lattice constants agree well with the existing results. In Table 3.2 we have tabulated the available results on lattice constants, structure type, magnetic moments and spin polarization of ternary $X_2Y'Z$ (X = Mn, Fe, Co ; Y′ = Sc to Cu and Z = Al, Si) compounds to compare our findings with Y′ = Y to Ag, keeping X and Z same. In case of lattice constants, we find that the lattice constants of ternary Heuslers are greater when X′ is an element with 4*d* electrons, in comparison to its counterpart with X′ an element with 3*d* electrons located right above the column in periodic table (Table 3.2). This trend can be explained purely on the basis of relative sizes of the atomic radii of the X′

Table 3.1: Calculated lattice constants, formation energies, structure type and magnetic moments of ternary $X_2X'Z$ compounds.

Systems (Type-I)	Lattice constant(Å)	Formation energy(eV)	Structure type	M ($\mu_B/f.u.$)
Mn_2YAl	6.52	-0.74	T_I	5.72
Mn_2ZrAl	6.15	-2.01	T_I	3.00
Mn_2NbAl	6.00 (6.005[174])	-1.56	T_I	2.00 (2.00[174])
Mn_2MoAl	5.90	-1.23	T_I	1.04
Mn_2TcAl	5.95	-1.94	T_{II}	0.04
Mn_2RuAl	5.95	-2.62	T_{II}	1.01
Mn_2RhAl	5.95	-2.08	T_{II}	1.86
Mn_2PdAl	6.05	-1.67	T_{II}	0.86
Mn_2AgAl	6.20	-0.29	T_{II}	0.31
Fe_2YAl	6.25	-0.47	T_I	1.95
Fe_2ZrAl	6.05	-1.96	T_I	0.91
Fe_2NbAl	5.90 (5.909[175])	-1.63	T_I	0.00
Fe_2MoAl	5.85	-0.77	T_I	0.82
Fe_2TcAl	5.85	-1.34	T_{II}	3.29
Fe_2RuAl	5.90	-1.97	T_{II}	5.20
Fe_2RhAl	5.90	-1.58	T_{II}	5.00
Fe_2PdAl	5.95	-1.25	T_{II}	4.84
Fe_2AgAl	6.05	0.25	T_{II}	4.75
Co_2YAl	6.20	-3.21	T_I	0.00
Co_2ZrAl	6.05	-4.32	T_I	1.00
Co_2NbAl	5.95	-3.31	T_I	2.00
Co_2MoAl	5.90	-2.36	T_I	2.84
Co_2TcAl	5.85	-3.14	T_I	3.91
Co_2RuAl	5.85	-3.38	T_{II}	3.87
Co_2RhAl	5.85	-2.84	T_{II}	3.37
Co_2PdAl	5.90	-2.56	T_{II}	3.04
Co_2AgAl	5.97	-1.28	T_{II}	2.77
Mn_2YSi	6.16	-1.01	T_I	3.02
Mn_2ZrSi	6.00 (6.004 [176])	-2.42	T_I	2.00[176]
Mn_2NbSi	5.87	-2.02	T_I	0.99
Mn_2MoSi	5.78	-1.61	T_I	0.00
Mn_2TcSi	5.83	-2.60	T_{II}	1.04
Mn_2RuSi	5.79	-3.10	T_{II}	2.00
Mn_2RhSi	5.81 (5.905 [177])	-2.09	T_{II}	3.00 (3.00 [177])
Mn_2PdSi	5.98	-1.39	T_{II}	0.95
Mn_2AgSi	6.11	0.14	T_{II}	0.59
Fe_2YSi	6.08	-0.87	T_I	0.96
Fe_2ZrSi	5.93 (5.899 [178])	2.55	T_I	0.00
Fe_2NbSi	5.84	-1.58	T_I	0.97
Fe_2MoSi	5.78	-0.71	T_I	1.79
Fe_2TcSi	5.79	-1.88	T_{II}	3.78
Fe_2RuSi	5.78	-2.37	T_{II}	4.69
Fe_2RhSi	5.80	-1.59	T_{II}	4.90
Fe_2PdSi	5.88	-0.91	T_{II}	5.07
Fe_2AgSi	5.97	0.77	T_{II}	4.69
Co_2YSi	6.12	-3.32	T_I	1.00
Co_2ZrSi	5.99	-4.36	T_I	2.00
Co_2NbSi	5.87	-3.01	T_I	1.71
Co_2MoSi	5.78	-2.16	T_{II}	0.01
Co_2TcSi	5.72	-3.22	T_{II}	0.21
Co_2RuSi	5.74	-3.60	T_{II}	3.20
Co_2RhSi	5.76	-2.65	T_{II}	3.27
Co_2PdSi	5.79	-2.14	T_I	2.35
Co_2AgSi	5.83	-1.20	T_I	0.20

component.

In order to first verify whether a compound indeed can be formed, we have calculated the formation energies the following way:

$$E_f = E_{X_2X'Z} - (2E_X + E_{X'} + E_Z)$$

Where $E_{X_2X'Z}$ are the total energies per formula unit of the $X_2X'Z$ and E_X, $E_{X'}$, E_Z, are the total energies of the bulk X, X′ and Z respectively in their ground state structures. The results are tabulated in Table 3.1. Except Fe_2AgAl, Mn_2AgSi and Fe_2AgSi most compounds are likely to form as the formation energies are negative and hence are thermally stable from the point of view of enthalpy. Thus, it is worth investigating further the properties of all these ternary Heusler compounds.

3.3.2 The Magnetic moments and the Slater-Pauling Rule

The necessary condition for a Heusler compound to be half-metal is that the total spin-magnetic moment per formula-unit is an integer and that it follows the Slater-Pauling rule, connecting the magnetic moment to the total number of valance electrons per formula unit [57–60]. In case of half-metallic ternary Heusler compounds $X_2X'Z$, the manifestation of this rule is that the total magnetic moment per formula unit, M and the number of valance electrons per formula unit, N_V are related by $M = |N_V - 18|$ or by $M = |N_V - 24|$ or by $M = |N_V - 28|$, depending on whether X is an early transition metal; or more precisely whether the Fermi-energy is placed in a gap after 9, 12 or 14 electronic states respectively [7, 59]. In Fig 3.2.(a), we have plotted the variations of M with N_V for $X_2X'Al$ (X′ = 4*d*, X = Mn, Fe, Co). Our results show that the moments of $Mn_2X'Z$ compounds follow the $M = |N_V - 24|$ rule with the exceptions of Mn_2YAl, Mn_2PdZ and Mn_2AgZ where the expected moments are smaller than those predicted by the Slater-Pauling rule. However, the moment of Mn_2PdAl lies close to $M = |N_V - 28|$ line. For $Fe_2X'Z$ series we find that for compounds with X′ an element after Mo, the moments of all compounds are much deviated from any of the Slater-Pauling lines. In case of $Co_2X'Al$ series the moments deviate from the line $M = |N_V - 24|$ for late transition metals (X′ = Ru, Rh, Pd, Ag), though Co_2PdAl lies close to $M = |N_V - 28|$ line. For the case of $Co_2X'Si$ series except Co_2YSi and Co_2ZrSi none of the compounds follow the $M = |N_V - 24|$ rule. Co_2MoSi with 28 valance electrons and having total moment zero lies on $M = |N_V - 28|$. Across the six series under investigation there are only two compounds, Mn_2ZrAl and Mn_2YSi having moments in conformation with both

Table 3.2: Lattice constants, structure type, magnetic moments and spin polarization of ternary $X_2Y'Z$ (X = Mn, Fe, Co ; Y = Sc to Cu and Z = Al, Si) compounds. The results are from the Heusler database http://heusleralloys.mint.ua.edu/. The numbers inside parantheses are reported values from other works.

Systems (Type-I)	Lattice constant(Å)	Structure type	M ($\mu_B/f.u.$)	Spin polarization %
Mn_2ScAl	6.16	T_I	4.0054	88.78
Mn_2TiAl	5.95 (5.967,5.920 [188, 189])	T_I	2.9865 (3.05)	75.34 (77)
Mn_2VAl	5.8019 (5.687, 5.875 [190, 191])	T_I	1.9994 (1.93, 1.82)	98.05 (93%)
Mn_2CrAl	5.72 (5.71 [192])	T_I	1.0406 (1.00)	91.76
Mn_2MnAl	5.3644 (5.80, 5.79[29, 193])	DO_{22} (DO_3)	1.7039 (0, 0.017)	55.07
Mn_2FeAl	5.75 (5.781, 5.725[194, 195])	T_{II}	1.0009 (1.00, 1.01)	98.43(100)
Mn_2CoAl	5.7349 (5.798, 5.76[83, 196])	T_{II}	1.9999 (2.00, 2.00)	100
Mn_2NiAl	5.8 (5.636[197])	T_{II}	1.1766	52.14
Mn_2CuAl	5.89 (5.855[198])	T_{II}	0.1841 (0.22)	52.14
Fe_2ScAl	6.02 (6.012[199])	T_I	1.9221 (1.92)	92.85
Fe_2TiAl	5.82 (5.878[200])	T_I	0.9442	88.76
Fe_2VAl	5.6925 (5.7129[114])	T_I	0	0
Fe_2CrAl	5.6599 (5.811[201])	T_I	0.9978	95.02
Fe_2MnAl	5.6711(5.673[194])	T_I	0.0001 (2.00)	0.01
Fe_2FeAl	5.74 (5.74[193])	T_I	5.9605 (5.98)	54
Fe_2CoAl	5.7006 (5.701[70])	T_{II}	4.9991 (5)	58.7
Fe_2NiAl	5.7455 (5.758[202])	T_{II}	4.777 (4.25)	10.33
Fe_2CuAl	-(5.048[202])	- (Regular tetragonal)	-(4.56)	-
Co_2ScAl	5.97 (5.961[203])	T_I	0.0001 (0.00)	0.05
Co_2TiAl	5.83 (5.849[204])	T_I	1.00 (0.75)	60.07
Co_2VAl	5.74 (5.75148, 5.7798[205, 206])	T_I	1.9985 (1.998)	94.88
Co_2CrAl	5.704 (5.73, 5.727[207, 208])	T_I	3.0 (3)	100
Co_2MnAl	5.7 (5.756[209])	T_I	4.0235 (4.01)	59.7
Co_2FeAl	5.7 (5.672[210])	T_I	4.991	74.69
Co_2CoAl	5.68	T_I	4.0336	67.49
Co_2NiAl	5.042	T_{II}	2.8742	72.15
Co_2CuAl	-(5.55[211])	- T_{II}	- (1.14)	-
Mn_2ScSi	5.9449	T_I	2.9809	93.9
Mn_2TiSi	5.77 (5.783[188])	T_I	1.9832	93.46
Mn_2VSi	5.65 (5.560[190])	T_I	0.9657 (0)	73.16
Mn_2CrSi	5.5899 (5.59[192])	T_I	0.0002 (0.00)	0.04
Mn_2MnSi	5.64 (5.65[193])	T_I (DO_3)	1.0071 (1)	95.93
Mn_2FeSi	5.6006 (5.60[195])	T_{II}	2.0077 (2.01)	84.51 (84)
Mn_2CoSi	5.621 (5.65, 5.621[196, 212])	T_{II}	3 (3.00)	100
Mn_2NiSi	5.7 (5.698[213])	T_{II}	1.0712	27.68
Mn_2CuSi	- (5.75[214, 215])	- (T_{II})	- (1.00)	- (100)
Fe_2ScSi	5.85	T_I	0.9336	91.16
Fe_2TiSi	5.685 (5.685[216])	T_I	0	0
Fe_2VSi	5.61 (5.674[217])	T_I	0.8056	81.91
Fe_2CrSi	5.4678	DO_{22} (T_I)	2.0 (1.98)	99.38 (98[218])
Fe_2MnSi	5.5942 (5.6686, 5.664 [219, 220])	T_I	3	100
Fe_2FeSi	5.61 (5.61[193])	T_I	0.8056 (5.01)	44.51
Fe_2CoSi	5.6086 (5.64[221])	T_{II}	4.9626 (4.99)	74.15 (100)
Fe_2NiSi	4.9287 (5.66[222])	DO_{22} (X_a/F-43m)	4.6756 (4.62)	2.56
Fe_2CuSi	-	-	-	-
Co_2ScSi	5.87 (5.8634[223])	T_I	1	100
Co_2TiSi	5.75 (5.733[204])	T_I	2 (1.96)	7.5
Co_2VSi	5.21 (5.6725[205])	DO_{22} (T_I)	0.9313 (3)	51.51
Co_2CrSi	5.6335 (5.699[224])	T_I	4 (4.006)	100
Co_2MnSi	5.6301 (5.654[209])	T_I	5 (5.07)	100
Co_2FeSi	5.628 (5.64[225])	T_I	5.48 (5.97)	72.34
Co_2CoSi	5.07	DO_{22}	2.8601	62.54
Co_2NiSi	5.0307/5.1124	Tetragonal/DO_{22}	2.2607/1.966	49.49/51.5
Co_2CuSi	5.02	Tetragonal	2.2312	59.15

$M = |N_V - 18|$ and $M = |N_V - 24|$ rules. In principle these system can have gaps after both 9 states and 12 states [212].

Fig 3.2 and Table 3.1 demonstrate that there are quite a few compounds with integer or close to integer moments following Slater-Pauling rule. These are the potential half-metals whose electronic structures need to be examined carefully before coming to any conclusion. In the next sub-section we discuss in detail the electronic structures of compounds in each series and try to understand the origin of half-metallicity in compounds with $4d$ elements.

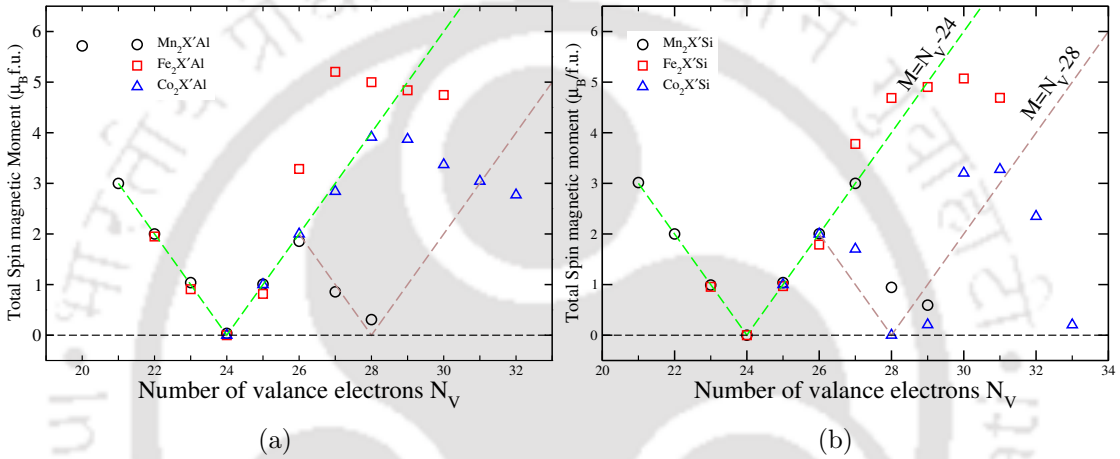

Figure 3.2: Total magnetic moments versus the total number of valence electrons N_V for (**a**) $X_2X'Al$ and (**b**) $X_2X'Si$ compounds respectively. The Slater-Pauling $M = |N_V - 24|$ and $M = |N_V - 28|$ lines are drawn as a guide to understand whether the compounds follow Slater-Pauling rule.

3.3.3 Electronic Structure

The origin of the half-metallic gap and the conformation to the Slater-Pauling rule by magnetic Heusler and inverse Heusler compounds can be understood from their electronic structures near the Fermi level by addressing the hybridizations between the constituents of the compounds [7, 59, 61]. In a ternary Heusler compound $X_2X'Z$, the *sp*-element Z provides 4 low lying (below d bands) states-one s and three p- in each spin channel. These $s-p$ bands lie well below the Fermi-energy, accommodate charges from the atoms with d electrons and stabilize the structure[5]. The d-orbitals of transition-metal atoms hybridize the following way: first the atoms on symmetric sites ($8c$ in the space group 225, $4c$ and $4d$ in space group-216) hybridize creating (i) 5 bonding d-hybrids (2 doubly-degenerate e_g and 3 triply degenerate t_{2g} hybrid orbitals) (ii) five non bonding hybrid d-orbitals (2 doubly-degenerate e_u and 3

triply degenerate t_{1u} hybrid orbitals)(Fig. 1.4(a) in chapter 1). The bonding e_g and t_{2g} orbitals, having tetrahedral symmetry, can only hybridize with *d*-orbitals of the remaining transition metal atom. Thus, ultimately we are left with five bonding and five anti-bonding states which are non-transforming with the *u* representation[7, 64] and can not couple with *d*-orbitals of the remaining transition atom (Fig. 1.4(b) in chapter 1).

In case of a half-metal there is an energy gap in one spin-channel, where the Fermi-energy is pinned in. The position of the Fermi-level in a spin-channel where the half-metallic gap is situated, determines which Slater-Pauling rule the material follows as the number of states in that particular spin-channel below the Fermi-level is always fixed and any extra electron would be placed in unoccupied states of other spin-channel. In this work we use the convention that if $N_V > 24$, the spin channel where the half-metallic gap is, will be considered the minority spin channel. Accordingly, from Fig. 1.4 in chapter 1 it is clear that position of E_F in the minority spin-channel would lead to the half-metals following different Slater-Pauling rules. If E_F is situated between t_{1u} and t_{2g} states, it would follow $M = |N_V - 18|$ rule. If the position of Fermi-energy is between t_{1u} and e_u states, the compound would follow $M = |N_V - 24|$ rule. Simple difference in electron count in both spin-channel leads us to this conclusion.

In Figs. 3.3 - 3.8 we present the spin-polarized total and atom projected densities of states of all $X_2X'Z$ compounds considered in this work in their respective ground state structures. The X atoms occupying the position (0, 0, 0) are denoted as X_I while the X atoms occupying the other positions are denoted as X_{II} throughout. In the following we discuss them series-wise. Selected band structures of the interesting compounds along the high symmetry directions in Brillouin zone are presented in Fig. 3.9 - Fig. 3.17.

3.3.3.1 $Mn_2X'Z$ compounds

The densities of states for compounds of $Mn_2X'Al$ ($Mn_2X'Si$) series with T_I and T_{II} structures are shown, respectively, In Fig 3.3.(a) and Fig 3.4.(a) (Fig 3.3.(b) and Fig 3.4.(b)). We find several features common to either the compounds with same structure type or even across the structure types: (a) for compounds in T_I structure and with possible half-metallic gaps, the gaps are flanked by Mn *d*-states, while for compounds in T_{II} structure, the contributions from Mn and X′ are significant; both consistent with the generalised hybridization picture described in chapter 1, (b) across the structures, as the atomic number increases, the contributions from X′

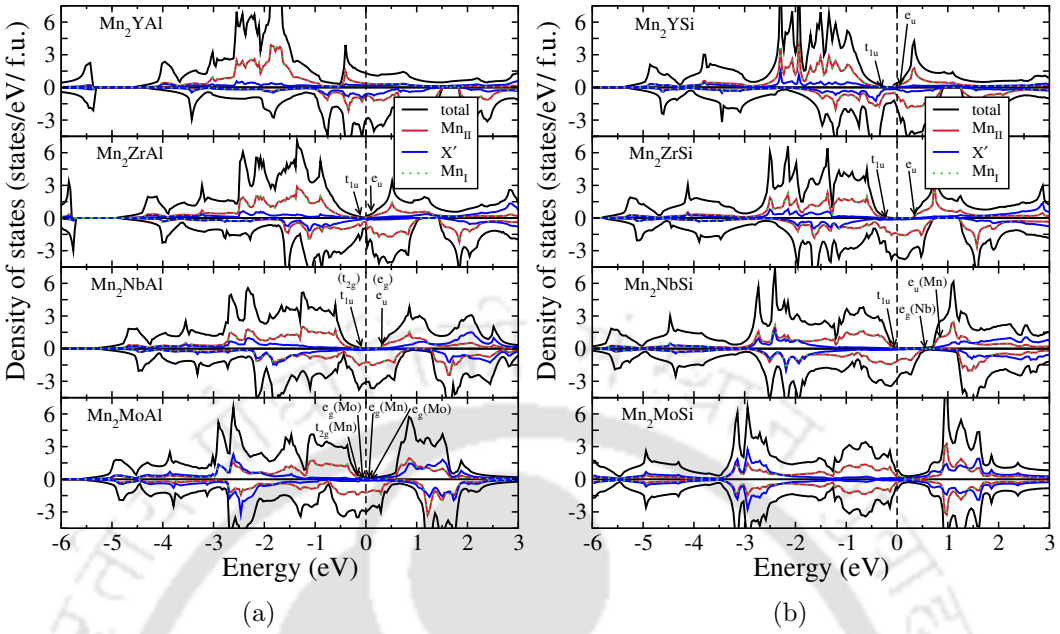

Figure 3.3: Spin polarized total and atom-projected densities of states for (**a**) $Mn_2X'Al$ and (**b**) $Mn_2X'Si$ (X′= Y, Zr, Nb, Mo) compounds. The ground states of these compounds are Type-I.

move gradually towards lower energies, (c) as long as structure types are same, the features in the densities of states of compounds from the two different series are very similar when N_V are same. This is reflected more in compounds with structure T_I. For example, Mn_2NbAl and Mn_2ZrSi both are half-metallic with N_V=22. Mn_2ZrAl and Mn_2YSi, Mn_2MoAl and Mn_2NbSi too have similar features in their densities of states. On the other hand, Mn_2MoSi and Mn_2TcAl, both are with N_V=24, yet have completely different features in their densities of states as the ground state structures are different.

In order to identify half-metals and understand their origin as N_V changes continuously, we now focus on the densities of states of the compounds in the two series systematically. We find that for compounds crystallising in T_I the origin of the gap in majority spin channel is due to the splitting of non-bonding t_{1u} and e_u states arising out of hybridizations between the Mn atoms. For Mn_2ZrAl and Mn_2YSi the separation between t_{1u} and e_u states are not enough to extend the gap cutting through the Fermi-level to make these compounds half-metallic. In Fig. 3.9, we present the spin-resolved band structure of Mn_2ZrAl. Although it has an integer magnetic moment of 3 μ_B per formula unit, the minority spin band structure shows that at the X point of the Brillouin zone, the top of the valence band

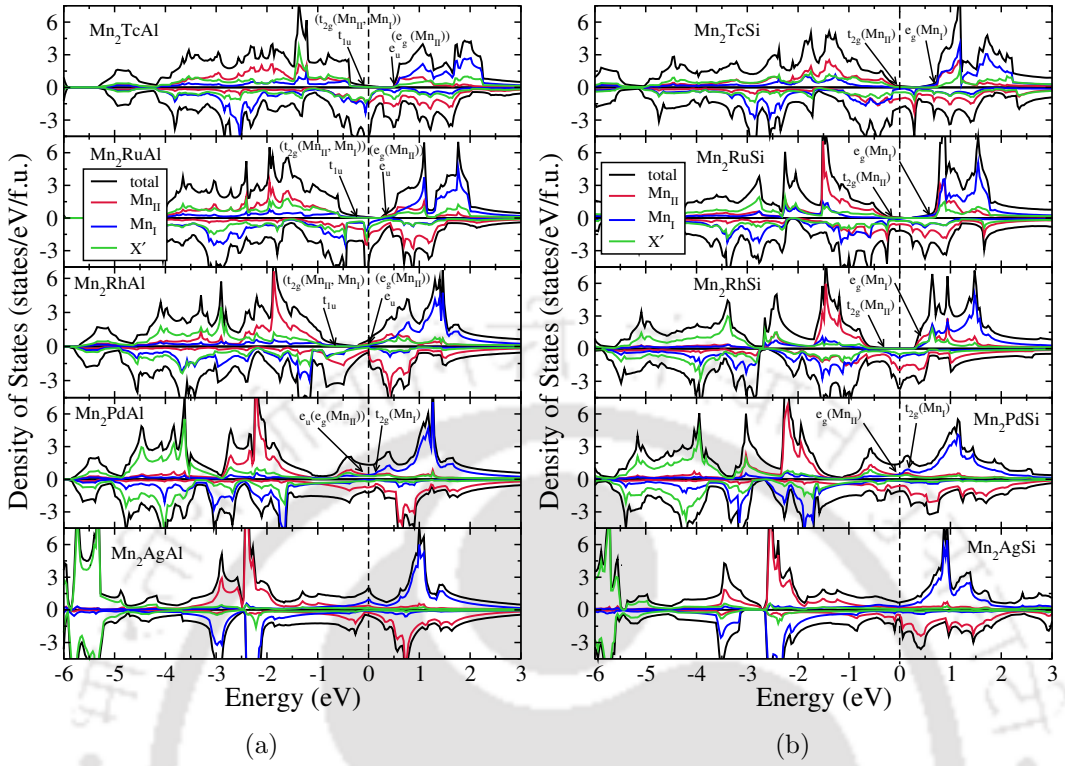

Figure 3.4: Spin polarized total and atom-projected densities of states for (**a**) $Mn_2X'Al$ and (**b**) $Mn_2X'Si$ (X′= Y, Zr, Nb, Mo) compounds. The ground states of these compounds are Type-II.

crosses the Fermi level, leading to a spin polarization of 74% and renders the system a normal metal. Thus, in spite of their magnetic moments being integer or near integer, these compounds are not half-metals. As we go from $Mn_2ZrAl(Mn_2YSi)$ to $Mn_2NbAl(Mn_2ZrSi)$, the extra electron is accommodated in one of the three t_{1u} states in the majority band opening a half-metallic gap. This is also reflected in the spin-resolved band structures of these compounds as shown in Fig. 3.10 and Fig. 3.12. The spin down band structures of $Mn_2NbAl(Mn_2ZrSi)$ clearly show a separation between the valence and the conduction bands with Fermi level falling in the gap. The spin up band structure on the other hand demonstrates a metallic character. Thus these materials are half-metals. In Mn_2MoAl (Mn_2NbSi) the extra electron is accommodated in one of the vacant t_{1u} or in the e_g states in the majority bands, thus producing high spin polarization but destroying the half-metallicity as these states cut through the Fermi levels. Once again, in spite of having near integer moments, these two compounds at best can be considered near half-metals with Mn_2NbSi having a spin polarization over 90%. Mn_2MoSi, with N_V=24, has same occupancy in both spin bands leading to zero magnetic moment, in conformation

with the Slater-Pauling rule. However, in spite of Mn_2TcAl having N_V=24 too, the electronic structure is different from that of Mn_2MoSi as the former crystallises in T_{II} structure. Though the moment is nearly zero in Mn_2TcAl (like Mn_2MoSi) it has a large spin polarization of 94%. This is because unlike Mn_2MoSi, it has a near half-metallic gap in the majority spin band arising out of the separation of bonding t_{2g} and non-bonding e_u states across the Fermi level. This, in fact, is part of the general features observed in the electronic structure of the compounds with T_{II} structure. In case of these compounds the bonding t_{2g} hybrid orbitals, originating from all the transition metal atoms and the non-bonding t_{1u} hybrids due to Mn and X′ atoms lie extremely close; same happens for anti-bonding e_g and non-bonding e_u states. Throughout the $Mn_2X'Z$ series with T_{II} structure, we find that the position of the gap and spin polarization is determined by this. As exemplary cases we have shown the spin-resolved band structures of Mn_2RuAl and Mn_2RhSi in figures 3.11 and 3.13. The band structure of Mn_2RuAl (Fig. 3.11) for the down spin shows that at Γ point the top of the valence band protrudes into the unoccupied part of the spectrum. Thus the material is near half-metal as can be understood also from the near zero densities of states at the Fermi level. Mn_2RhSi is the only half-metallic compound in $Mn_2Y'Z$ series, crystallising in the inverse Heusler structure. The semiconducting gap in one of the spin channels of the band structure of Mn_2RhSi is clearly seen in Fig. 3.13.

Thus, in $Mn_2X'Z$ series we found three true half-metals (Mn_2NbAl, Mn_2ZrSi and Mn_2RhSi), four near half-metals *i.e.* materials with high spin polarization (greater than 90%) (Mn_2TcAl, Mn_2RuAl, Mn_2NbSi, Mn_2RuSi). Out of the three true half-metals, Mn_2RhSi has also been found to be a potential thermoelectric material [177]. On the other hand, near half-metal Mn_2TcAl with it's high spin polarization and near zero magnetic moment is a potential compensated ferrimagnet. It may be noted that Mn_3Al in DO_3 structure is a well known compensated ferrimagnet [29] and that Mn_2TcAl is isoelectronic to it (derived by replacing one Mn with Tc), implying that the physical properties of magnetic Heusler compounds obtained by replacing one $3d$ element with a $4d$ may depend solely on N_V. We find a signature of this when we compare Mn_2YAl and Mn_2ScAl. Our calculations show that Mn_2YAl is not a half-metal at all, neither does it have a significant spin polarization. However, it has exceptionally large magnetic moment exactly like Mn_2ScAl, which is isoelectronic.

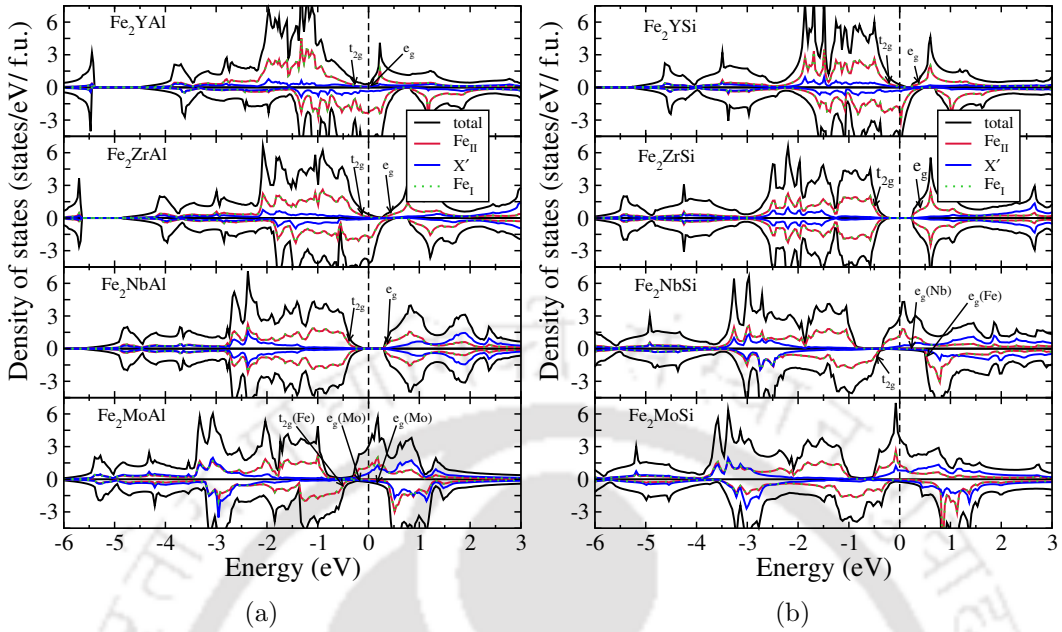

Figure 3.5: Spin polarized total and atom-projected densities of states for (**a**) $Fe_2X'Al$ and (**b**) $Fe_2X'Si$ (X′= Y, Zr, Nb, Mo) compounds. The ground states of these compounds are Type-I.

3.3.3.2 $Fe_2X'Z$ compounds

Atom and spin resolved densities of states of $Fe_2X'Z$ series are presented in the Fig 3.5 and Fig 3.6. Fig 3.5.(a) and Fig 3.5.(b) (Fig 3.6.(a) and Fig 3.6.(b)) are the densities of states for compounds with structure type T_I(T_{II}). We find substantial similarities between $Fe_2X'Z$ and $Mn_2X'Z$ as far as some of the general features in the electronic structures are concerned. Like in $Mn_2X'Z$ series, the main contributions to densities of states for compounds in $Fe_2X'Z$ near Fermi levels come from the Fe atoms in case of compounds with structure T_I whereas in case of compounds with T_{II} structure, the main contributions come from the tetrahedrally co-ordinated Fe and X′ atoms. We also find that with increasing atomic number the X′ *d*- states lie deeper into the valence band, a feature similar to the $Mn_2X'Z$ series. The major difference, however, between the compounds in two series, is that none of the 18 compounds in $Fe_2X'Z$ series is found to be half-metallic. This difference originates from the fact that the Fe states are more delocalised as compared to Mn states. As a result, often the Fe states or the ones with hybridizations with Fe atoms, extend into the unoccupied part, leaving no possibility of opening up of a half-metallic gap. However, in almost all compounds, there is either a pseudo gap in the occupied part of one spin channel and a gap like valley cutting through the Fermi level in the

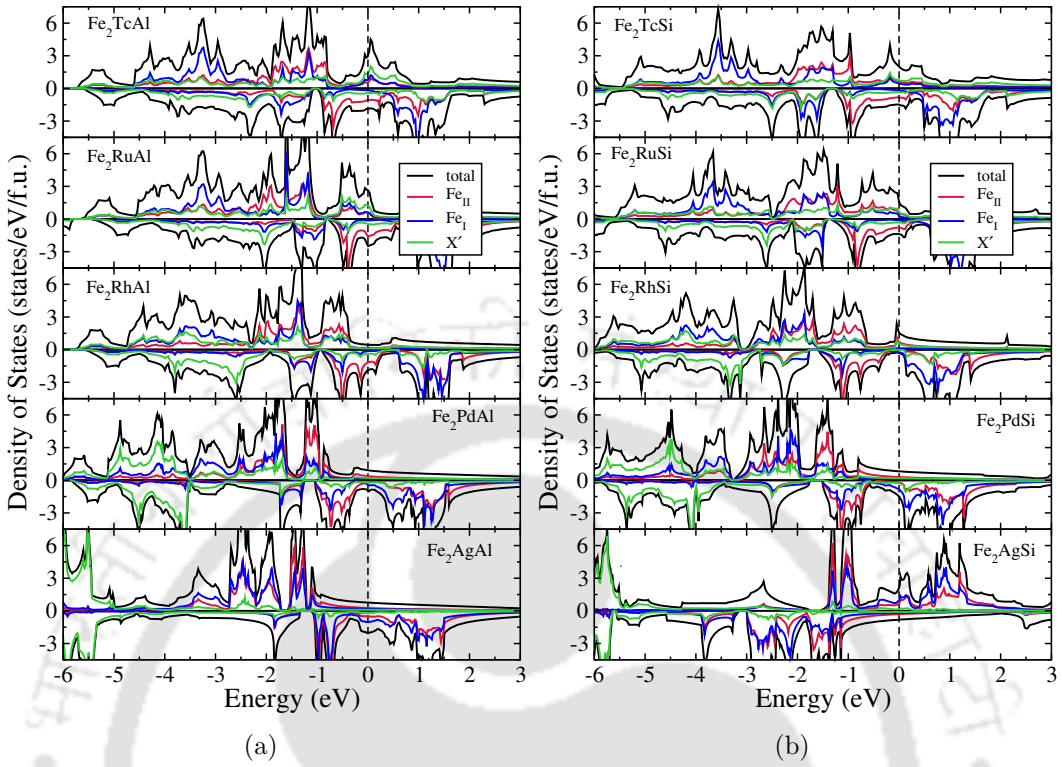

Figure 3.6: Spin polarized total and atom-projected densities of states for (**a**) $Fe_2X'Al$ and (**b**) $Fe_2X'Si$ (X′= Y, Zr, Nb, Mo) compounds. The ground states of these compounds are Type-II.

other. The trends in the features of the electronic structures as one goes through the compounds in a series and with a given crystal structure, are same across the Al and Si series. The electronic structures are very similar if N_V is same. For compounds with structure type T_I, the electronic structure near the Fermi level is contributed mostly by the t_{2g} and e_g Fe states in occupied and unoccupied parts respectively. We find the only near half-metal in Fe-series compounds to be Fe_2NbSi with spin polarization 95% crystallising in T_I structure. The compound right before Fe_2NbSi in the series is Fe_2ZrSi which has 24 valence electrons and turns out to be a non-magnetic semiconductor. It is interesting to note that unlike $Mn_2X'Z$, the changes in the electronic structure of $Fe_2X'Z$ compounds, when N_V changes from 23 to 24 are drastic. In the Mn-series, the changes in electronic structures between Mn_2NbAl (N_V=23) and Mn_2MoAl (N_V=24) bore a continuity while the changes from Fe_2ZrAl (Fe_2YSi) to Fe_2NbAl (Fe_2ZrSi) are sharp and substantial. The changes from Fe_2NbAl (Fe_2ZrSi) to Fe_2MoAl (Fe_2NbSi) again are systematic, following a trend. The extra electron in Fe_2MoAl (in comparison to Fe_2ZrAl) is accommodated in the spin-up band, which reflects in a pseudo gap inside the occupied part of spin

up channel. The semiconducting gap of Fe_2NbAl in the spin down channel would have been intact if the hybridizations near the Fermi level wouldn't have changed upon replacement of Nb with Mo. The hybridizations of Mo and Fe states near the Fermi level produce a valley cutting through the Fermi level, reducing the magnetic moment significantly from the Slater-Pauling predicted value, bringing down the spin polarization as well. The semiconducting gap of spin down channel in Fe_2ZrSi nearly survives in Fe_2NbSi as the Nb e_g and Fe t_{2g} hybridizations near Fermi level are weak as compared to Fe_2MoAl. For the compounds with structure type T_{II}, the proximity of *d* states of Fe and X′ mix the states substantially in both spin channels, leaving little possibility of a semiconducting gap in any of the spin channels.

3.3.3.3 $Co_2X'Z$ compounds

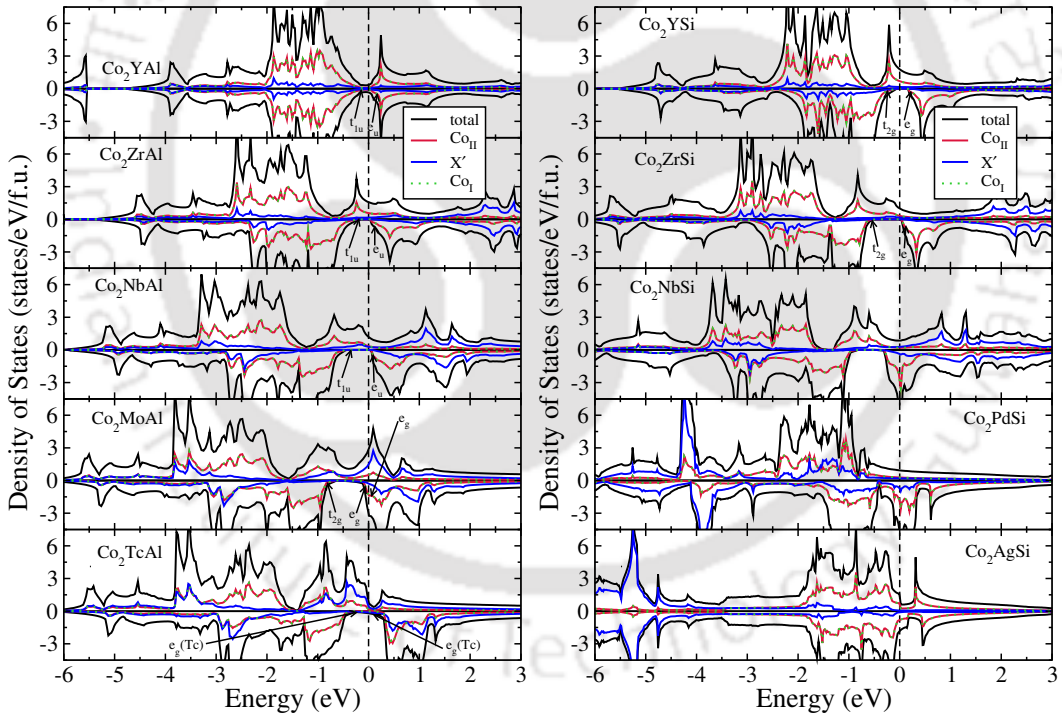

Figure 3.7: Spin polarized total and atom-projected densities of states for (**a**) $Co_2X'Al$ and (**b**) $Co_2X'Si$ (X′= Y, Zr, Nb, Mo) compounds. The ground states of these compounds are Type-I.

In Figs 3.7 - 3.8 we show the total and partial densities of states of $Co_2X'Z$ compounds. Like observed in cases of Mn_2 and Fe_2 based compounds, the Co_2 based compounds with structure T_I have Co states dominating the features near the half-

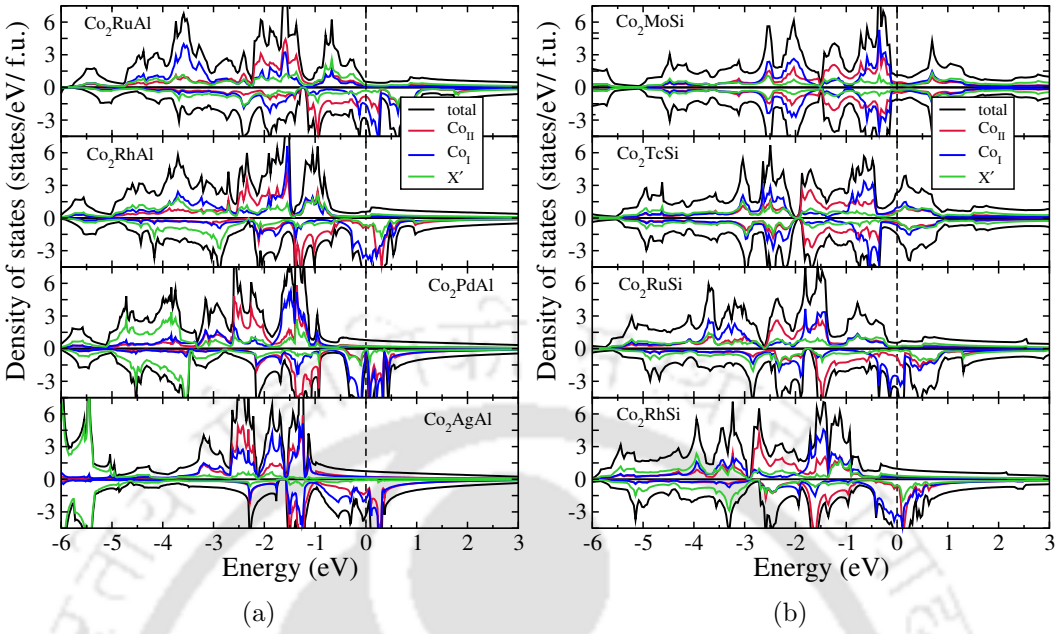

Figure 3.8: Spin polarized total and atom-projected densities of states for (**a**) $Co_2X'Al$ and (**b**) $Co_2X'Si$ (X′= Y, Zr, Nb, Mo) compounds. The ground states of these compounds are Type-II.

metallic gaps for half-metals. We find more half-metals with 100% spin polarizations among $Co_2X'Z$ compounds in comparison to compounds in other two series. All the half-metals in Co_2-compounds are with T_I structure, arising because of the Co states, localised more in comparison to Mn or Fe in Mn_2 and Fe_2 based compounds respectively. This feature is also seen in the more familiar $Co_2X'Z$ compounds with X′ a $3d$ element [7, 226, 227]. The Co-based compounds studied in the present work have N_V greater than or equal to 24. Thus the half-metallic gaps are found in the spin down channels. In Fig 3.7.(a) and Fig 3.7.(b) we see that the main contributions to densities of states comes from Co-t_{2g} or Co-t_{1u} below the Fermi-level and from Co-e_g or Co-e_u above the Fermi-level in both $Co_2X'Al$ and $Co_2X'Si$ series. Co_2YAl, having $N_V = 24$, is a non-magnetic compound where each spin band has exactly 12 electrons. In Co_2ZrAl -Co_2NbAl (Co_2YSi-Co_2ZrSi) minority spin channel have 12 electrons and the extra electrons are fully accommodated in the majority spin channel opening the gap in minority spin channel. In Figs. 3.14- 3.17, we show the electronic structures of the Co_2 based half-metals identified in this study. The band structures in all these cases clearly show a semiconducting gap in the minority spin channels.

In Co_2MoAl (Co_2NbSi) the extra electron is not fully accommodated in the

next e_g band in spin up channel, instead it is shared by both the spin channels, thus destroying the half-metallicity. In Co_2TcAl the extra electron, as expected, is not placed totally in the anti-bonding e_g states in spin up channel and there is considerable mixing of Co and Tc e_g states near Fermi level leaving little chance of half-metallicity. Co_2PdSi and Co_2AgSi, the other two compounds with T_I structure have different hybridization pattern where delocalised Pd and Ag states hybridize considerably with Co states near Fermi level, leading them to behave like normal metals.

The compounds with T_{II} structures have significant hybridizations between Co and X′ states in both spin channels and thus there is no possible half-metals with this crystal structure. Like the Mn_2 and Fe_2 series, this is an artefact of the atomic arrangement in T_{II} structure. Thus, in $Co_2X'Z$ series we find four half-metals, Co_2ZrAl, Co_2NbAl, Co_2ZrSi and Co_2NbSi, having 100% spin polarization.

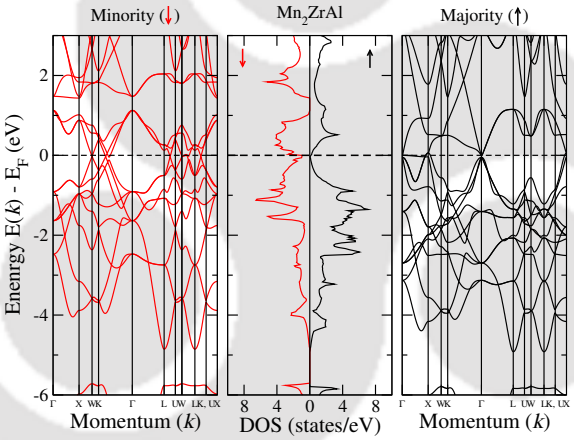

Figure 3.9: Spin-resolved band structure and density of states for Mn_2ZrAl

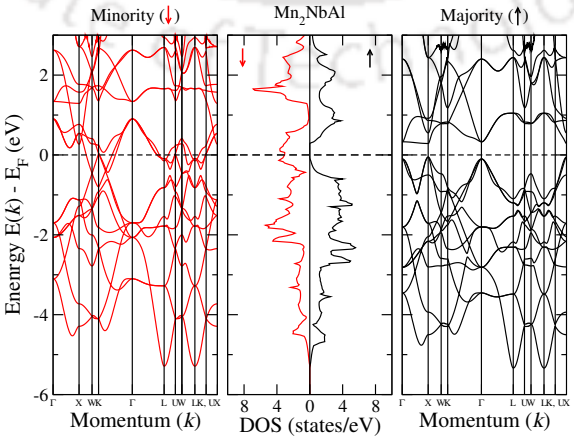

Figure 3.10: Spin-resolved band structure and density of states for Mn_2NbAl

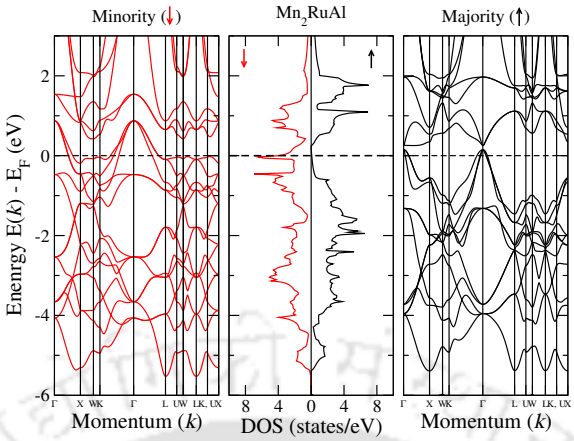

Figure 3.11: Spin-resolved band structure and density of states for Mn_2RuAl

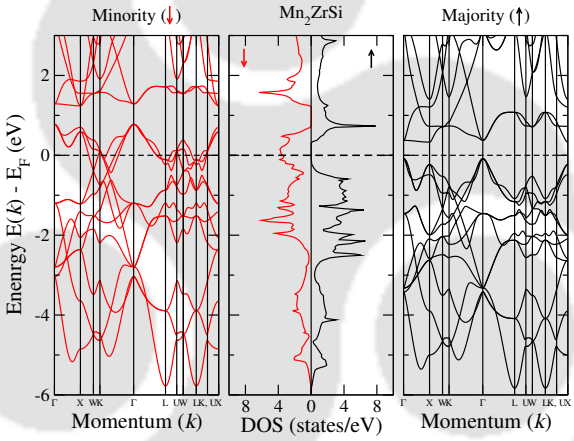

Figure 3.12: Spin-resolved band structure and density of states for Mn_2ZrSi

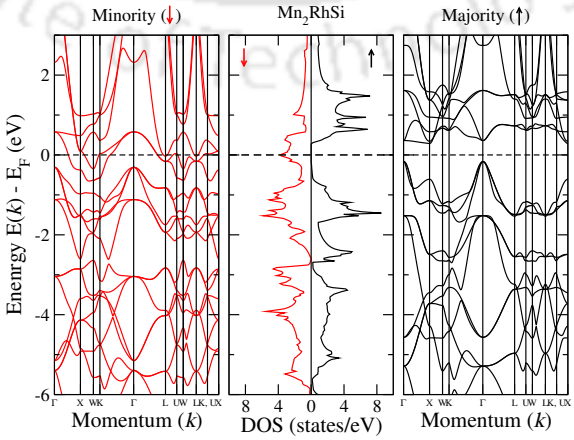

Figure 3.13: Spin-resolved band structure and density of states for Mn_2RhSi

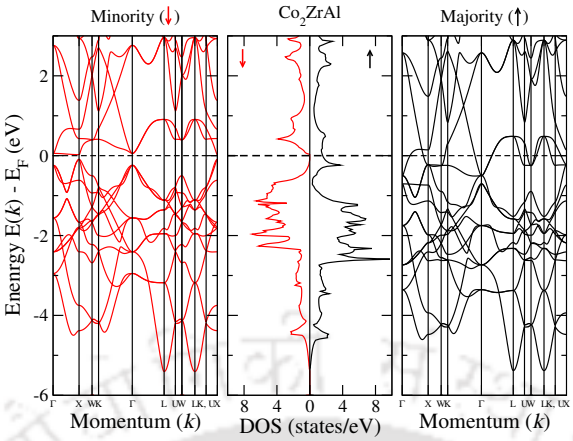

Figure 3.14: Spin-resolved band structure and density of states for Co_2ZrAl

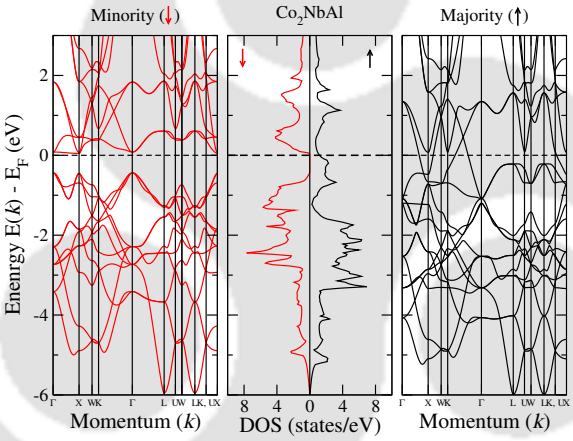

Figure 3.15: Spin-resolved band structure and density of states for Co_2NbAl

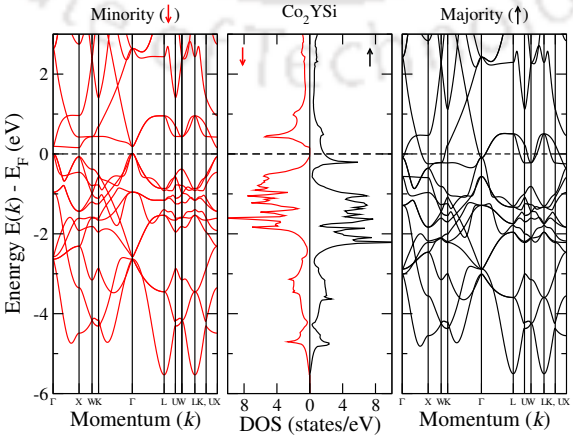

Figure 3.16: Spin-resolved band structure and density of states for Co_2YSi

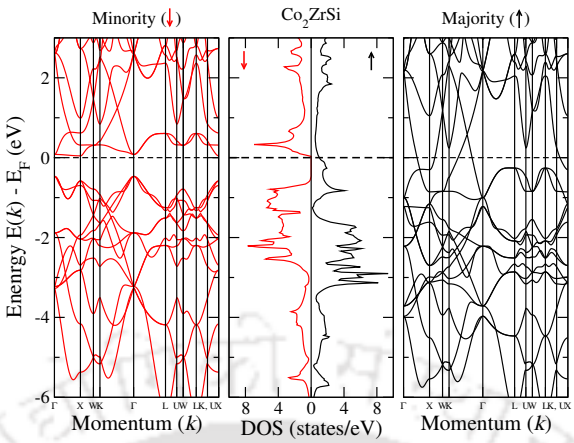

Figure 3.17: Spin-resolved band structure and density of states for Co_2ZrSi

3.3.4 Trends in the local magnetic moments

In Tables 3.3 to 3.8 we present the total and site projected magnetic moments along with the spin polarizations for all the compounds considered here. We try to understand the magnetic structures, the contributions of each transition metal atom towards the total moments, and the trends in variations of the atomic moments across series and structures. We also intend to relate such trends with the trends in the electronic structures discussed in previous sub-section.

The $3d$ elements contribute most towards the magnetic structure and the overall magnetisation in all the compounds studied here. This is a reflection of the facts that the electronic structures of these compounds evolve around the electronic structures of the $3d$ constituents throughout the series. For compounds with structure type T_I we find that the moments of the $3d$ constituents are very close across the corresponding Al and Si series, the only exceptions being Co_2MoAl and Co_2NbSi. For compounds with structure type T_{II}, there is no such trend. For Mn_2-compounds, Mn moments differ substantially between the compounds in Al series and those in Si series. The moments of Mn_I, the Mn atoms at the 4c sites, are considerably reduced in the compounds of Si series, as compared to those in the Al series. The trend is not so in cases of the Fe- and Co-series, except few cases like Fe_2RuAl-Fe_2TcSi and Co_2RuAl-Co_2TcSi pairs.

The moments of Mn atoms in both $Mn_2X'Al$ and $Mn_2X'Si$ series decrease with N_V for compounds with structure type T_I. The opening of the gap in the spin up band and subsequent increase in the electrons in the spin down band, as explained in the previous sub-section, is responsible for such trend. For compounds with structure type T_{II}, the two Mn atoms are ferrimagnetically coupled due to they

Table 3.3: Total and atomic magnetic moment of $Mn_2X'Al$ systems in $\mu_B/f.u.$. N_V is the number of valence electron of the systems. M is the total moment and M_i is the moment of constituent i. P is the spin polarization.

Systems(T_I)	N_V	M	M_{Mn_I}	$M_{Mn_{II}}$	$M_{X'}$	M_{Al}	P(%)
Mn_2YAl	20	5.72	2.99	2.99	-0.13	-0.07	39
Mn_2ZrAl	21	3.00	1.73	1.73	-0.34	-0.05	74
Mn_2NbAl	22	2.00	1.21	1.21	-0.36	-0.03	100
Mn_2MoAl	23	1.04	0.68	0.68	-0.31	-0.01	88
Systems(T_{II})	N_V	M	M_{Mn_I}	$M_{X'}$	$M_{Mn_{II}}$	M_{Al}	P(%)
Mn_2TcAl	24	0.04	-2.35	-0.37	2.75	0.03	94
Mn_2RuAl	25	1.01	-2.18	0.06	3.07	0.02	96
Mn_2RhAl	26	1.86	-1.84	0.34	3.26	0.01	6
Mn_2PdAl	27	0.86	-2.80	0.13	3.45	0.01	4
Mn_2AgAl	28	0.31	-3.12	0.03	3.40	0.01	59

Table 3.4: Total and atomic magnetic moment of $Mn_2X'Si$ systems in $\mu_B/f.u.$. N_V is the number of valence electron of the systems. M is the total moment and M_i is the moment of constituent i. P is the spin polarization.

Systems(T_I)	N_V	M	M_{Mn_I}	$M_{Mn_{II}}$	$M_{X'}$	M_{Si}	P(%)
Mn_2YSi	21	3.02	1.64	1.64	-0.10	-0.07	66
Mn_2ZrSi	22	2.00	1.12	1.12	-0.20	-0.04	100
Mn_2NbSi	23	0.99	0.59	0.59	-0.17	-0.02	93
Mn_2MoSi	24	-0.00	-0.00	-0.00	0.00	0.00	0
Systems(T_{II})	N_V	M	M_{Mn_I}	$M_{X'}$	$M_{Mn_{II}}$	M_{Si}	P(%)
Mn_2TcSi	25	1.04	-1.38	-0.30	2.63	0.05	87
Mn_2RuSi	26	2.00	-0.85	0.07	2.70	0.03	91
Mn_2RhSi	27	3.00	-0.44	0.30	3.04	0.02	100
Mn_2PdSi	28	0.95	-2.59	0.08	3.37	0.04	13
Mn_2AgSi	29	0.59	-2.88	0.02	3.39	0.04	15

Table 3.5: Total and atomic magnetic moment of $Fe_2X'Al$ systems in $\mu_B/f.u.$. N_V is the number of valence electron of the systems. M is the total moment and M_i is the moment of constituent i. P is the spin polarization.

Systems(T_I)	N_V	M	M_{Fe_I}	$M_{Fe_{II}}$	$M_{X'}$	M_{Al}	P(%)
Fe_2YAl	22	1.95	1.17	1.17	-0.18	-0.04	89
Fe_2ZrAl	23	0.91	0.54	0.54	-0.12	-0.01	85
Fe_2NbAl	24	0.00	0.00	0.00	0.00	0.00	0
Fe_2MoAl	25	0.82	0.48	0.48	-0.07	-0.01	84
Systems(T_{II})	N_V	M	M_{Fe_I}	$M_{X'}$	$M_{Fe_{II}}$	M_{Al}	P(%)
Fe_2TcAl	26	3.29	1.51	-0.26	2.06	-0.01	22
Fe_2RuAl	27	5.20	2.23	0.49	2.59	-0.03	2
Fe_2RhAl	28	5.00	1.98	0.39	2.77	-0.04	62
Fe_2PdAl	29	4.84	2.00	0.14	2.78	-0.04	1
Fe_2AgAl	30	4.75	2.19	-0.00	2.63	-0.04	44

being nearest neighbours. We find that in both Al- and Si-series, the moment of Mn_{II}, the Mn atom at the 4a sites, is much robust and increases gradually with N_V. This is because of the fact that the Mn_{II} spin up band is nearly full with a near gap close to the Fermi level while the spin down band gradually becomes empty. The Mn_I atom, on the other hand, hybridizes well with X′ as they occupy symmetric positions and thus loses the robustness in it's moment. The re-distributions of states among the spin bands due to the hybridizations of Mn and X′ *d*-orbitals are more prominent in the compounds of the Si-series which is responsible for the substantial reductions in the Mn_I moments.

The drastic changes in the electronic structures of Fe_2-compounds crystallising in T_I structure when N_V is equal to or greater than 24 reflect in the Fe moments. The Fe moment decreases significantly from Fe_2YAl to Fe_2ZrAl. The extra electron in Fe_2ZrAl occupies the spin down band of Fe reducing the moment. The moment starts to pick up after N_V is beyond 24. The extra electron now starts to occupy the Fe spin up band primarily. This explains the trends in the $Fe_2X'Si$ compounds. Like observed in the Mn-series, Fe_{II} moment in compounds with structure type T_{II} is robust. Although the magnetic interaction between Fe atoms is ferromagnetic, substantial states in Fe_I close to Fermi level , an artefact of hybridizations with X′, reduces it's moment in comparison to Fe_{II}.

In contrast, Co moment in $Co_2X'Z$ compounds with structure type T_I increases with N_V, the only exception being Co_2NbSi where the Co moment decreases in comparison to that in Co_2ZrSi. The electronic structures provide clue to this trend.

Table 3.6: Total and atomic magnetic moment of $Fe_2X'Si$ systems in $\mu_B/f.u.$. N_V is the number of valence electron of the systems. M is the total moment and M_i is the moment of constituent i. P is the spin polarization.

Systems(T_I)	N_V	M	M_{Fe_I}	$M_{Fe_{II}}$	$M_{X'}$	M_{Si}	P(%)
Fe_2YSi	23	0.96	0.54	0.53	-0.05	-0.02	89
Fe_2ZrSi	24	0.00	0.00	0.00	-0.00	-0.00	0
Fe_2NbSi	25	0.97	0.60	0.60	-0.14	-0.01	95
Fe_2MoSi	26	1.79	0.96	0.96	-0.05	-0.01	88
Systems(T_{II})	N_V	M	M_{Fe_I}	$M_{X'}$	$M_{Fe_{II}}$	M_{Si}	P(%)
Fe_2TcSi	27	3.78	1.37	-0.05	2.43	0.01	16
Fe_2RuSi	28	4.69	1.65	0.34	2.74	-0.02	8
Fe_2RhSi	29	4.90	1.72	0.38	2.85	-0.03	71
Fe_2PdSi	30	5.07	2.08	0.18	2.79	-0.02	31
Fe_2AgSi	31	4.69	2.07	0.00	2.62	-0.02	46

Table 3.7: Total and atomic magnetic moment of $Co_2X'Al$ systems in $\mu_B/f.u.$. N_V is the number of valence electron of the systems. M is the total moment and M_i is the moment of constituent i. P is the spin polarization.

Systems(T_I)	N_V	M	M_{Co_I}	$M_{Co_{II}}$	$M_{X'}$	M_{Al}	P(%)
Co_2YAl	24	0.00	0.00	0.00	0.00	0.00	0
Co_2ZrAl	25	1.00	0.59	0.59	-0.10	-0.00	100
Co_2NbAl	26	2.00	1.02	1.02	0.01	0.00	100
Co_2MoAl	27	2.84	1.19	1.19	0.47	-0.01	4
Co_2TcAl	28	3.91	1.36	1.36	1.25	-0.03	56
Systems(T_{II})	N_V	M	M_{Co_I}	$M_{X'}$	$M_{Co_{II}}$	M_{Al}	P(%)
Co_2RuAl	29	3.87	1.32	0.70	1.94	-0.01	69
Co_2RhAl	30	3.37	1.31	0.39	1.80	-0.02	79
Co_2PdAl	31	3.04	1.46	0.04	1.63	-0.01	54
Co_2AgAl	32	2.77	1.34	-0.02	1.56	-0.02	64

Table 3.8: Total and atomic magnetic moment of $Co_2X'Al$ systems in $\mu_B/f.u.$. N_V is the number of valence electron of the systems. M is the total moment and M_i is the moment of constituent i. P is the spin polarization.

Systems(T_I)	N_V	M	M_{Co_I}	$M_{Co_{II}}$	$M_{X'}$	M_{Si}	P(%)
Co_2YSi	25	1.00	0.58	0.58	-0.12	0.01	100
Co_2ZrSi	26	2.00	1.04	1.04	-0.07	0.04	100
Co_2NbSi	27	1.71	0.83	0.83	0.04	0.03	72
Systems(T_{II})	N_V	M	M_{Co_I}	$M_{X'}$	$M_{Co_{II}}$	M_{Si}	P(%)
Co_2MoSi	28	0.01	0.02	-0.00	-0.01	-0.00	0
Co_2TcSi	29	0.21	0.04	0.02	0.14	0.00	22
Co_2RuSi	30	3.20	1.12	0.48	1.67	-0.01	74
Co_2RhSi	31	3.27	1.34	0.44	1.56	-0.01	65
Systems(T_I)	N_V	M	M_{Co_I}	$M_{Co_{II}}$	$M_{X'}$	M_{Si}	P(%)
Co_2PdSi	32	2.35	1.17	1.17	0.11	-0.04	69
Co_2AgSi	33	0.20	0.12	0.12	-0.01	-0.01	18

As the extra electrons available with increasing N_V are gradually accommodated primarily in the spin up bands, the moment increases. In case of Co_2NbSi, the extra electron available with respect to Co_2ZrSi is shared between both spin bands, thus departing from the general trend. Same trend is seen Co_{II} moment in compounds with structure type T_{II}. The Co_I moments, though reduced in comparison to those of Co_{II}, the reduction is less substantial in comparison to Mn_2- and Fe_2-compounds. The extra electron available as N_V increases is accommodated primarily in the spin down band, reducing the moment of Co_{II}. The moment of Co_I, on the other hand, hardly changes from compound to compound.

In all the compounds, the X′ atom contributes to the overall magnetic moment, mostly for structure type T_{II}. The greater hybridization with the $3d$ element, as a consequence of geometry, is responsible for this. Al and Si atoms have vanishingly small contributions in all cases.

3.3.5 Exchange interactions and Curie temperature

In Fig 3.18 and 3.19 we show the variations of Curie temperatures with with changes in the valance electron number for $X_2X'Al$ (X = Mn, Fe, Co) and $X_2X'Si$ (X = Mn, Fe, Co) series respectively. Our results show that the variations in the Curie temperatures can be classified in two distinct regions based on structure types. Though the region-wise variations are not uniform it gives a qualitative idea of dependence

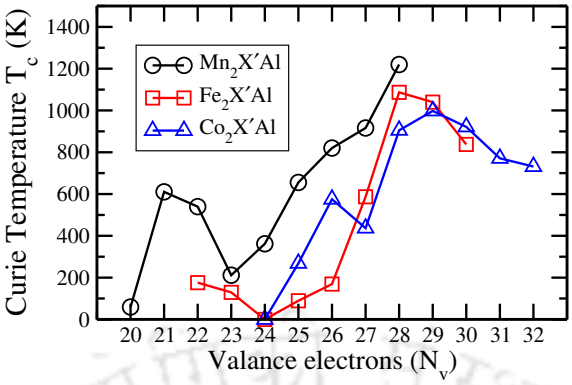

Figure 3.18: Variations in the Calculated Curie temperature with total number of valence electron for $X_2X'Al$ (X = Mn, Fe, Co) series.

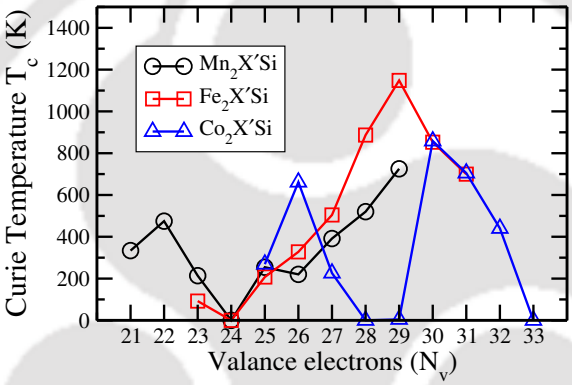

Figure 3.19: Variations in the calculated Curie temperature with total number of valence electron for $X_2X'Si$ series.

of Curie temperatures on the ordering of the atoms. we analyse the trends in the variations of Curie temperatures by inspecting the variations of different effective exchange parameters $J^{eff}_{\mu\nu}$ (Fig. 3.20 and Fig. 3.21) being given as $J^{eff}_{\mu\nu} = \sum_j J^{0j}_{\mu\nu}$; 0 fixed on μ sub-lattice and j runs over ν sub-lattice.

For $Mn_2X'Z$ compounds with structure type T_I, the Mn-Mn ferromagnetic interactions decide the variations in the Curie temperature T_c. This is true for $Fe_2X'Z$ and $Co_2X'Z$ series with compounds crystallising in T_I. The highest T_c is thus obtained for Mn_2ZrAl and Mn_2ZrSi for Mn-series, Fe_2YAl and Fe_2MoSi for Fe-series, Co_2NbAl and Co_2ZrSi for Co-series. Among them, the Co-compounds have the highest T_c and the Fe-compounds have the lowest T_c. This trend can be understood from the higher J^{eff} for Co-compounds and relatively lower ones in Fe-compounds. In case of Co-compounds, along with Co-Co, Co-X′ ferromagnetic interactions too play a significant role in deciding T_c. We find that both J^{eff} are maximum for N_V=26 across the Z series for Co-compounds. This can be attributed to the changes in

the behaviour of the exchange average, the average of exchange energies associated with low temperature spin excitations. This variation in the exchange average is related to the availability of spin down states below Fermi level. A gap in the spin down bands starting below Fermi level and extending beyond would lead to a larger value of exchange average and consequently a larger Curie temperature [110]. This, exactly, is happening for Co-compounds considered here. The same explanation can be used for Mn_2- compounds. The absence of such clear gaps around Fermi level of Fe-compounds imply that this argument cannot be used and thus the trends in variations of T_c is qualitatively different.

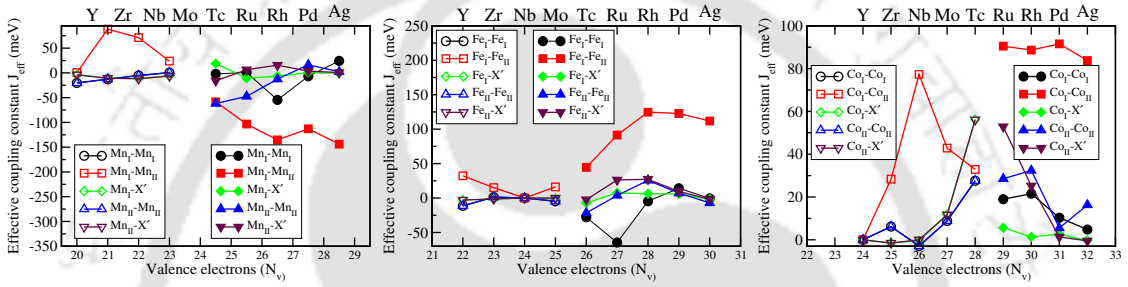

(a) (b) (c)

Figure 3.20: Effective exchange parameters for (**a**) $Mn_2X'Al$, (**b**) $Fe_2X'Al$, (**c**) $Co_2X'Al$ compounds. Open symbols are for structure type T_I, filled symbols are for structure type T_{II}.

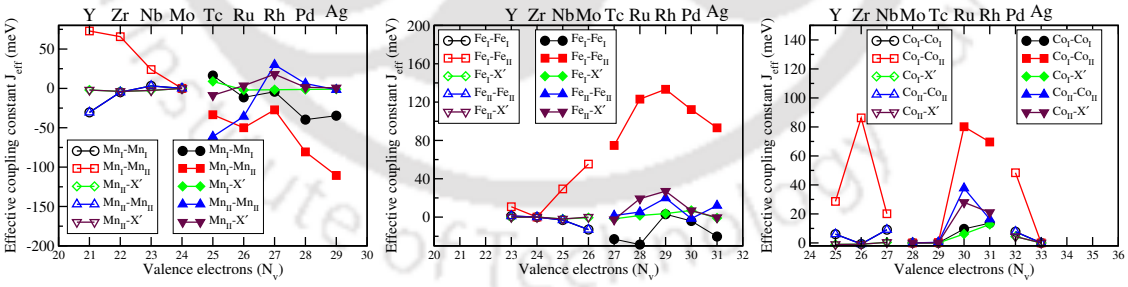

(a) (b) (c)

Figure 3.21: Effective exchange parameters for (**a**) $Mn_2X'Si$, (**b**) $Fe_2X'Si$, (**c**) $Co_2X'Si$ compounds.Open symbols are for structure type T_I, filled symbols are for structure type T_{II}.

The dominant exchange interactions for compounds with structure type T_{II} are $Mn_I(Co_I,Fe_I)$-$Mn_{II}(Co_{II},Fe_{II})$, Mn_{II}-Mn_{II} (Co_{II}-Co_{II}, Fe_{II}-Fe_{II}) and Mn_{II}-X′(Co_{II}-X′, Fe_{II}-X′). For Mn-compounds, the Mn_I-Mn_{II} interactions are strongly antiferromagnetic while the interactions between the $3d$ magnetic atoms are ferromagnetic for

compounds in other two series. In case of Mn-compounds, the T_c for Si-series is generally less than Al-series. The reason is that in the compounds in Si series there are competing antiferromagnetic and ferromagnetic interactions with the ferromagnetic ones coming from Mn_{II}-Mn_{II} and Mn_{II}-X′ interactions. The variations in the T_c for compounds in each series are controlled by the variations in the various dominant J^{eff}.

In summary, the effective exchange couplings (Fig. 3.20 and Fig. 3.21) show the differences due to different structure types. While in cases of $Fe_2X'Z$ and $Co_2X'Z$ compounds, the ferromagnetic Fe-Fe and Co-Co exchange interaction is the strongest and determines the qualitative variations in the Curie temperature T_c as the number of valence electrons vary, in case of $Mn_2X'Z$ compounds with structure type T_{II} several competing antiferromagnetic and ferromagnetic exchange interactions determine the variations in T_c.

3.3.6 Trends in the electronic properties upon replacing a 3*d* X′ constituent with an isoelectronic 4*d* element

There are lot more half-metals and SGS discovered among $X_2X'Z$ Heusler compounds with all transition metal atoms from 3*d* series. It would, thus, be interesting and important to understand the impact of replacing a 3*d* X′ constituent with an isoelectronic 4*d* element. A comparison into the half-metallic aspects of the isoelectronic compounds which are either half-metals or near half-metals with high spin polarization in either or both series (one with X′ a 3*d* element and another with X′ an isoelectronic 4*d* element) would shed light to the following: (a) whether electronic properties like half-metallicity primarily depends on N_V and not on whether X′ is a 3*d* element or a 4*d* element and (b) if not, then which are the possible factors that can explain the comparative trends in the isoelectronic compounds where in each case a 3*d* X′ is replaced with its isoelectronic 4*d* counterpart. Addressing this issue would help in prediction and design of new half-metals.

In Table 3.2, the structural, magnetic and electronic properties associated with half-metallicity of $X_2X'Z$ (X=Co, Mn, Fe; X′= an element with 3*d* electrons; Z = Al, Si) obtained from various existing resources are tabulated. Focusing solely on the compounds with integer or near integer magnetic moments and spin polarization equal to or close to 100% , we find that Mn_2VAl and Mn_2CoSi are half-metals, Mn_2TiSi and Mn_2FeAl are near half-metals while Mn_2CoAl is a SGS; Fe_2MnSi is a half-metal while Fe_2CrAl and Fe_2CrSi are near half-metals; Co_2TiAl, Co_2CrAl,

Co_2ScSi and Co_2CrSi are half-metals while Co_2VAl is a near half-metal. For each of these compounds, we look at the spin polarizations of the isoelectronic counterpart in the series with X′ a 4*d* element and find the following: (i) Mn_2VAl-Mn_2NbAl and Mn_2CoSi-Mn_2RhSi pairs are half-metals, Mn_2FeAl-Mn_2RuAl pairs are near half-metals with high spin polarization, Mn_2TiSi is a near half metal while isoelectronic Mn_2ZrSi is a half-metal, Mn_2CoAl in structure type T_{II} is a SGS while Mn_2RhAl is an ordinary metal, (ii) Fe_2MoAl and Fe_2MoSi are ordinary metals while their isoelectronic counterparts with X′ a 3*d* element, Fe_2CrAl and Fe_2CrSi, respectively are compounds with high spin polarizations. Fe_2TcSi is an ordinary metal while Fe_2MnSi is a half-metal, (iii) Co_2TiAl-Co_2ZrAl and Co_2ScSi-Co_2YSi are half-metal pairs, Co_2CrAl and Co_2MnSi are half-metals while their isoelectronic counterparts Co_2MoAl and Co_2TcAl, respectively, are ordinary metals with low spin polarizations,Co_2VAl is a near half metal while Co_2NbAl is a half metal. Co_2TiSi is an ordinary metal while Co_2ZrSi is a half-metal. Co_2CrSi is a half-metal while Co_2MoSi is a non-magnetic material.

In order to understand the trend observed, we take recourse to the comparisons of the electronic structures of each pairs of compounds considered above. In Fig. 3.22-3.24 we show the total and partial densities of states of some of the pairs. In cases of Mn_2VAl-Mn_2NbAl and Mn_2CoSi-Mn_2RhSi pairs (Fig. 3.22 (a),(b)), we find that the electronic structures of a given pair are near identical around the Fermi levels. In cases of inverse Heusler (structure type T_{II}) Mn_2CoSi and Mn_2RhSi, the half-metallic gaps are artefacts of the separation of the t_{2g} and e_g spin up states. However, there is a difference between the contributors to these states between the two compounds: In Mn_2RhSi, the states bordering the gap are primarily Mn_I t_{2g} and a hybridiZed Mn_{II}-Rh e_g while in Mn_2CoSi, the t_{2g} states too are hybridized Mn_I-Co. In case of the pair Mn_2VAl-Mn_2NbAl, both in regular Heusler structure (structure type T_I), the electronic structures in the majority band is identical-the half-metallic gap being flanked by Mn states only. In Fig. 3.22 (c) we show the densities of states of the pair Mn_2TiSi-Mn_2ZrSi, the later is a half-metal while the former is a near half-metal with integer moment and above 90% spin polarization (Table 3.2). The densities of states reveal that the difference in the electronic properties originates from the positions of the t_{2g} and e_g states flanking the half-metallic gap; in Mn_2TiSi, the position of the top of the t_{2g} spin up bands in the occupied part coming from the Mn atoms cut through the Fermi level while this is not so in case of Mn_2ZrSi. The little trace of densities of states at the Fermi level reduces the spin polarization in Mn_2TiSi. The striking difference in electronic properties in the context of half-

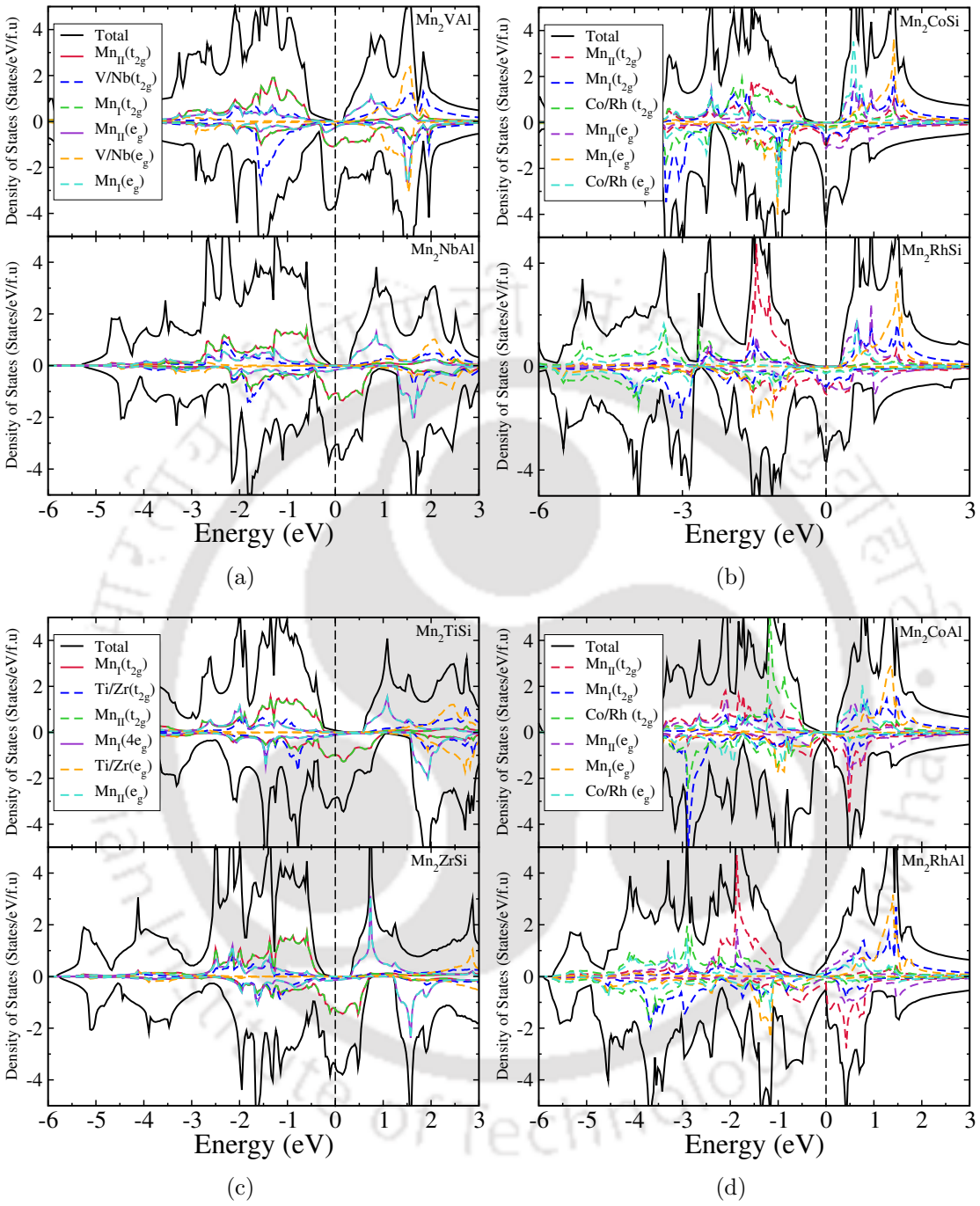

Figure 3.22: Spin polarized total and atom-projected densities of states for pairs of isoelectronic compounds (**a**) Mn_2VAl-Mn_2NbAl (**b**) Mn_2CoSi-Mn_2RhSi (**c**) Mn_2TiSi-Mn_2ZrSi (**d**) Mn_2CoAl-Mn_2RuAl . In each pair of compounds X and Z are identical, while X′ is a 3*d* element in one while in another it is an isoelectronic 4*d* element. The results show that the features of the densities of states for a pair of isoelectronic compounds are very similar. The positions of the bands in one of the spin channels with respect to Fermi levels determine their electronic properties.

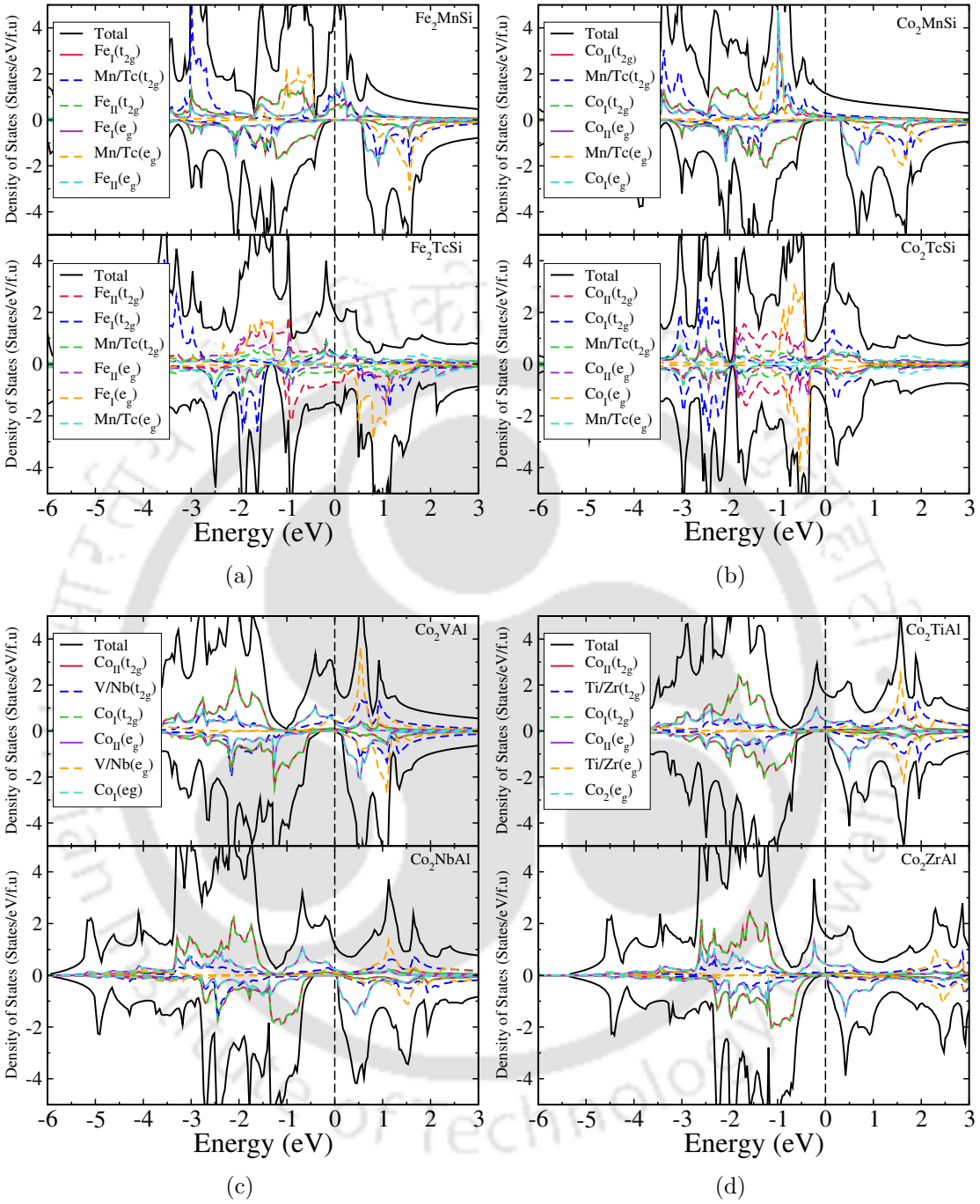

Figure 3.23: Spin polarized total and atom-projected densities of states for pairs of isoelectronic compounds (**a**) Fe_2MnSi-Fe_2TcSi (**b**) Co_2MnSi-Co_2TcSi (**c**) Co_2VAl-Co_2NbAl (**d**) Co_2TiAl-Co_2ZrAl . In each pair of compounds X and Z are identical, while X′ is a $3d$ element in one while in another it is an isoelectronic $4d$ element. The results show that the features of the densities of states for a pair of isoelectronic compounds are very similar. The positions of the bands in one of the spin channels with respect to Fermi levels determine their electronic properties.

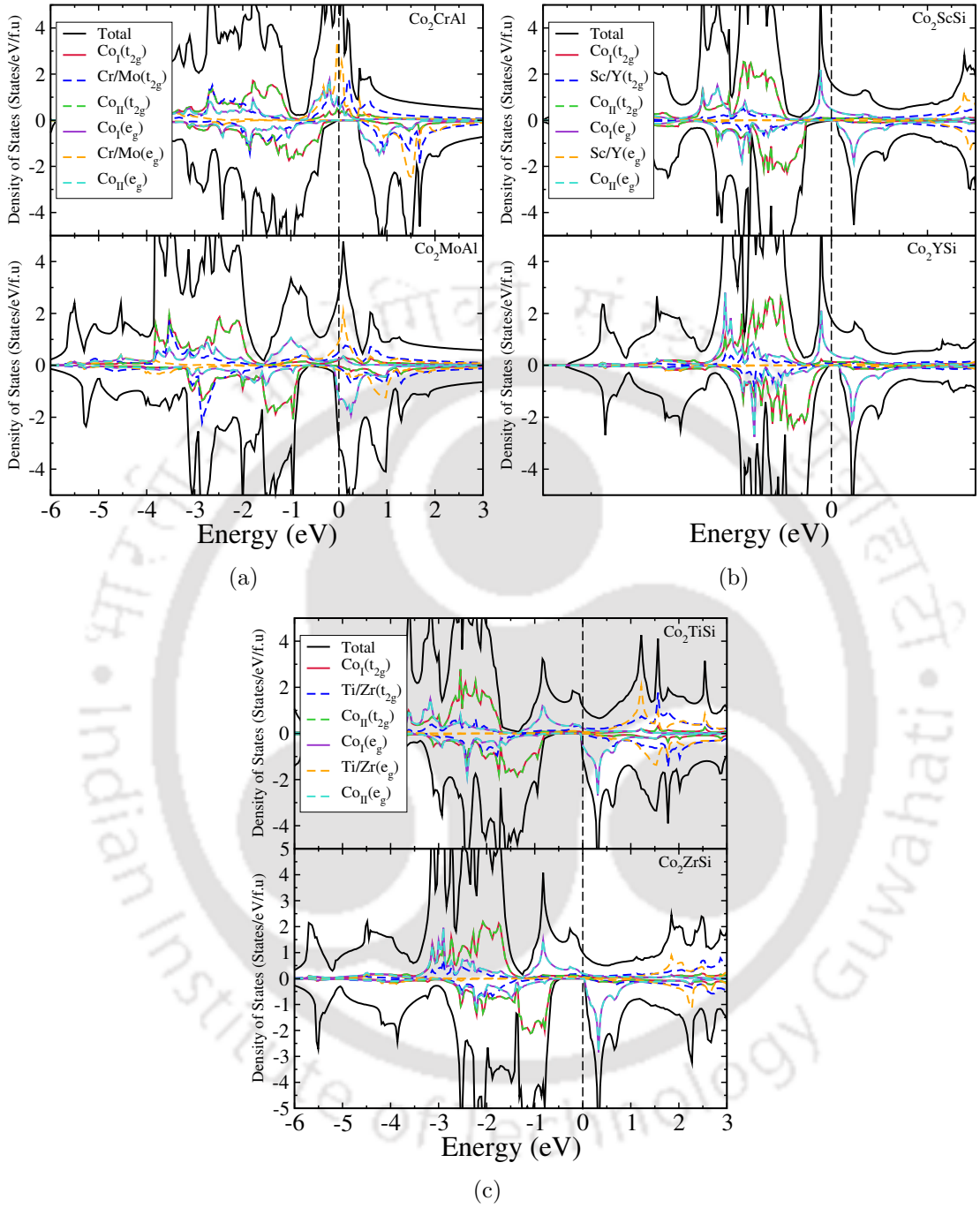

Figure 3.24: Spin polarized total and atom-projected densities of states for pairs of isoelectronic compounds (**a**) Co_2CrAl-Co_2MoAl (**b**) Co_2ScSi-Co_2YSi (**c**) Co_2TiSi-Co_2ZrSi. In each pair of compounds X and Z are identical, while X′ is a 3*d* element in one while in another it is an isoelectronic 4*d* element. The results show that the features of the densities of states for a pair of isoelectronic compounds are very similar. The positions of the bands in one of the spin channels with respect to Fermi levels determine their electronic properties.

metallicity is observed in the pair Mn_2CoAl-Mn_2RhAl with the former being a SGS and both are of structure type T_{II}. A close inspection into the densities of states (Fig. 3.22 (d)), however, reveals that the electronic structures of the two compounds are not so different from each other, in both compounds top of the valence band and bottom of the conduction band touch each other forming zero gap in the spin down band. A difference occurs in the spin up bands. In Mn_2CoAl, there is a clear half-metallic gap with the top of the valence band having contributions from Mn_{II} and Co t_{2g} states and the bottom of the conduction band having contributions from the e_g states of the same pair of atoms. In Mn_2RhAl, we find another zero gap in the spin up bands, however, not at the fermi level but inside the occupied part of the spectrum. The t_{2g} and e_g bands in this case are more delocalised, possibly due to hybridizations with more delocalised $4d$ states of Rh as compared to $3d$ states of Co, thus, diminishing chances of getting SGS or half-metallic properties in this compound.

The origin of different properties in Fe_2MnSi-Fe_2TcSi pair can be traced to the structures they crystallise in: the former in T_I and the later in T_{II}. In Fig. 3.23 (a), we compare the densities of states of two compounds. The half-metallic behaviour of Fe_2MnSi stems from the unavailability of spin down states on either side of Fermi level with the gap being flanked by Fe t and e states. In Fe_2TcSi, the T_{II} structure leaves no such scope as there is substantial hybridizations between Fe and Tc states across the Fermi level. The pairs Fe_2CrAl-Fe_2MoAl and Fe_2CrSi-Fe_2MoSi all crystallise in same structure (type T_I) but their spin polarizations differ significantly. However, the densities of states of each pair of compounds are qualitatively similar. The highlights of the electronic structure in both Fe_2CrAl [201] and Fe_2MoAl are a pseudogap in the spin up band and a gap cutting through the Fermi level in the spin down band, although in case of Fe_2MoAl, it is more like a pseudo gap reducing it's spin polarization. This difference in the electronic structure once again stems from the availability of states near and at Fermi level in case of Fe_2MoAl, presumably because of the hybridizations of Fe with delocalised Mo states. Similar differences explain the differences in spin polarizations of Fe_2CrSi and Fe_2MoSi.

In Fig. 3.23 (b)-(d), we show the densities of states for three pairs of Co_2-compounds. The Co_2TiAl-Co_2ZrAl pair is a half-metal one, in Co_2VAl-Co_2NbAl pair, the later is a half-metal while the former is a near half-metal with spin polarization of 95%. In the pair Co_2MnSi-Co_2TcSi, the former is a half-metal and the later an ordinary metal. In Fig. 3.24 (a)-(c) we show the electronic structures of another three pairs Co_2CrAl-Co_2MoAl, Co_2ScSi-Co_2YSi and Co_2TiSi-Co_2ZrSi respectively.

We find that the electronic structures of Co_2TiAl and Co_2ZrAl are identical with the Co states on either sides of the gaps being located even at same energies. Same happens in case of Co_2ScSi-Co_2YSi pair. The differences in the electronic structures near the Fermi levels of Co_2VAl and Co_2NbAl are minimal. Unlike Co_2NbAl, there is a trace of hybridization between Co and V states around the Fermi level reducing the spin polarization by a few percent than that of an ideal half-metal. A major difference is observed between Co_2MnSi and Co_2TcSi. This, clearly, is due to the different crystal structures (Co_2MnSi has structure type T_I, Co_2TcSi has structure type T_{II}), the reflections are there in the densities of states. Similar is the case with Co_2CrSi [224] and Co_2MoSi. Analysing the cases where both members of an isoelectronic pair crystallise in structure type T_I but one of them is a half-metal while the other is a metal with medium spin polarization (Fig. 3.24 (a) and Fig. 3.24 (b)), we find that the electronic structures are very similar for the compounds in a pair. For example, in both Co_2TiSi-Co_2ZrSi and Co_2CrAl-Co_2MoAl pairs, the noteworthy feature in the densities of states is the presence of a clear gap in the spin down bands. The differences in the spin polarization arise due to different positions of the Fermi levels. In Co_2TiSi, the bottom of the conduction band which consists of e_g states of Co falls behind the Fermi level while they are above the Fermi level in Co_2ZrSi. Similar is the case with the other pair of compounds.

3.4 Conclusions

Employing first-principles electronic structure calculations, in this chapter, we have systematically studied the structural, electronic and magnetic properties of 54 $X_2X'Z$ ternary Heusler compounds where X= Mn, Fe, Co; Z = Al, Si and X′ represents 9 elements with 4*d* electrons in their valance shells. In pursuit of finding new half-metallic magnets from ternary series with both 3*d* and 4*d* electrons in the same compounds we found only seven half-metals Mn_2NbAl, Mn_2ZrSi, Mn_2RhSi, Co_2ZrAl, Co_2NbAl, Co_2YSi and Co_2ZrSi with 100% spin polarization. We also find the compounds Mn_2TcAl, Mn_2RuAl, Mn_2NbSi, Mn_2RuSi, Fe_2NbSi with high spin polarization (greater than 90%) and a gap like feature in one of the spin-channel near the Fermi-level. These compounds can be identified as “near half-metals”. Tuning the positions of their Fermi levels by application of pressure such that the gap cuts through the Fermi levels may induce half-metallicity in them.

From the present study the hybridization picture that has been in use to explain the origin of half-metallicity in ternary Heusler compounds with magnetic compo-

nents being the ones with 3*d* elements only, is found to be valid in case of compounds with both 3*d* and 4*d* elements as constituents. This leads to a general framework in understanding the origin of half-metallic behaviour in Heusler $X_2X'Z$ compounds where X′ can be either a 3*d* element or one from the group of 4*d*. An one-on-one comparison between $X_2X'Z$ compounds where X′ is a 3*d* element in one case and a 4*d* element in other, shows that as long as N_V, the number of valence electrons are same, the electronic properties like half-metallicity or near half-metallicity with high spin polarization, by an large, remain intact if a 4*d* element replaces a 3*d* one as X′ provided both compounds crystallise in the same ground state structure. Even in cases where the spin polarizations, and subsequent half-metallic features are different, the electronic structures are very similar for compounds with same N_V and same structure type. The differences in electronic properties in regard to half-metallicity occurs due to the relative positions of the bottom of the conduction band and the Fermi energy which is a consequence of the positions of the X and X′ states near the Fermi level. Therefore, N_V can be a good predictor to explore possible new half-metals.

The trends in the Curie temperature, T_c, in the compounds with X′ a 4*d* element, is found to be correlated with the trends in the dominant exchange interactions. We find that across the series, the X-X exchange interactions determine the trends in T_c for compounds with structure type T_I which in turn can be correlated to the dominance of X-X hybridizations in their electronic structures. In case of compounds with structure type T_{II}, the dominant exchange interactions are X_I-X_{II} and X_{II}-X′ deciding the trends in T_c. This, once again, can be correlated to the dominant hybridizations in their electronic structures. The present work, thus, systematically explores the physics behind occurrence of half-metallicity in compounds with magnetic constituents from both 3*d* and 4*d* series and provides with a generalised microscopic picture applicable to a large number of heusler compounds. This would be useful for experimentalists in particular, to explore new materials with novel magnetic applications.

Chapter 4

Investigation of half-metallic behaviour in quaternary Heusler compounds CoX′Y′Z (X′ = $4d$ elements, Y′ = Mn, Fe and Z = Al, Si)

4.1 Introduction

Quaternary Heusler (XX′Y′Z) compounds are less explored in comparison to the ternary $X_2X'Z$ ones as mentioned in chapter 1. On top of that, most of the studies on quaternary Heuslers are on the compounds where all three transition metal constituents, X, X′ and Y′ are from $3d$ series [66, 76, 180, 229–234]. Fewer attempts have been made to systematically explore quaternary compound series with at least one or more than one transition metal elements with $4d$ electrons. In this chapter, we present our results on structural, electronic and magnetic properties of 4 quaternary series CoX′Y′Z with Y′ = Mn, Fe while X′ are 9 transition elements varied from Y to Ag along the series in the periodic table and Z = Al, Si. In section 1.8 we have mentioned the reason behind our judicious choice on these particular six quaternary series.

The results and discussions on CoX′Y′Si series in this chapter are published in Scientific Reports **7**, 1803 (2017) and the results and discussions on CoX′Y′Al series in this chapter are from [228], physica status solidi (b) **256**, 1900039 (2019).

In a bid to systematically understand the physics of half-metallic behaviour in quaternary Heusler compounds where one of the magnetic elements is from the 4*d* series of periodic table, in this work, we have computed the structural, electronic and magnetic properties of compounds in four quaternary Heusler series, CoX′Y′Z, where X′ is an element with 4*d* electrons and Z is Al or Si. We also perform a comparative study of these four series CoX′Y′Z. Apart from the quest for new half-metals, following are the issues we attempt to address:

1. to understand how the similarities and differences between the arrangements of atoms in various crystallographic sites in the ground states, and the electronic structures, influence the possibility of half-metallic behaviour in quaternary compounds with 4*d* elements.

2. to understand the key factors influencing half-metallic behaviour in quaternary compounds by qualitative comparison between compounds where all magnetic atoms are from 3*d* atoms and where one of the magnetic atoms are from 4*d* series.

3. to observe whether half-metallic behaviour is transferable to daughter quaternary compounds with 4*d* elements whose parent compounds are ternary Heuslers. This is important in the light of the work presented in previous chapter.

4. to find out the role of 4*d* transition metal elements by successively changing it along the series of 4*d* transition metal elements so that the total number of valance electron changes continuously, on the properties of compounds where one of the 3*d* elements remains fixed with the other changes.

This chapter is organised as follows. In the next section we present computational details and the methods. Next we have discussed the calculated results on structural, electronic and magnetic properties of the above mentioned quaternary compounds with a comparative understanding with compounds having only 3*d* elements as the magnetic components. While discussing series wise we have chosen Z = Si series first because one of the prototype parent compounds, $Co_2X'Z$, has more half-metals with Z = Si compared to Z = Al series (as seen from Table 3.2). At the end, discussions on calculated results is followed by the conclusions and future outlook.

4.2 Computational Details

Using Vienna Ab-initio Simulation Package (VASP) [137–139], we have used spin-polarized DFT based projector augmented wave method for calculating electronic structure with Generalized Gradient Approximation (GGA) [172]. 450 eV energy cut-off and a Monkhorst-Pack [173] 25 x 25 x 25 k-mesh were used for self-consistent calculations while we used a larger 31 x 31 x 31 k-mesh for the densities of sates. The energy and the force convergence criteria were set to 10^{-6} eV and 10^{-2} eV/Å respectively. We checked our results by turning on the spin-orbit coupling as systems had $4d$ electrons. However, the results did not change.

The magnetic pair exchange parameters ($J^{ij}_{\mu\nu}$) were calculated with multiple scattering Green function formalism as implemented in SPRKKR code[140] using a Heisenberg Hamiltonian for the spin interaction of sites using the equation (2.53). We have used full potential spin polarized scalar relativistic Hamiltonian with angular momentum cut-off $l_{max} = 3$ to calculate the energy differences by the SPRKKR code. A uniform k-mesh of 22 x 22 x 22 is used for Brillouin zone integration. The Green's functions were calculated for 32 complex energy points distributed on a semi-circular contour. For the self-consistent cycles, the energy convergence criterion was set to 10^{-6} Ry . The calculated $J^{ij}_{\mu\nu}$ were used further to compute the Curie temperatures T_c using the mean field approximation[167].

4.3 Results and Discussions

4.3.1 Structural Properties

As mentioned in section 1.2 when one of the X atoms in $X_2Y'Z$ compound is substituted by a different transition metal element X′, a quaternary Heusler alloy(QHA) with composition XX′Y′Z is formed. The prototype structure of QHA is LiMgPdSn(Space group no. 216; $F\bar{4}3m$) [237] with X, X′ and Y′ occupying 4c, 4d and 4b

Table 4.1: Possible structure types of XX′Y′Z compounds.

	4a (0, 0, 0)	4b (1/2, 1/2, 1/2)	4c (1/4, 1/4, 1/4)	4d (3/4, 3/4, 3/4)
Type-I (T_I)	Z	X′	X	Y′
Type-II (T_{II})	Z	Y′	X	X′
Type-III (T_{III})	Z	X	X′	Y′

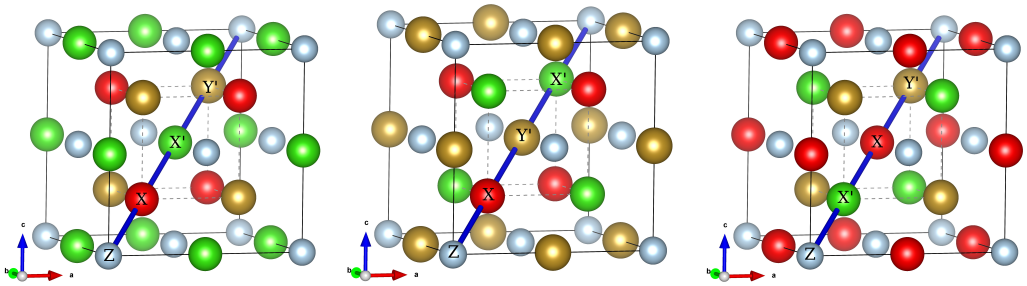

(a) (b) (c)

Figure 4.1: Crystal structures of quaternary Heusler compounds XX′Y′Z: (**a**) structure type T_I (X and Y′ are in symmetric positions 4c and 4d respectively; 4a and 4b sites are occupied by Z and X′) (**b**) structure type T_{II} (X and X′ are in symmetric positions 4c and 4d; 4a and 4b sites are occupied by Z and Y′.) (**c**) structure type T_{III}(X′ and Y′ are in symmetric positions 4c and 4d).

				Mn 1.55	Fe 1.83	Co 1.88		Si 1.90
Y 1.22	Zr 1.33	Nb 1.60	Mo 2.16	Tc 1.90	Ru 2.20	Rh 2.28	Pd 2.20	Ag 1.93

Figure 4.2: Schematic representation of preferred ground state structures (Red - Type-I; Green - Type-II) of CoX′Y′Si compounds . The number attached to each element represent its electronegativity(Pauli scale).

positions respectively, making the arrangement of atoms along the body diagonal of the Heusler lattice as X-Y′-X′-Z. It has been found out that if the number of valence electrons decreases along X, X′, Y′ then LiMgPdSn structure is the most stable [61]. However, there are other two inequivalent configurations possible if one fixes the position of Z at site 4a and permutes the occupancies of the three other sites. The three resulting configurations[61, 101, 179] are shown in Table 4.1 and Fig. 4.1.

In order to find the ground state crystal structures of the CoX′Y′Si compounds considered in the present study, we have calculated the total energies of each of the compounds in all three structure types listed in Table 4.1. The results are shown in Table 4.2. Our calculations show that the structure Type-III is energetically always higher than the other two structure types for all the compounds considered. Thus, the compounds crystallize either in structure Type-I(T_I) or in Type-II(T_{II})(Fig.4.1). It may be noted that the order of magnitude of energy differences (ΔE, $\Delta E'$) is consistent with those obtained for quaternary Heusler compounds with 3*d* magnetic atoms only [238]. The results also suggest that the argument with respect

Table 4.2: Calculated lattice constants, formation energies, magnetic moments and energy differences between possible structures of quaternary CoX′Y′Si compounds. The energy differences between Type-II (T_{II}) and Type-I(T_I) structures are given by ΔE=$E_{T_{II}}$-E_{T_I} . A positive ΔE implies T_I as the ground state. The energy differences between Type-III(T_{III}) and Type-I or Type-II structures are given by $\Delta E'$=$E_{T_{III}}$-$E_{T_{I/II}}$. For the systems which crystallise in Type-II(T_{II}), $\Delta E'$=$E_{T_{III}}$-$E_{T_{II}}$; for the systems which crystallise in Type-I(T_I), $\Delta E'$=$E_{T_{III}}$-E_{T_I}.

Systems (Type-I)	Lattice constant(Å)	Formation energy(eV)	ΔE (eV/f.u.)	$\Delta E'$ (eV/f.u.)	Structure type	M ($\mu_B/f.u.$)
CoYMnSi	6.30	-1.94	0.39	0.05	T_I	4.55
CoZrMnSi	5.96	-2.23	1.14	0.82	T_I	0.00
CoNbMnSi	5.85	-1.74	0.69	0.85	T_I	1.00
CoMoMnSi	5.84	-1.90	-0.21	0.67	T_{II}	2.33
CoTcMnSi	5.79	-3.14	-0.89	0.84	T_{II}	3.00
CoRuMnSi	5.79	-2.70	-1.38	0.85	T_{II}	4.00
CoRhMnSi	5.83 (5.84[235])	-2.82	-1.46	0.81	T_{II}	5.00 (5.00[235])
CoPdMnSi	5.90	-2.06	-0.67	0.51	T_{II}	4.90
CoAgMnSi	5.96	-0.38	0.05	0.28	T_I	3.53
CoYFeSi	6.08	-2.14	0.91	0.81	T_I	0.00
CoZrFeSi	5.96 (5.97[233])	-3.33	1.19	1.24	T_I	1.00 (1.00[233])
CoNbFeSi	5.88	-2.31	0.77	1.06	T_I	1.99
CoMoFeSi	5.84	-1.42	-0.05	0.39	T_{II}	2.83
CoTcFeSi	5.80	-2.65	-0.67	0.49	T_{II}	3.89
CoRuFeSi	5.78 (5.773[236])	-3.12	-1.02	0.52	T_{II}	4.66 (4.80[236])
CoRhFeSi	5.80	-2.10	-0.78	0.21	T_{II}	4.90
CoPdFeSi	5.86	-1.48	-0.23	0.06	T_{II}	4.00
CoAgFeSi	5.88	-0.10	0.09	0.18	T_I	2.71

to the number of valence electrons of each transition metal atom, in explaining the structure type in which a particular compound crystallizes to, is not valid for all the compounds studied. According to that argument, CoMoMnSi, CoTcFeSi and CoMoFeSi should have crystallized in Type-I structures while CoAgMnSi and CoAgFeSi should have crystallized in Type-II structures.

A better understanding of the ground state site occupancies displayed by these compounds can be achieved if one provides an argument only in terms of relative electronegativities of the transition metal components in these systems. If one fixes the position of the main group element at 4a site, then the 4b site should be occupied by the least electronegative one out of the three transition metal atoms. Thus the main group element and the least electronegative element of the remaining three occupy the octahedral sites while the other two occupy the tetrahedral sites. For example, in CoMoMnSi, Mn is the least electronegative among the three transition metal atoms and so it occupies the 4b site, giving rise to a Type-II structure. The reason behind unfavourable Type-III structure for all compounds, too, can be ex-

Table 4.3: Calculated lattice constants, formation energies, magnetic moments and energy differences between possible structures of quaternary CoX′Y′Al compounds. The energy differences between Type-II (T_{II}) and Type-I(T_I) structures are given by $\Delta E = E_{T_{II}} - E_{T_I}$. A positive ΔE implies T_I as the ground state. The energy differences between Type-III(T_{III}) and Type-I or Type-II structures are given by $\Delta E' = E_{T_{III}} - E_{T_{I/T_{II}}}$. For the systems which crystallize in Type-II(T_{II}), $\Delta E' = E_{T_{III}} - E_{T_{II}}$; for the systems which crystallize in Type-I(T_I), $\Delta E' = E_{T_{III}} - E_{T_I}$.

Systems (Type-I)	Lattice constant(Å)	Formation energy(eV)	ΔE (eV/f.u.)	$\Delta E'$ (eV/f.u.)	Structure type	M ($\mu_B/f.u.$)
CoYMnAl	6.41 (6.412[239])	-2.01	0.70	0.35	T_I	4.00 (4[239])
CoZrMnAl	6.08 (6.0746[240])	-2.87	0.95	0.49	T_I	0.98 (1.0030[240])
CoNbMnAl	5.94	-2.41	1.19	1.09	T_I	0.00
CoMoMnAl	5.87	-1.77	0.34	0.88	T_I	0.91
CoTcMnAl	5.85	-2.94	-0.47	0.92	T_{II}	2.11
CoRuMnAl	5.85	-3.42	-1.05	0.73	T_{II}	3.02
CoRhMnAl	5.88 (5.8924[235])	-2.98	-1.34	0.80	T_{II}	4.05(4.04[235])
CoPdMnAl	5.97	-2.68	-1.09	0.73	T_{II}	5.00
CoAgMnAl	6.08	-1.07	-0.42	0.40	T_{II}	4.59
CoYFeAl	6.22	-1.76	0.74	0.67	T_I	0.86
CoZrFeAl	6.04	-3.23	1.45	1.40	T_I	0.00
CoNbFeAl	5.93 (5.9482[241])	-2.36	1.15	1.42	T_I	1.00 (1.00[241])
CoMoFeAl	5.87	-1.63	0.50	1.04	T_I	1.93
CoTcFeAl	5.86	-2.33	-0.12	0.60	T_{II}	3.05
CoRuFeAl	5.85	-3.09	-0.74	0.62	T_{II}	4.20
CoRhFeAl	5.88	-2.60	-1.12	0.60	T_{II}	4.86
CoPdFeAl	5.94	-2.08	-0.79	0.29	T_{II}	4.41
CoAgFeAl	6.02	-0.64	-0.37	0.10	T_{II}	3.82

tracted from this logic. In Type-III structure, Co and Si, the two elements having the highest electronegativities occupy the octahedral sites, thus making it impossible to form the rocksalt sub-lattice with octahedral coordination. However, the exceptions to this empirical rule are observed in cases of CoNbMnSi, CoAgMnSi and CoAgFeSi. The reason behind the exception in case of CoNbMnSi could be due to the fact that the electronegativities of Nb and Mn are very close. In cases of CoAgMnSi and CoAgFeSi, the energy differences between Type-I and Type-II structures are very small(Table 4.2), indicating that the structure Type-I is not strongly preferred over structure Type-II and a thermally induced disordered structure can be the ground state for them. Nevertheless, the site preferences for a large number of QHA can be explained by this suggested empirical rule[101, 116–119, 179–186]. A schematic representation of preferred structures of CoX′Y′Si compounds under consideration is given in Fig.4.2.

For CoX′Y′Al compounds too, we first optimised the ground state structures for each of the compounds by computing their total energies in each of the three structures. In Table 4.3 we have tabulated the calculated lattice constants, the

formation energies and total magnetic moments for each of the 18 quaternary Heusler compounds in their respective ground state. Here too, we find that structure type T_{III} is energetically always higher. This, along with the structure types in which each of these CoX′Y′Al compounds investigated crystallise, can be explained on the basis of relative electronegativities as mentioned earlier. Except CoNbY′Al (Y′ = Fe,Mn) this empirical rule works well for all other quaternary compounds. Fixing the position of Al at 4*a* site we find Y and Zr having electronegativities lower than Co, Mn,Fe in CoX′Y′Al occupy 4*b* site leading CoYMnAl(CoYFeAl) and CoZrMnAl(CoZrFeAl) to crystallise in T_I validating the empirical rule. Similarly for other CoX′Y′Al (X′ = Tc, Ru, Rh, Pd and Ag , Y′=Mn, Fe) compounds, fixing the position of Z atom at 4*a* implies that the least electronegative one of the remaining three transition element atoms will occupy the 4*b* site producing the structure Type-II (Fig 4.1(b)). It is also to be noted that irrespective of the electronegativitiy of the *sp*-element at the 4*a* site, 4*b* site is always occupied by the least electronegative of the transition metal elements. The closeness in electronegativities of Nb and Mn (Co and Fe) (The electronegativities of Nb,Mn,Fe and Co are 1.6,1.55,1.83 and 1.88 respectively), might explain the reason behind CoNbY′Al (Y′ = Mn, Fe) being the exception to the empirical rule. Another exception is that of CoMoY′Al. In this case, Al being the least electronegative of all four atoms, 4*b* site is occupied by the highest electronegative element Mo. Thus, the octahedral sites are occupied by the main group element and the least electronegative of the remaining three making a rocksalt sub-lattice, while the tetrahedral sites are fixed with other two transition metal elements, leading to a structure type T_I. The energy differences between different structures with respect to ground state-type (ΔE, $\Delta E'$) are not very small indicating the ground state structure types, given in Table 4.3 are strongly preferred, unlike the cases of CoAgX′Si compounds where the deviations from the empirical rule was explained in terms of closeness of energies in T_I and T_{II} [187]. A comparison with CoX′Y′Si compounds point out another difference: the Mo-compounds crystallised in T_{II} as expected from the empirical rules. The difference can be explained by the fact that Si has a electronegativity of 1.9, much higher than Al and certainly not the least among the four constituents.

The quaternary Heusler XX′Y′Z can be considered as a daughter compound derived from the parent ternary compounds $X_2Y'Z$ [116, 119, 237]. Depending on the choice of parent ternary compounds there exist a number of possible combinations that yield quaternary Heuslers, at least theoretically. In this work we only considered $X_2X'Z$ and $Y'_2X'Z$ as the parent compounds. For example, CoX′Y′Al can

be considered to be derived from parents $Co_2X'Al$ and $Y'_2X'Al$. Considering T_I as equivalent to that of the regular Heusler structure and T_{II} as that of the "inverse" Heusler structure of ternary compounds we find that except CoTcMnAl, CoTcFeAl, CoMoMnSi, CoMoFeSi, CoPdMnSi, CoPdFeSi and CoAgMnSi all the CoX′Y′Z (Z = Al, Si) compounds follow the same structure type preferred by parent ternary compounds [168, 187]. Co_2TcAl (Mn_2TcAl) prefers T_I(T_{II}) as ground state [168] implying that the daughter compound can assume any of the two types depending on the energy cost. This is the case for other such deviant daughters as well.

The calculated lattice constants agree well with the available results for select systems. The optimized lattice constants in the ground state structures of CoX′Y′Z systems and their formation energies are also given in tables 4.2 and 4.3. The variations in the lattice constants across compounds are consistent with that in the atomic radii of X′. Comparing the results CoX′Y′Al with those of CoX′Y′Si series, we find that change in lattice constant is in accordance with the changes in the size of the main group element.The formation energies are expressed as

$$E_f = E_{CoX'Y'Z} - (E_{Co} + E_{X'} + E_{Y'} + E_Z)$$

where $E_{CoX'Y'Z}$ is the total energies per formula unit of the CoX′Y′Z and E_{Co}, $E_{X'}$, $E_{Y'}$ and E_Z are the total energies of the bulk Co, X′, Y′ and Z respectively in their ground state structures. Out of these compounds, only CoRuFeSi has been experimentally synthesised [236] and the lattice constant for this system agree very well with the experimental result. From Tables 4.2 and 4.3, we see that for all Quaternary compounds formation energies are negative, hence thermodynamically stable and are probable to form. Therefore further investigations into their properties are worth a shot.

4.3.2 The Magnetic moments and the Slater-Pauling Rule

The necessary condition for half-metallic behaviour in Heusler compounds is that the total magnetic moment per formula unit is an integer and that it follows the Slater-Pauling rule, [57–60] which connects the total magnetic moment to the number of valence electrons. For $X_2Y'Z$ Heusler compounds, the magnetization M and the number of valence electrons N_V are related either by $M = |N_V - 18|$or by $M = |N_V - 24|$ or by $M = |N_V - 28|$, depending on whether X is an early transition metal or not [7, 59]. It was observed that half-metallic quaternary Heusler compounds too obey these rules [61].

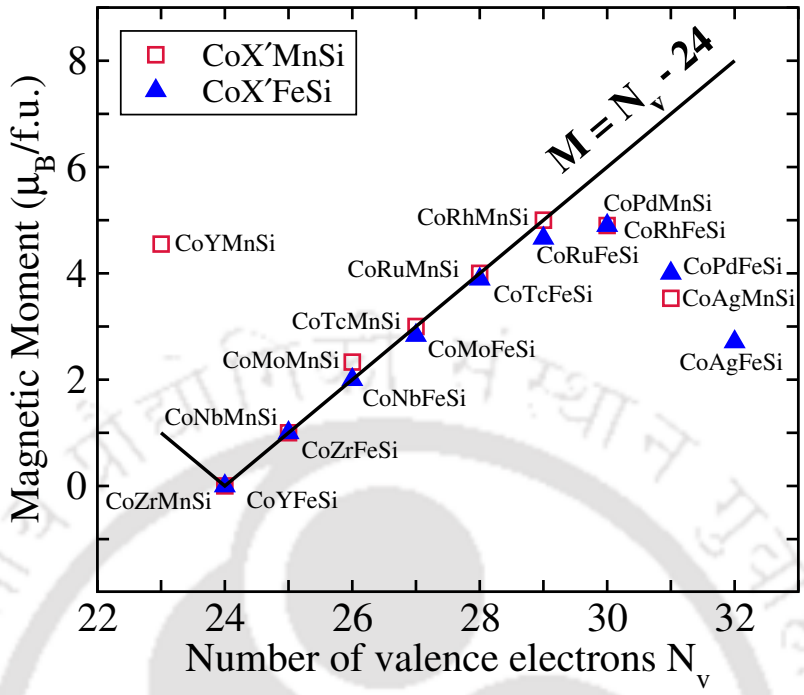

Figure 4.3: Total magnetic moments versus the total number of valence electrons N_V for CoX′Y′Si compounds. The Slater-Pauling $M = |N_V - 24|$ line is drawn as a guide to understand whether the compounds follow Slater-Pauling rule.

Since CoX′Y′Si systems are derived from Co_2Y′Si(Y′=Mn, Fe) compounds which follow $M = |N_V - 24|$ Slater-Pauling rule [7], we intend to investigate whether the systems under study in the present work conform to that. Accordingly, we have plotted total magnetic moments (Table 4.2) of all compounds in Fig.4.3 along with $M = |N_V - 24|$ line. We find that the magnetic moments for most of the compounds in CoX′Y′Si series lie on or very close to the $M = |N_V - 24|$ line. The significant deviants from the Slater-Pauling line are the ones where X′ element is a late transition metal. The magnetic moments of most of these deviants, shown in Table 4.2, actually do not seem to follow any of the Slater-Pauling rules mentioned above and thus are not interesting from the perspective of half-metallic magnets. CoYMnSi, in spite of deviating from the Slater-Pauling line $M = |N_V - 24|$ significantly (M should have been -1 μ_B according to $N_V - 24$ rule) comes close to following $M = |N_V - 18|$. CoPdFeSi, on the other hand, has an integer moment, yet does not fit into any of the Slater-Pauling rules.

The variations in the total spin-magnetic moment per formula unit (M) with N_V for the CoX′Y′Al compounds considered in this work are shown in Fig 4.4. Like CoX′Y′Si compounds, most of the CoX′Y′Al compounds are found to follow $M = |N_V - 24|$ rule closely except for the cases when X′ are late transition metal

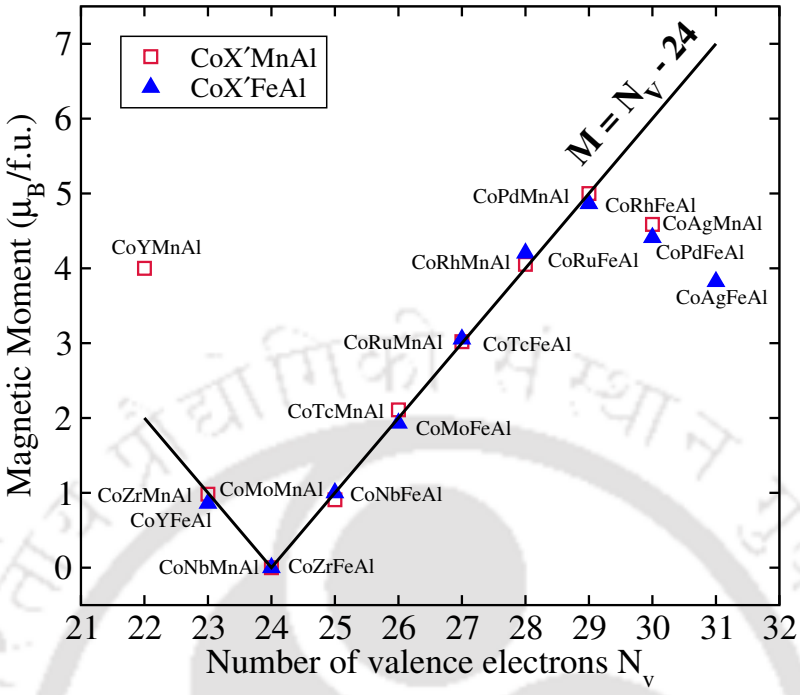

Figure 4.4: Total magnetic moments versus the total number of valence electrons N_V for CoX′Y′Al compounds. The Slater-Pauling $M = |N_V - 24|$ line is drawn as a guide.

elements; CoAgMnAl, CoPdFeAl, CoAgFeAl deviate substantially. The compound CoMnYAl has total moment 4 $\mu_B/f.u.$ with $N_V = 22$, thus follows $M = |N_V - 18|$ rule.

Thus, the results on magnetic moments suggest that from CoX′Y′Si series only six compounds (CoNbMnSi, CoTcMnSi, CoRhMnSi, CoRuMnSi, CoZrFeSi, CoNbFeSi) and seven compounds (CoYMnAl, CoZrMnAl, CoRuMnAl, CoRhFeAl, CoPdMnAl, CoNbFeAl, CoTcFeAl) from CoX′Y′Al series with non-zero magnetic moments follow the $M = |N_V - 24|$ Slater-Pauling rule and are, therefore, potential half-metallic magnets. In the next sub-section, we discuss their electronic structures to confirm whether they indeed can be considered as new half-metallic magnets.

4.3.3 Electronic Structure

The origin of the half-metallic gap in $Co_2Y'Z$ compounds has been understood from the features in their electronic structures near the Fermi level. In these compounds, a gap in the spin down bands arise due to the hybridizations between the *d* orbitals of Co and Y′. The *d* orbitals of the Co atoms hybridize and create 5 bonding hybrids(2 e_g and 3 t_{2g}) which further hybridize with the d orbitals of the Y′ element resulting in 5 bonding and 5 anti-bonding hybrids. Five non bonding hybrids(2

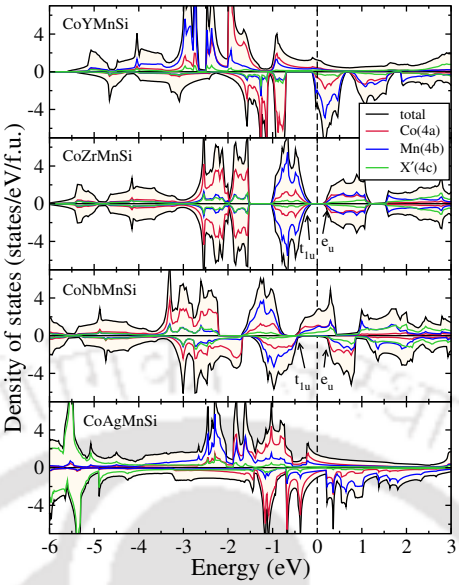

Figure 4.5: Spin polarized total and atom-projected densities of states for CoX′MnSi (X′= Y, Zr, Nb, Ag) compounds. The Ground states of these compounds are Type-I.

e_u and 3 t_{1u}) of the octahedral Co atoms can not hybridize with the d orbitals of tetrahedral Y′ atoms as shown in Fig. 1.4 in chapter 1. The gap in the spin down bands arise from these non bonding states[7]. For most of half-metallic $Co_2Y'Z$ compounds, the half-metallic gaps are due to the separations between the bottom of the conduction bands consisting of e_u states and the top of the valence bands made up of non bonding t_{1u} hybrids. This pattern of hybridization is largely followed in case of $X_2Y'Z$ compounds (X,Y′ are $3d$ transition metals) having Inverse Heusler arrangement whose magnetisations follow either $M = |N_V - 18|$ or $M = |N_V - 24|$ Slater-Pauling rules [59]. Since the structure Type-I and Type-II in the present study are the quaternary counterparts of the ternary $X_2Y'Z$ Inverse Heusler and regular Heusler compounds with one X atom replaced with an element from $4d$ series, respectively, it would be interesting to explore how the hybridization picture in case of $X_2Y'Z$ with all magnetic atoms from $3d$ series gets modified for the systems presented here. In the following the electronic structures of theses 36 quaternary compounds in their respective ground state structures are discussed series wise.

4.3.3.1 CoX′Y′Si compounds

The densities of states of CoX′Y′Si compounds in their respective ground state structures are presented in Fig.4.5, 4.6, 4.7 and 4.8. In Fig.4.5, we show the densities of states of four CoX′MnSi systems, which crystallise in structure Type-I. We find that

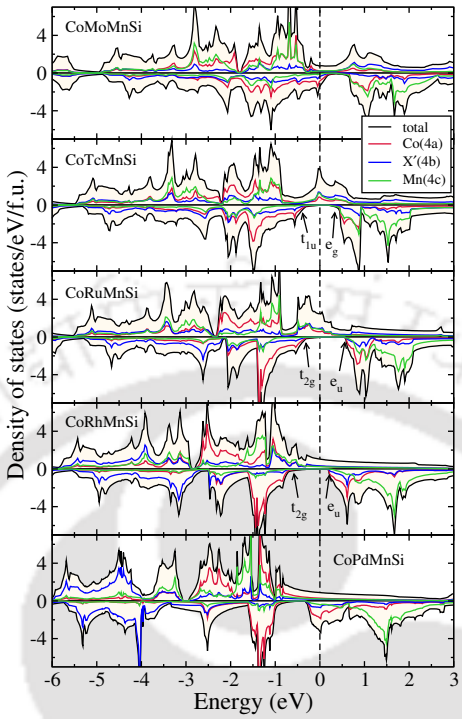

Figure 4.6: Spin polarized total and atom-projected densities of states for CoX′MnSi (X′= Mo, Tc, Ru, Rh, Pd) compounds. The ground states of these compounds are Type-II.

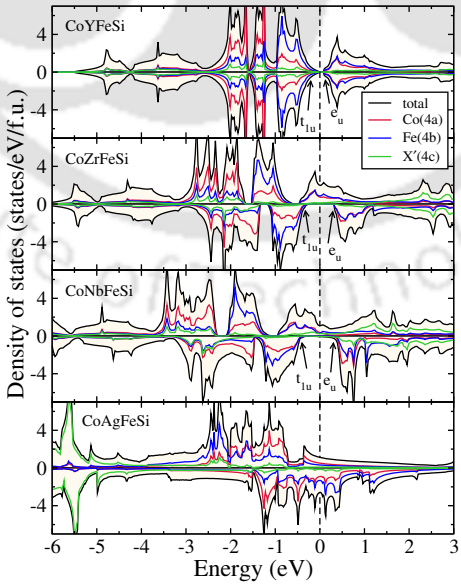

Figure 4.7: Spin polarized total and atom-projected densities of states for CoX′FeSi (X′= Y, Zr, Nb, Ag) compounds. The ground states of these compounds are Type-I.

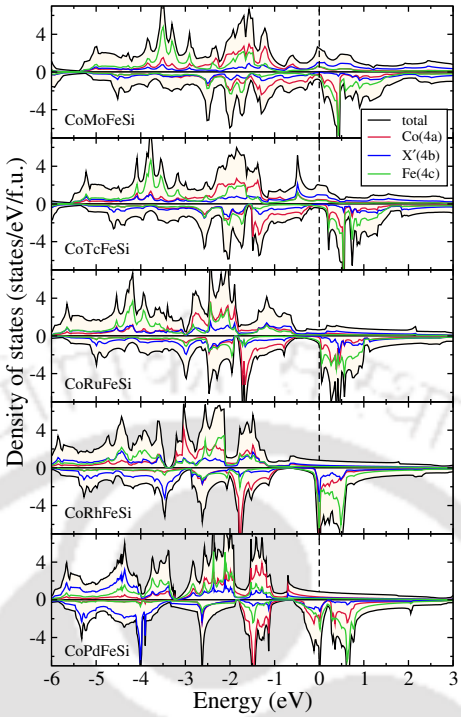

Figure 4.8: Spin polarized total and atom-projected densities of states for CoX′FeSi (X′= Mo, Tc, Ru, Rh, Pd) compounds. The ground states of these compounds are Type-II.

CoYMnSi is distinctly different from the other compounds with the same structure. In CoYMnSi, the spin up bands are nearly full along with a large gap in the spin down band but the Fermi level does not fall into the gap. Upon analysis of the fat bands (not shown here), we find that the origin of the gap in the spin down band is due to the splitting of bonding t_{2g} (due to hybridization between all transition metals) and nonbonding t_{1u} coming from Co and Mn. The separations between the bonding t_{2g} and nonbonding t_{1u} states are not enough to extend the gap till the Fermi level and lead to half-metallic behaviour. It may be noted that these features have been observed in ternary $X_2Y'Z$ compounds following $M = |N_V - 18|$ Slater-Pauling rule[59] and crystallising in Inverse Heusler structures. Thus, even with a quaternary compound having a $3d$ element replaced with a $4d$ element, the origin of the gap in the spin down band remains intact. The band structure of this compound presented in Fig.4.9 shows that the minority bands cross the Fermi level at the L point. If the states crossing the Fermi level can be pushed into the higher energy region by adjusting the lattice constant or by doping with another element so that the total number of electrons is reduced, a half-metallic gap can be opened in this compound. CoZrMnSi having exactly 24 electrons, opens a semiconducting gap due to well separated e_u and t_{1u} hybrids coming from the Co and Mn atoms.

Once again, this pattern is in agreement with that in ternary $X_2Y'Z$ compounds in Inverse Heusler structure following the same Slater-Pauling rule. CoNbMnSi, with one extra electron than CoZrMnSi, fills one out of two e_g states in the spin up band. The covalent nature of Co-Nb and Nb-Mn bonds enables this extra electron to be shared between Co and Mn. Therefore, the e_g states near the Fermi level are contributed mainly by Co and Mn. Since no electrons are accommodated in the down spin band, the semiconducting gap in spin down band remains. However, a very close inspection of the band structure (Fig.4.10) of this compound reveals that in the down spin channel, a band crosses the Fermi level only slightly at the X point. Thus, although the magnetic moment of this system is integer, in strict sense, this is not a half-metal but can be considered as near half-metal. A little change in the lattice constant or suitable doping may push these states to the higher energy level and bring out the half-metallicity.

In Fig.4.6, we show the densities of states of five compounds that have Type-II as their ground state structures. Although CoNbMnSi and CoMoMnSi differ by only one electron, the trend observed from CoZrMnSi to CoNbMnSi is not followed when the compounds crystallise in a different structure. Substantial re-distribution of states near the Fermi level happens as one goes from CoNbMnSi to CoMoMnSi. We now see that the extra electron, in comparison to CoNbMnSi, is not solely accommodated in the spin up band of CoMoMnSi, resulting in spin down states at the Fermi level, followed by a gap. As the number of electrons starts to increase when one goes from CoMoMnSi to CoRhMnSi, the extra electrons get accommodated in the spin up band, opening up a semiconducting gap at the spin down channel, and gradually filling up the spin up bands. As a result, CoTcMnSi, CoRuMnSi and CoRhMnSi exhibit half-metallicity with nearly 100% spin polarization as is shown in Table 4.4. In order to establish that they indeed are half-metals (Unlike CoYMnSi and CoNbMnSi), we show the band structure of CoRhMnSi in Fig.4.11. The origin of the half-metallicity in these compounds with structure Type-II is, however, do not reflect the established reason in case of ternary $X_2Y'Z$ compounds in regular Heusler structures [7]. Unlike Co_2MnSi, in the present case, the Co and the Mn atoms sitting in different symmetry sites, have energy levels closer to each other. As a result the bonding t_{2g} hybrids originating from Co, Mn and X′ atoms and the non-bonding t_{1u} hybrids due to the Co and X′ atoms lie extremely close; same happens for anti-bonding e_g and non-bonding e_u states. Consequently, top of the spin down valence bands in case of CoMoMnSi and CoTcMnSi are due to the t_{1u} states while bottom of the conduction bands are due to the e_g states. For CoRuMnSi and

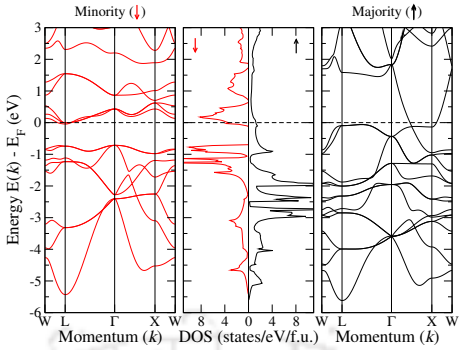

Figure 4.9: Spin-resolved band structure and density of states for CoYMnSi

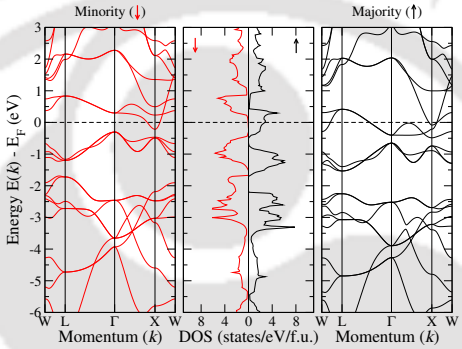

Figure 4.10: Spin-resolved band structure and density of states for CoNbMnSi

CoRhMnSi, they are due to the bonding t_{2g} and non-bonding e_u states respectively. The half-metallicity is destroyed in CoPdMnSi. Since the spin up is completely filled in CoRhMnSi, the extra electron in CoPdMnSi is accommodated in the spin down band, thus, pushing the e_u states towards lower energy and destroying half-metallic behaviour. The CoAgMnSi is significantly different as the d shell is completely filled in Ag, and the system crystallises in Type-I structure. The Ag states are now lying deep in energy. The Co and Mn hybridizations are weak, with a large spin polarization of Mn states.

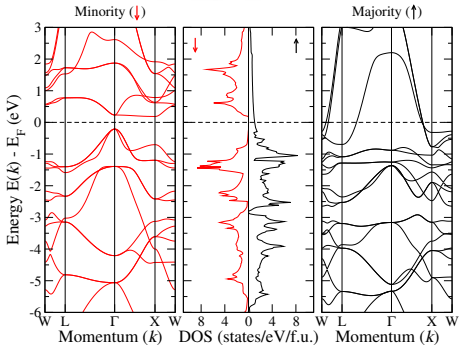

Figure 4.11: Spin-resolved band structure and density of states for CoRhMnSi

Thus, in the CoX′MnSi series, we can identify one compound as nearly half-metal, CoNbMnSi and three compounds as half-metals, CoTcMnSi, CoRuMnSi and CoRhMnSi, with integer moments following Slater-Pauling rule and nearly 100 % spin polarization (Table 4.3). In Fig.4.7 and 4.8 we show the densities of states of CoX′FeSi compounds in Type-I and Type-II structures respectively. A comparison with the densities of states of CoX′MnSi compounds reveal that the features are very similar. CoYFeSi has 24 valence electrons and turns out to be a semiconductor with zero moment, with the gap in both spin bands coming out from separations in t_{1u} and e_u non bonding hybrids of Co and Fe. One extra electron in CoZrFeSi, like CoNbMnSi, occupies the spin up e_u states, leading to a semiconducting gap in the down spin channel. This compound, thus, turns out to be a half-metal with 100% spin polarization (Table 4.3 and 4.4). One more electron in CoNbFeSi fills up more states in the spin up band. However, though it seems like that the gap in the spin down band is intact, a close up view shows that few spin down states are there at the Fermi level. Thus the spin polarization in this material is only 87%. None of the materials in Type-II structure qualify to be half-metals as all of them are characterised by the finite number of states at the Fermi level. As the number of electron increases while one goes from CoMoFeSi to CoRhFeSi, the extra electrons are accommodated in the spin down e_u bands, thus shifting the peak towards lower energy. For CoRhFeSi and CoPdFeSi, the peak in the spin down band falls exactly at the Fermi energy. This signifies structural instabilities in these compounds and may lead to ground state structures of different symmetries. This qualitative difference with respect to CoX′MnSi compounds is due to the extra electron of Fe in comparison to Mn. Since, like CoX′MnSi compounds in Type-II structure, the spin up bands in CoX′FeSi bands get filled, the extra electron in Fe is to be accommodated in the spin down band, leading to filling up states in the gap, and subsequent loss of possible half-metallicity.

Therefore, in the CoX′FeSi series, we find only CoZrFeSi to be half-metallic with integer magnetic moment, in accordance with Slater-Pauling rule, and high value of spin polarization. CoNbFeSi could be considered nearly half-metal. Suitable doping with an element which reduces the total number of electrons may push the states at the Fermi level towards higher energies and bring in a complete spin polarization in this compound. Among the compounds in Type-II structure, CoRuFeSi and CoRhFeSi have spin polarizations close to 90%. Experimentally, CoRuFeSi has been claimed to be a half-metal [236], however through indirect evidence. This discrepancy between theory and experiment could be resolved by more direct experimental

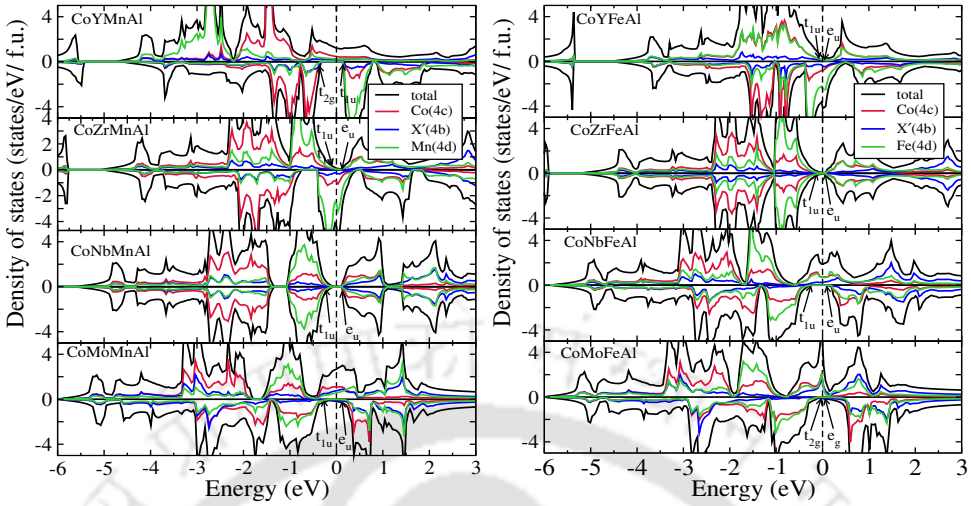

Figure 4.12: Spin polarized total and atom-projected densities of states for (**a**) CoX′MnAl and (**b**) CoX′FeAl (X′ = Y, Zr, Nb, Mo) compounds. The ground states of these compounds are T_I.

evidences like measurement of the spin polarization.

4.3.3.2 CoX′Y′Al compounds

In this sub-section we present the spin-polarized total and atom projected densities of states for all CoX′Y′Al compounds in their respective ground state structures, determine the compounds that are half-metals and compare them with the compounds in the Si series [187] to obtain a generalised picture across series of compounds. The densities of states of all compounds are presented in Fig 4.12 and Fig 4.13. Fig 4.12.(a) and Fig 4.12.(b) show the electronic structures of the compounds with structure type T_I. We find that CoYMnAl and CoNbFeAl are the two half-metals with a semiconducting gap in the spin down band, resulting in 100% spin polarization. CoZrMnAl and CoMoFeAl are another pair of compounds with high spin polarizations (more than 90%). Their electronic structures too have distinct features of a near gap in one of the spin bands. In case of CoYMnAl, the gap originates due to separation of t_{2g} (due to hybridization of all transition metal d orbitals) and t_u states (due to Co and Mn states). The pattern of hybridization is same as CoYMnSi [187]. However, CoYMnSi is not a half-metal as the t_u states were below the Fermi level. This presumably occurred as the the deeper lying Si states (compared to Al) pulled the d states downward in energy. In case of CoNbFeAl, the gap is created due to the separations of t_u and e_u states. CoZrFeAl, having exactly 24 electrons, have

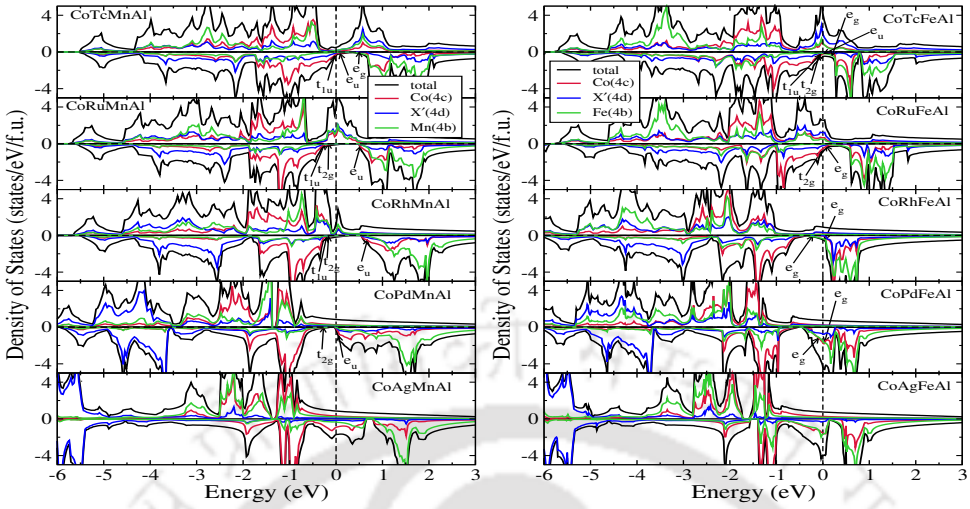

Figure 4.13: Spin polarized total and atom-projected densities of states for (**a**) CoX′MnAl and (**b**) CoX′FeAl (X′ = Tc, Ru, Rh, Pd, Ag) compounds. The ground states of these compounds are Type-II.

equal distributions among the spin channels, resulting in a zero moment and opening of gaps in both spin channels. The extra electron in CoNbFeAl is accommodated in the spin up band, thus retaining the semiconducting gap in the spin down band. One more electron in CoMoFeAl, fills the spin up states almost completely. However, the t_{2g} bands from the occupied part of the spectrum in the spin down channel move closer to the Fermi level producing small number of states there and reducing the spin polarization to 96%. This material, therefore, can be categorised as a "near half-metal" with high spin polarization. Among the other members of CoX′MnAl, we do not find any more half-metal due to the nature of band filling. CoZrMnAl has features very similar to CoZrFeAl in it's spin up densities of states. The highlight is a small near-gap bordered with t_u and e_u non-bonding states, while the extra electron as compared to CoYMnAl fills the spin down band. As a result, the system is a near half-metal with a spin polarization of 95%. CoNbMnAl has exactly 24 electrons, distributed evenly between two spin bands rendering this compound a non-magnetic semiconductor like CoZrFeAl. In fact the electronic structure of CoNbMnAl changes drastically with respect to CoZrMnAl. The densities of states of CoMoMnAl is quite similar to that of CoMoFeAl with a near-gap in the spin down band bordered by t_u and e_u hybrids. However, the position of the *e* states of CoMoMnAl is lower in energy in comparison to those of CoMoFeAl, producing states at the Fermi level thereby lowering of the spin polarization to 86%.

Among the compounds with structure type T_{II}, we do not find any half-metal in CoX′Y′Al series. Only CoRuMnAl can be considered a near half-metal as the spin polarization is 94%. Qualitatively this is distinctly different from the Si-series quaternary compounds where two half-metals were found [187]. Among the CoX′MnAl compounds with structure T_{II}, we find that in cases of four out of five compounds, there is indeed a gap in the spin down band. However, the gap does not extend through the Fermi level for any of the compounds. Once again this is due to the positions of the t bands, primarily, with respect to the Fermi levels. A comparison with Si-series compounds [187] reveals that the t bands in Si-series compounds were lying deeper in the spectrum, ostensibly due to the presence of deep lying Si states pulling the d bands of transition metals towards lower energies. In case of CoX′FeAl compounds, the extra electrons as one goes from T_I CoMoFeAl to CoTcFeAl and onwards, are accommodated in the spin down e bands, thus, pulling them closer to Fermi levels and destroying any possibility of having a half-metallic gap. Similar was the situation for CoX′FeSi series with structure type T_{II}. We present the spin-resolved band structures of three compounds CoYMnAl,CoZrMnAl and CoRuMnAl in figures 4.14- 4.16. These band structures corroborate that the first one is a half-metal while the other two are near half-metals. In case of CoYMnAl, we do see a clear separation of the valence and conduction bands with Fermi level falling in the gap. This is an indirect gap as the top of the valence band is at Γ point while the bottom of the conduction band is at L point. In case of CoRuMnAl, we find the top of the valence band protruding into the conduction region at Γ point. This implies that tuning the number of states in that small pocket of protrusion, by alloying suitably, the material may be converted to a half-metal. In case of CoZrMnAl, though the densities of states may give an impression of a zero gap majority spin channel, the band structure demonstrates it is not so. At the X point, there is band crossing from valence to conduction region across the Fermi level. Once again, little tuning by alloying or by suitable pressure to reduce the states protruding across Fermi level, can make this material a half-metal.

A comparison between CoX′Y′Al and CoX′Y′Si series show one interesting pattern: the densities of states for compounds with same N_V have striking resemblances. CoYMnSi and CoZrMnAl have similar features in the densities of states in both spin channels. So are CoZrMnSi-CoNbMnAl, CoMoMnAl-CoNbMnSi, CoYFeSi-CoZrFeAl, CoZrFeSi-CoNbFeAl, CoNbFeSi-CoMoFeAl. There are resemblances too in the spin down bands of CoMoMnSi-CoRuMnAl, CoTcMnSi-CoRhMnAl, CoRuMnSi-CoPdMnAl and CoRhMnSi-CoAgMnAl pairs, all with structure type

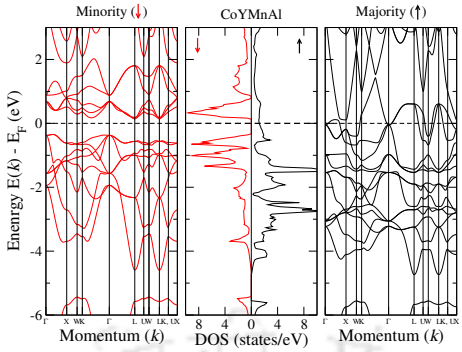

Figure 4.14: Spin-resolved band structure and density of states for CoYMnAl

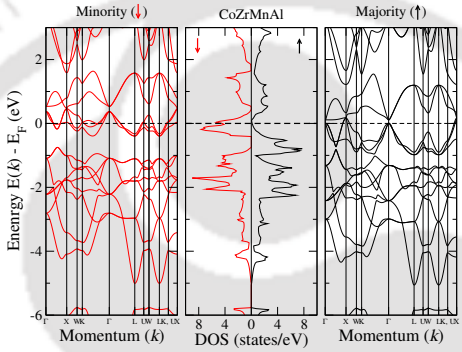

Figure 4.15: Spin-resolved band structure and density of states for CoZrMnAl

T_{II}. This can be easily understood by considering how the bands in one of the spin channels are filled continuously, depending upon N_V, across the series.

4.3.4 Trends in the local magnetic moments

In order to understand the trends in the total magnetic moments and the features in the densities of states, we look into the trends in the local magnetic moments associated with each species across the series studied. In Tables 4.4 and 4.5, results

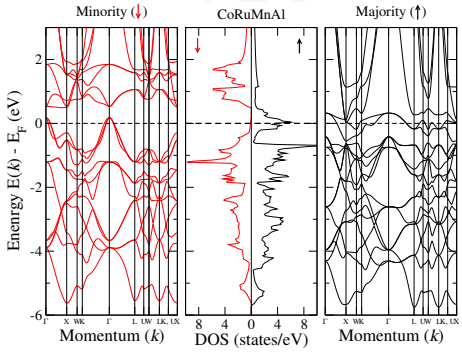

Figure 4.16: Spin-resolved band structure and density of states for CoRuMnAl

Table 4.4: Total and atomic magnetic moment of CoX′MnSi systems in $\mu_B/f.u.$. N_V is the number of valence electrons of the systems. M is the total magnetisation. P is the spin polarization.

Systems(T_I)	N_V	M	M_{Co}	M_{Mn}	$M_{X'}$	M_{Si}	P(%)
CoYMnSi	23	4.55	1.20	3.37	-0.09	0.00	46
CoZrMnSi	24	0.00	0.00	0.00	0.00	0.00	0
CoNbMnSi	25	0.99	0.71	0.30	0.00	0.00	96
Systems(T_{II})	N_V	M	M_{Co}	$M_{X'}$	M_{Mn}	M_{Si}	P(%)
CoMoMnSi	26	2.33	0.68	-0.58	2.27	-0.01	31
CoTcMnSi	27	3.00	0.67	-0.34	2.60	0.02	100
CoRuMnSi	28	4.00	0.92	0.13	2.94	-0.01	97
CoRhMnSi	29	5.00	1.21	0.43	3.33	-0.02	100
CoPdMnSi	30	4.90	1.11	0.21	3.47	-0.01	58
Systems(T_I)	N_V	M	M_{Co}	M_{Mn}	$M_{X'}$	M_{Si}	P(%)
CoAgMnSi	31	3.53	0.49	3.08	0.02	0.08	14

for total and the site projected magnetic moments for all the compounds in the CoX′MnSi and CoX′FeSi series, respectively, are presented. We find that the trend in the local magnetic moments is same for compounds irrespective of the series, as long as the structure type is same. The compounds having Type-I arrangement as their ground states and having valence electrons equal to or more than 24 follow the same trend in both series: both Co and Y′ element have low moments with Y′ having a vanishingly small moment. As number of electrons increase due to a different X′, the moments start to increase. The low exchange-splitting of the stronger magnet Y′ in both series can be understood from the neighbourhood around Y′ in Type-I structure. In Type-I structure, nearly non-magnetic $4d$ elements and Si form the neighbourhood around the Y′ element. This weakens the exchange field associated with the Y′ element and prevents building up of local moment in Y′. When an extra electron is added to the system due to a different $4d$ element, the covalent bonding between Co and Y′ makes them share the electron, resulting in nearly uniform increase in spin polarizations of both Co and Y′. The notable differences to this trend are found in cases of CoYMnSi, CoAgMnSi and CoAgFeSi, where both Mn and Fe have large spin polarizations. In these cases, the lattice constants of the systems are significantly larger in comparison to the other compounds with the same structure. Due to this, the Y′ atoms hybridize very little with the other atoms, thus, almost retaining their atomic moments. The most suitable example of this is CoYMnSi where the lattice constant is the largest and the Mn atom has a

Table 4.5: Total and atomic magnetic moment of CoX′FeSi systems in $\mu_B/f.u.$. N_V is the number of valence electrons of the systems. M is the total magnetisation. P is the spin polarization.

Systems(T_I)	N_V	M	M_{Co}	M_{Fe}	$M_{X'}$	M_{Si}	P(%)
CoYFeSi	24	0.00	0.00	0.00	0.00	0.00	0
CoZrFeSi	25	1.00	0.56	0.62	-0.12	0.00	100
CoNbFeSi	26	1.99	1.12	0.99	-0.06	0.02	87
Systems(T_{II})	N_V	M	M_{Co}	$M_{X'}$	M_{Fe}	M_{Si}	P(%)
CoMoFeSi	27	2.83	0.84	-0.33	2.31	0.04	59
CoTcFeSi	28	3.89	1.01	0.15	2.68	0.03	64
CoRuFeSi	29	4.66	1.26	0.53	2.87	0.01	87
CoRhFeSi	30	4.90	1.44	0.57	2.87	0.01	89
CoPdFeSi	31	4.00	1.08	0.07	2.84	-0.01	73
Systems(T_I)	N_V	M	M_{Co}	M_{Fe}	$M_{X'}$	M_{Si}	P(%)
CoAgFeSi	32	2.71	0.69	2.14	0.03	-0.06	41

moment greater than 3 μ_B. In case of systems with Type-II arrangement, Co and Y′ are nearest neighbours. The strong exchange field associated with them leads to large exchange splittings in the Y′ components. This gives rise to sizeable magnetic moments on Y′ and Co sites. The local magnetic moments systematically increases as the total number of electrons increase with change of X′ element. The changes in Fe moment is small compared to that in Mn as the number of electrons increase. This indicates that the Fe moments are more localised than the Mn moments. This, in turn, implies that the effects of localisation are to be included for compounds having Fe as has been mentioned earlier. Due to the strong exchange fields in the Type-II structures, the 4*d* elements too get slightly polarized.

In Tables 4.6 and 4.7 we present the total and site projected magnetic moments of CoY′MnAl and CY′FeAl compounds, respectively. Analysing the trends as a function of N_V and structure type, we find near identical behaviour with CoX′Y′Si series [187]. Across the series and structures, the total moment continuously increases with N_V for compounds with $N_V > 24$ and upto 29. This is understood from the hybridization and band filling picture discussed in the previous sub-section. We find that the continuous building up of the moment is due to building up of Co and Y′ moments. This is more prominent for compounds in structure type T_{II} where the moments on the 3*d* elements build up due to they being nearest neighbours leading to large exchange splitting primarily on Y′ elements. The changes in Fe moments

Table 4.6: Total and atomic magnetic moment of CoX′MnAl systems in $\mu_B/f.u.$. N_V is the number of valence electrons of the systems. M is the total magnetisation. P is the spin polarization.

Systems(T_I)	N_V	M	M_{Co}	M_{Mn}	$M_{X'}$	M_{Al}	P(%)
CoYMnAl	22	4.00	0.80	3.41	-0.13	-0.04	100
CoZrMnAl	23	0.98	0.10	0.94	-0.07	-0.01	95
CoNbMnAl	24	0.00	-0.00	0.00	-0.00	-0.00	0
CoMoMnAl	25	0.91	0.82	-0.09	0.22	-0.01	86
Systems(T_{II})	N_V	M	M_{Co}	$M_{X'}$	M_{Mn}	M_{Al}	P(%)
CoTcMnAl	26	2.11	0.57	-0.62	2.21	-0.02	20
CoRuMnAl	27	3.02	0.53	-0.13	2.66	-0.01	94
CoRhMnAl	28	4.05	0.84	0.25	3.07	-0.03	77
CoPdMnAl	29	5.00	1.27	0.25	3.48	-0.03	39
CoAgMnAl	30	4.59	1.07	0.03	3.48	-0.03	33

with N_V are smaller compared to Mn moments, implying Fe moments are more localised. The moments on the $4d$ compounds are small. They gain moment due to polarizing effect of strong exchange fields of $3d$ elements. For compounds with $N_V >$ 29, the total moments start decreasing with increasing N_V. The corresponding compounds are CoPdFeAl, CoAgFeAl and CoAgMnAl. The electronic structure reveals that the Pd states are deep in energy and both spin bands are nearly filled. Since it has a filled d shell, this is only natural that there will be a relatively weak exchange field associated with Pd. As a result, the moment on Pd drastically reduces compared to the X′ element in the preceding compound in the series. This brings the overall moment down. Ag has s states in it's valence band, which are further deep in energy leaving no scope of any spin polarization of the X′ component. Therefore, even though the Co and Y′ moments do not change significantly, the moments of CoAgFeAl and CoAgMnAl decrease with respect to the preceding compounds in their respective series.

The exchange splittings in compounds with structure type T_I are smaller, an artefact of the neighbourhood around the $3d$ components. The exception is CoYMnAl where Mn has a large moment. A significantly large lattice constant in this compound is a hindrance for Mn to hybridize with the other components leading to it retaining it's local moment in the atomic state. The densities of states of this compound is consistent with this assessment. One can see that in the spin up channel, the Mn states are deep lying and are well separated from the Co states, along with the fact that Mn down band is nearly empty.

Table 4.7: Total and atomic magnetic moments of CoX′FeAl systems in $\mu_B/f.u.$. N_V is the number of valence electron of the systems. M is the total magnetisation. P is the spin polarization.

Systems(T_I)	N_V	M	M_{Co}	M_{Fe}	$M_{X'}$	M_{Al}	P(%)
CoYFeAl	23	0.86	0.04	0.93	-0.04	-0.02	84
CoZrFeAl	24	0.00	0.00	-0.00	0.00	0.00	0
CoNbFeAl	25	1.00	0.62	0.56	-0.09	-0.01	100
CoMoFeAl	26	1.93	1.14	0.77	0.10	-0.01	96
Systems(T_{II})	N_V	M	M_{Co}	$M_{X'}$	M_{Fe}	M_{Al}	P(%)
CoTcFeAl	27	3.05	0.77	-0.14	2.43	0.01	78
CoRuFeAl	28	4.20	1.14	0.40	2.77	-0.01	51
CoRhFeAl	29	4.86	1.40	0.55	3.00	-0.02	32
CoPdFeAl	30	4.41	1.37	0.15	2.92	-0.02	72
CoAgFeAl	31	3.82	1.20	-0.02	2.74	-0.03	69

4.3.5 Exchange coupling and Curie temperature

In this section, we present the results on inter atomic effective exchange coupling constant(J_{eff}) and Curie temperatures T_c for CoX′Y′Z compounds in all the series. The variations of the Curie temperatures with different X′ atoms i.e. with changes in the valence electron numbers are shown in figures 4.17 and 4.20. First we'll consider the CoX′Y′Si series. From Fig.4.17 we find two compounds, CoRhMnSi and CoRuFeSi, having very high Curie temperatures, 1012K and 1052K respectively. The experimental Curie temperature for CoRuFeSi is 867K[236]. Our results are overestimated in comparison to the experimental one as we have used mean field approximation. Apart from these two, there are few other compounds with Curie temperatures between 600K and 800K(Fig.4.17). The results show that the variations in the Curie temperatures can be classified in two distinct regions based on the structure types in which the compounds crystallise. In each region, however, the variations are not uniform. This is true for the two different series (Y′ = Mn, Fe) also. For Type-I structures, the Curie temperatures are low. For Type-II structures they increase with N_V steadily upto a critical point N_V after which it steadily decreases. The maximum Curie temperature in both CoX′MnSi and CoX′FeSi are, therefore, obtained when N_V.

In order to explain such behaviour of Curie temperatures, we take recourse to the calculated inter-atomic magnetic exchange coupling parameters, and the features in the densities of states. In Fig.4.18 and 4.19, we show the various effective

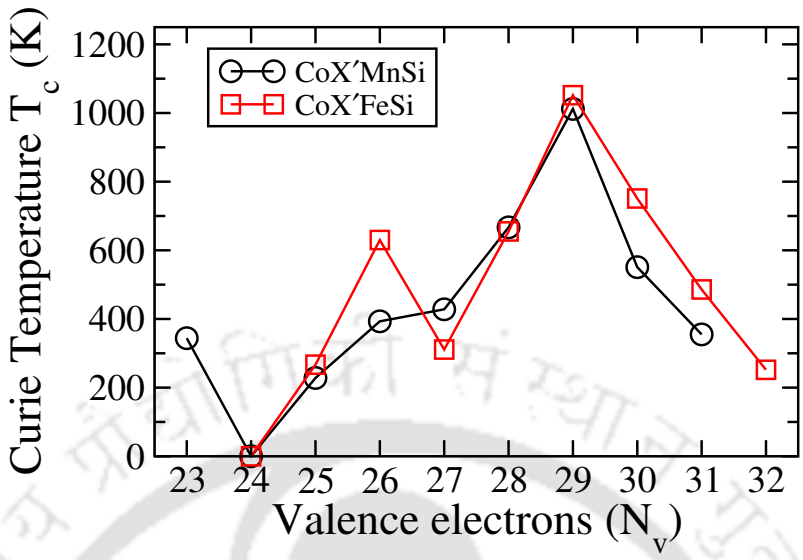

Figure 4.17: Calculated Curie temperature with total number of valence electron for CoX′Y′Si series.

exchange coupling parameters (J_{eff}). We find that the Co-Co, Co-Y′ and Y′-Y′ effective exchange parameters are the dominant ones. The other exchange interactions are very weak and do not contribute to the understanding of the trends in the Curie temperature. Analysing the results for exchange interactions in compounds with two different structure types, we see that Co-Y′ interaction is the dominant one irrespective of the structure type. In general, the Co-Y′ effective exchange parameters for compounds in structure Type-II are significantly larger than for those in structure Type-I. The weaker Co-Y′ interactions for compounds in structure Type-I are due to the fact that Co and Y′ interactions are mediated via the weak magnet X′ in structure Type-I while the interactions are direct in structure Type-II. A notable exception to this trend is found in case of CoNbFeSi which has structure Type-I as the ground state but the Co-Y′ exchange parameter is larger than that in CoMoFeSi, the first compound in the series having structure Type-II as the ground state. That the variations in the Co-Y′ exchange parameter decides the variations in the Curie temperature is visible upon comparing the trends of both quantities. Thus, a stronger Co-Y′ exchange parameter in CoNbFeSi leads to a higher Curie temperature in comparison to CoMoFeSi, in spite of the former crystallising in structure Type-I and thus, having an indirect Co-Y′ exchange. The other exchange parameters have similar variations qualitatively across the two series, and they only contribute to the absolute values of the Curie temperatures. The prominent ones except Co-Y′ are the X′-Y′ and the intra-atomic Y′-Y′ interactions. The exceptional behaviour of

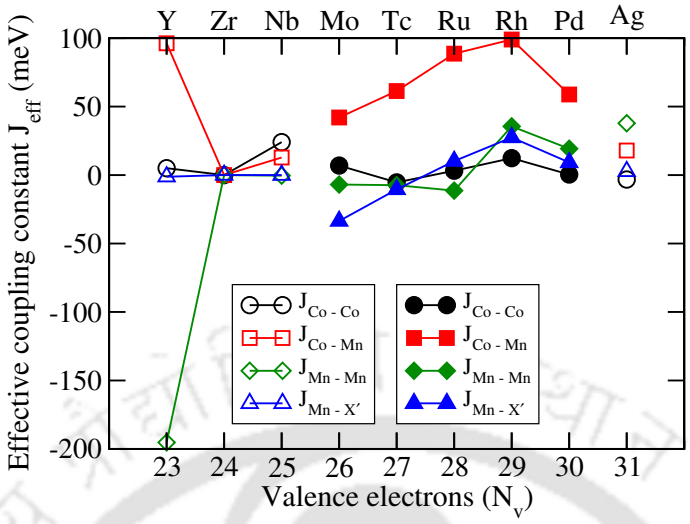

Figure 4.18: Effective exchange coupling constant for CoX′MnSi compounds. Open symbols: Type-I structure, Filled symbols: Type-II structure

CoYMnSi in the context of total magnetic moment is also observed here. In case of this compound, the Co-Mn interaction strength is of the same order as that of CoRhMnSi, the compound having the maximum value of Curie temperature in the series. However, this strong ferromagnetic Co-Y′ interaction is completely compensated by a stronger Mn-Mn interaction, which is antiferromagnetic in nature, leading to a smaller value of Curie temperature.

The result on Curie temperatures revel another interesting fact. We find that the half-metals with 100% spin polarizations having structure Type-II have high Curie temperatures(428K for CoTcMnSi and 1012K for CoRhMnSi) while the only half-metal with 100% spin polarization having structure Type-I, CoZrFeSi, has a rather low Curie temperature of 267K. This suggests that the half-metallicity cannot be always correlated with occurrence of high Curie temperature. As the discussion in the preceding paragraph suggest, the magnitude of Curie temperature is decided by the select exchange interaction and their magnitudes, which in turn are dependent upon the structure types. Thus, the crystal structure plays the most important role influencing the magnitude of the Curie temperatures.

The question that remains to be answered is that why the J_{eff} values have the maximum at N_V followed by a decrease upon increase in N_V. Kubler *et al* [110], in their investigations into a similar behaviour in the ternary $Co_2Y'Z$ compounds found a similar behaviour in the variations of the Curie temperatures with N_V. They attributed this to the changes in the behaviour of the "Exchange average", the average of exchange energies associated with low temperature spin excitations.

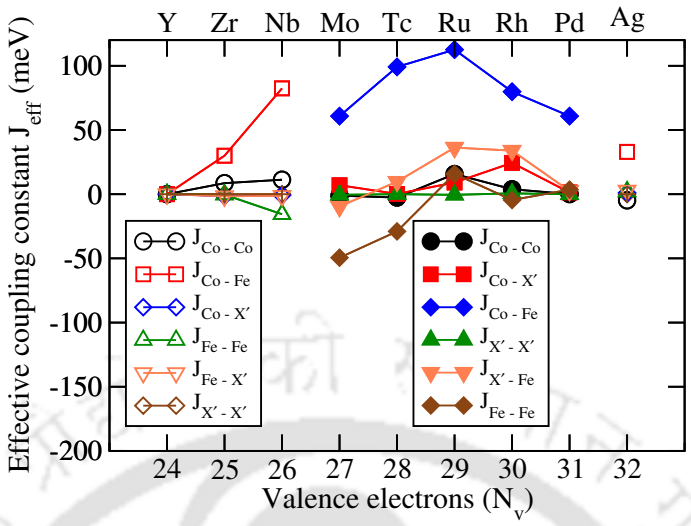

Figure 4.19: Effective exchange coupling constant for CoX′FeSi compounds. Open symbols: Type-I structure, Filled symbols: Type-II structure

This variation in the "Exchange average" is related to the availability of spin down states below Fermi level. They showed that a gap in the spin down bands starting below Fermi level and extending beyond it would lead to a larger value of "Exchange average" and consequently a larger Curie temperature. Extending this idea to the compounds in the present work, we find that the unavailability of the states in the spin down bands gradually increases as N_V increases and is maximised at $N_V = 29$. Thus the "Exchange average" is maximised at $N_V = 29$ and we see its manifestations in the maximisations of the J_{eff}. Upon further increase of N_V, we see states in the spin down bands at the Fermi level. This reduces the "Exchange average" and the J_{eff} and Curie temperatures decrease beyond $N_V = 29$.

The results on J_{eff} and T_c for the CoX′Y′Al compounds considered in our study are presented in Figures 4.20-4.22. Fig 4.20 shows the variations of T_c with different X′ atoms *i.e.* with changes in N_V for CoX′Y′Al. The two half-metals CoYMnAl and CoNbFeAl have T_c of 430K and 232K respectively. Our result for CoYMnAl agrees well with the value of 482K obtained by Rahmoune *et al*[239]. Looking at Fig 4.20 we find that qualitative variations in T_c depends on the ground state structure type of the compounds in the series implying that the arrangements of the atoms in crystallographic sites play a significant role in deciding T_c as well. We find that in general, compounds with structure type T_{II} have T_c higher than those of compounds with structure type T_I. The highest T_c for both series is obtained at N_V=29, a result exactly same as the quaternary Si-series [187]. Similar to CoX′Y′Si

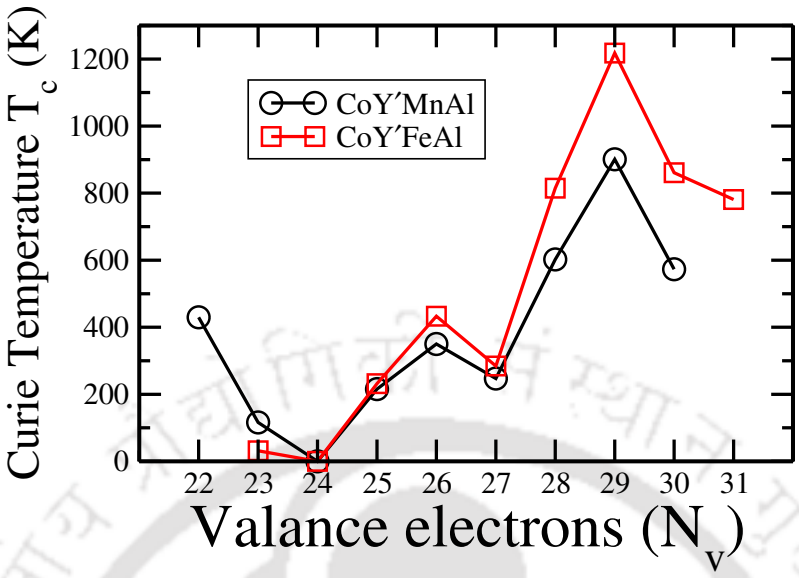

Figure 4.20: Calculated Curie temperature with total number of valence electron for CoY′X′Al series.

series[187] we find that, Co-Y′ J_{eff} are the dominant interactions and the variations in T_c closely follow the variations in this particular effective exchange parameter. Other prominent exchange parameters are for Co-Co, Y′-Y′, Y′-X′ ones. As was seen in Si-based compounds [187], Co-Y′ interactions for compounds in structure type T_{II} are notably stronger than those of compounds in structure T_I. The reason for this is that, Co-Y′ interaction is direct in T_{II} whereas weak magnet X′ is the mediator for Co and Y′ interactions in T_I.

Though qualitatively the variations of T_c across series and structure types in CoX′Y′Al are exactly same as that in CoX′Y′Si compounds, there are quantitative differences. In general, CoX′FeAl (CoX′MnAl)have higher (lower)T_c than CoX′FeSi(CoX′MnSi). The difference is prominent in compounds with T_{II} structure type. In CoX′FeAl compounds with structure T_{II}, we find that Co-Fe and Fe-X′ interactions are stronger than those in CoX′FeSi compounds. This along with more ferromagnetic Fe-Fe interactions in Al-series compounds lead to higher T_c in them. In the CoX′MnZ compounds, we find that in Si-series, the dominant Co-Mn interactions are stronger than that in Al-series; the other prominent interactions being of comparable strength. This, then, decides the quantitative differences in T_c of the two series.

Finally the reason behind T_c being maximum at $N_V = 29$ across the series irrespective of Y′ and Z element can be explained in terms of "Exchange average"[110], exactly the way was done for Si series [187]. Inspecting the densities of states for

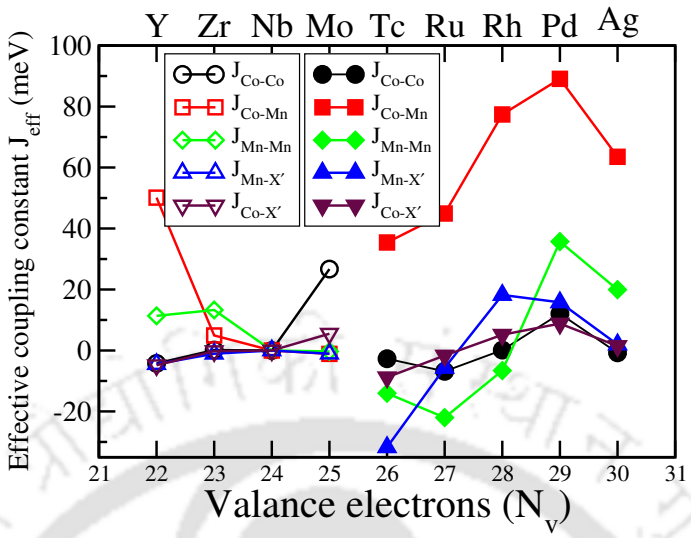

Figure 4.21: Effective exchange coupling constant for CoX′MnAl compounds. Open symbols: structure type T_I, Filled symbols: structure type T_{II}.

compounds with structure type T_{II}, we see that lower the value of the number of states in spin down channel at Fermi level in the compounds with structure Type-II, higher is the "Exchange average" and subsequently the T_c. For both Al and Si-series quaternary compounds we see that as N_V increases, the number of states at the Fermi level keeps decreasing and that in turn increases the "Exchange average" and T_c upto a particular N_V. The subsequent fall of T_c can also be attributed to the fall in "Exchange average" with increasing N_V as the electronic structure shows a fall in the number of available states at the Fermi level in spin down bands. Thus we conclude that the significant similarity in the qualitative trends in the variations of T_c across Y′ and Z series of Co and 4*d* transition metal based quaternary Heuslers can be correlated to the similarities in the trends in the variations in their electronic structures which is dependent upon structure types and N_V.

4.3.6 Qualitative comparison with quaternary Heuslers having all magnetic components 3*d* transition metals

Our results in this chapter provide significant insights into the roles of atomic arrangement, the number of valence electrons, and the hybridizations towards achieving half-metallic behaviour. In order to gain deeper insights and evolve a generalised picture of half-metallicity in quaternary Heusler compounds, we now make a qualitative comparison between the series where the only difference is that X′ a 4*d* element in one and a 3*d* element (one of Sc to Cu in the row of 3*d* transition metals in the

Table 4.8: Lattice constants, structure type,magnetic moments and electronic behaviour of quaternary CoX′Y′Z (X′ = Sc to Cu ; Y′ = Mn , Fe and Z = Al, Si) compounds. The sources of the information are explicitly mentioned.

Systems (Type-I)	Lattice constant(Å)	Structure type	M ($\mu_B/f.u.$)	Whether Half-metal(HM) or metal (M) or semiconductor (SC)
CoScMnAl	-	-	-	-
CoTiMnAl	5.86	T_I	0.98	HM[61]
CoVMnAl	5.80	T_I	0	SC[242]
CoCrMnAl	5.76	T_I	1	HM[242]
CoMnMnAl (Mn_2CoAl)	5.73	T_{II}	1.99	HM[83, 196]
CoFeMnAl	5.79	T_I	3	HM[242]
CoCoMnAl (Co_2MnAl)	5.7	T_I	4.023	M[209]
CoNiMnAl	5.79	T_I	5	HM[242]
CoCuMnAl	-	-	-	-
CoScFeAl	-	-	-	-
CoTiFeAl	5.85	T_I	0	SC[242]
CoVFeAl	5.73	T_I	0.97	HM[61]
CoCrFeAl	5.70	T_I	2	HM[61, 63]
CoMnFeAl	5.79	T_I	3	HM[242]
CoFeFeAl(Fe_2CoAl)	5.701	T_{II}	5	M[70]-
CoCoFeAl(Co_2FeAl)	5.7	T_I	4.99	M[210]
CoNiFeAl	-	-	-	-
CoCuFeAl	-	-	-	-
CoScMnSi	-	-	-	-
CoTiMnSi	5.73	T_I	0	SC[61]
CoVMnSi	5.65	T_I	0.97	HM[61]
CoCrMnSi	5.65	T_I	2	HM[63]
CoMnMnSi(Mn_2CoSi)	5.62	T_{II}	3 0	HM[196, 212]
CoFeMnSi	5.66	T_I	4	HM[242] SGS[63]
CoCoMnSi(Co_2MnSi)	5.63	T_I	5	HM[209]
CoNiMnSi	5.67	T_I	4.69	M[243]
CoCuMnSi	-	-	-	-
CoScFeSi	-	-	-	-
CoTiFeSi	5.73	T_I	1	HM[61]
CoVFeSi	5.66	T_I	1.97	HM[61] SGS[63]
CoCrFeSi	5.63	T_I	3	HM [242]
CoMnFeSi	5.66	T_I	4	HM[242]
CoFeFeSi(Fe_2CoSi)	5.60	T_{II}	4.96	M[221]
CoCoFeSi(Co_2FeSi)	5.62	T_I	5.48	M[225]
CoNiFeSi	-	-	-	-
CoCuFeSi	-	-	-	-

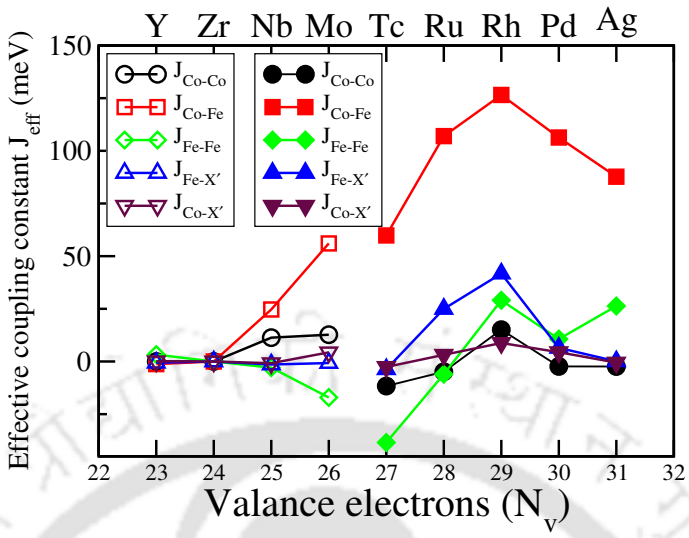

Figure 4.22: Effective exchange coupling constant for CoX′FeAl compounds. Open symbols: structure type T_I, Filled symbols: structure type T_{II}.

periodic table) in another. In Table 4.8, we have compiled the available results on the quaternary compounds CoX′Y′Z with main group element either Si or Al, Y′ either Mn or Fe and X′ one of the 3*d* transition metals. From the compiled results we find that the in the quaternary family with all magnetic components 3*d* transition metals, there are significantly higher number of materials reported to be half-metals or even SGS [61, 63, 116]. Since the results in the present work, that of Reference [187] and [168] on ternary and quaternary Heusler compound series with one of the magnetic element a 4*d* transition metal indicate that N_V is a significant predictor of half-metallic behaviour, we first compare the electronic properties, in the context of half-metallic behaviour, of compounds across the families with same N_V.

We first observe that there are four pairs of half-metals (with same N_V), one each from two families, one with X′ a 3*d* element and another with X′ the isoelectronic 4*d* element. They are CoNbFeAl-CoVFeAl, CoZrFeSi-CoTiFeSi, CoTcMnSi-Mn_2CoSi and CoRhMnSi-Co_2MnSi. Strictly speaking the X′ a 3*d* element contingent in the last two pairs is not a quaternary compound. The ground state structures of all four compounds in the first two pairs are T_I while that of the third pair is T_{II}. In the fourth pair, CoRhMnSi has T_{II} structure but Co_2MnSi crystallises in T_I. There are another five pairs of compounds having nearly identical behaviour in the context of half-metallicity. In the pair CoMoFeAl-CoCrFeAl, CoMoFeAl is a near half-metal while CoCrFeAl is a SGS; both compounds in the pair CoNbMnSi-CoVMnSi are near half-metals. In the pairs CoZrMnAl-CoTiMnAl, CoRuMnAl-CoFeMnAl, CoRuMnSi-CoFeMnSi, the constituents with 4*d* element as X′ are all near half-

metals while the other ones are all half-metals. Apart from the last two pairs, the components in the other three pairs have identical ground state structures, T_I. CoRuMnAl and CoRuMnSi crystallise in T_{II} while CoFeMnAl and CoFeMnSi have T_I as their ground states.

There are another eight pairs of isoelectronic compounds whose electronic behaviours are different. In each of these pairs compounds with 4*d* elements are metals while the ones with all magnetic components beingf 3*d* transition metals are half-metals. These pairs are CoNiMnAl-CoPdMnAl, CoMnFeAl-CoTcFeAl, CoCrFeSi-CoMoFeSi, CoMnFeSi-CoTcFeSi, CoCrMnSi-CoMoMnSi, CoVFeSi-CoNbFeSi, CoCrMnAl-CoMoMnAl and $CoMn_2Al$-CoTcMnAl. The constituents of the first five pairs have different ground state structures; the compounds with all 3*d* magnetic components have structure type T_I while the ones with one 4*d* constituent are in structure type T_{II}. Out of the remaining three pairs, the constituents of the first two pairs crystallise in T_I while the last one crystallise in T_{II}.

These observations clearly indicate that N_V can be considered a predictor for half-metallic behaviour of quaternary Heuslers as long as structure types are same as that of existing isoelectronic half-metals. This was also observed in cases of ternary Heusler compounds [168]. The reason can be traced back to the similarities in the electronic structures and band-fillings for isoelectronic compounds across various different series with transition metal elements from different rows of the periodic table. Although the systematic analysis of evolution of properties with changes in N_V through an analysis of evolutions in the partial densities of states providing a clear picture of element-specific hybridizations is not available in literature for quaternary compounds with all magnetic elements from 3*d* row of periodic table, one can intuitively conclude that since the hybridizations in structure type T_I compounds mostly come from the 3*d* elements, the similarities in electronic structures for isoelectronic compounds across series and thus in the electronic properties like half-metallic behaviour are only natural consequences.

Another observation regarding the parents and daughter compounds in CoX′Y′Z considered here is quite insightful. None of the quaternary daughters predicted to be half-metals among the compounds in these four series have both ternary parents as half-metals. We find that out of the five half-metals CoYMnAl, CoNbFeAl, CoTcMnSi, CoRhMnSi and CoZrFeSi found in the quaternary series considered, Co_2YAl is a non-magnetic semiconductor, Mn_2YAl a metal; Co_2NbAl is a half-metal, Fe_2NbAl a non-magnetic semiconductor; both Co_2TcSi and Mn_2TcSi are normal metals; Co_2RhSi a metal while Mn_2RhSi a half-metal, Co_2ZrSi a half-metal and while

Fe_2ZrSi is a non-magnetic semiconductor. This indicates that the half-metallicity in CoNbFeAl and CoZrFeSi might be coming solely from the half-metallicity of one of the ternary half-metal parents. This is because the other parent is a non-magnetic semiconductor and thus replacing one Fe with a Co in each one of them must have filled one of the spin bands rendering it metallic while the other spin band remains semiconducting. The origin of half-metallicity in the other three compounds would be indeed intriguing as there are three different combinations in their ternary parents: metal-metal, metal-non-magnetic semiconductor and metal-half-metal. This aspect is worth investigating in future.

4.3.7 Conclusions

We have made a detailed investigations into the structural, electronic and magnetic properties of 36 quaternary Heusler compounds spanning the series CoX′Y′Z, where X′ stand for 9 elements with 4*d* electrons in their valence shells, and Y′ being Fe and Mn, the two strong magnets with unfilled 3*d* electrons in their outer shells and Z being Al and Si. Our search for new half-metallic ferromagnets from quaternary series with both 3*d* and 4*d* electrons in the same compound throws up interesting facts. We find that although there are thirteen compounds with integer values of their magnetic moments, all of them do not qualify to be half-metals or even near half-metals.

We find that three compounds CoTcMnSi, CoRhMnSi and CoZrFeSi can be identified as truly half-metals from CoX′Y′Si series. However, there are few other compounds like CoYMnSi, CoNbMnSi, CoRuMnSi and CoNbFeSi, which can be identified as near half-metals. Application of moderate pressure or controlled doping in a way that the total number of electrons in these systems reduce, should make these systems half-metallic too. We found two half-metallic ferromagnet CoYMnAl and CoRuMnAl with 100% spin polarization and three "nearly" half-metallic compounds with a gap like feature in minority spin channel and spin polarization greater than 90% in CoX′Y′Al series.

We provide an understanding of the types of site occupancies observed in the compounds of the two series in terms of relative values of electronegativities of Co, X′ and Y′. This explanation towards the preferred structure types of quaternary Heusler compounds addresses ground state structure types of large numbers of compounds in the quaternary family outside of the two series studied in this work. The trends in the magnetic properties and the electronic structures of these compounds

are found to be due to the neighbourhood of the magnetic atoms, which differ between the two preferred structure types. Consequently, the magnetic interactions between the stronger magnetic elements, Co and Y′, get modified as the structure type or the element X′ changes. We find that the magnetic exchange interactions between Co and Y′ atoms are the strongest and their behaviour with number of valence electrons is responsible for the trends in the Curie temperature, another quantity of interest for assessing a half-metal in the context of its potential for spintronics applications. We make an assessment of the variations in the magnetic exchange averages across the compounds from the features in their densities of states and conclude that the variations of the Curie temperatures can be understood from it. The compounds crystallising in Type-I structures have lower Curie temperatures due to weaker exchange interactions between the constituents, making the average exchange lower. The compounds with structure Type-II have higher Curie temperature due to stronger Co-Y′ exchange interactions which make the average exchange stronger. In both series we find that the maximum Curie temperature is achieved for compounds with N_V=29, and in general high values of Curie temperatures are obtained if the number of valence electrons are in a range of 28-30.

Accordingly, out of the compounds identified as half-metals in the present study, CoTcMnSi and CoRhMnSi have significantly high values of Curie temperature and hence these two can be considered as new functional materials for magnetic applications. If CoNbFeSi, CoTcFeSi,CoRuFeSi and CoRhFeSi turn out to be half-metals under moderate pressure, they also would fall into this category as they too have high values of Curie temperature.

This work offered a broader perspective to the physics of half-metallic quaternary Heuslers. We systematically compared the results on CoX′Y′Al series with the results on another series with same Y′ and X′, CoX′Y′Si [187]. We found that as long as N_V and structure types are the same, the electronic and magnetic properties of the compounds from the two series are nearly identical. The minor changes somewhat affecting the possibilities of half-metallic behaviour were due to the changes in the positions of the 3*d* states with respect to the Fermi levels, an artefact of the deeper lying Si states pulling the *d* bands towards lower energies as compared to the Al states. We further compared the impacts of the X′ component on half-metallic behaviour by comparing the results of isoelectronic quaternary pairs where X′ is a 3*d* element in one case, and 4*d* in the other. We once again observed that unless the structure types are identical, it is not possible to obtain half-metallicity in isoelectronic compounds from both series. Thus, rather than the chemical element

X′, the N_V and the structure types are more important in determining half-metallic behaviour in quaternary Heuslers. We attributed this to the general picture of hybridizations between the transition metal atoms which were found to be transferrable across various quaternary series. Thus, manipulating the N_V by substitution at the Z site may transform near half-metals to half-metals with 100% spin polarization as the hybridization between the transition metals is not expected to be affected substantially due to such substitution. Finally, we investigated the transferability of the half-metallic properties of parent ternary Heuslers making up a daughter quaternary compound. We found that neither of the quaternary Heusler compounds considered here showing half-metallic behaviour have half-metallicity in both parent ternary compounds. This poses an interesting open question regarding the emergence of half-metallic behaviour through substitution at select sites which will be addressed in the future. This work, therefore, provides a number of useful insights into evolving a broader picture of half-metallicity which can help predict and design future half-metals for spintronics applications. The importance of this work is that instead of focusing on prediction of new half-metals from a new series of compounds, which is what available mostly in literatures, it makes an attempt to address the microscopic physics governing a large group of materials in a systematic and coherent way.

Chapter 5

Site dependent substitution and half-metallic behaviour in Heusler compounds: a case study for Mn_2RhSi, Co_2RhSi and CoRhMnSi

5.1 Introduction

In the last two chapters we have extensively studied ternary and quaternary compounds with one 4*d* element [168, 187, 228]. Our primary goal was to understand the basic trends in electronic and magnetic properties of ternary and quaternary Heusler compounds across different series and their connections to the half-metallic behaviour. One of the interesting find of this study is that if we consider the quaternary Heusler compounds as the daughter compounds, derived from the parent ternary compounds, none of the half-metallic quaternary compounds have half-metallicity in both the ternary parents. This throws up a possibility of emergence of half-metallic behaviour through substitution at select sites of ternary compounds which are not half-metals. In this chapter, we address this by considering Mn_2RhSi, Co_2RhSi and CoRhMnSi as a case study. In the previous two chapters, we have found that CoRhMnSi and Mn_2RhSi are half-metals while Co_2RhSi is a normal metal. This makes this combination of parent-daughter compounds suitable to investigate how site-dependent substitution give rise to half-metallicity. In this chapter we approach CoRhMnSi compound from two directions: one, by systematically replacing one Mn with Co in Mn_2RhSi and two, by systematic replacement of one Co by Mn in

The contents of this chapter have been Accepted in Computational Condensed Matter

Co_2RhSi. We investigate the effects of composition on the electronic structure and magnetic properties and try to find if half-metals at intermediate compositions can be obtained as well as try to understand how site specific substitution is related to the origin of half-metallic behaviour. The chapter is organised as follows: Computational details and the methods, used in this chapter are given in the next section. In the subsequent section (Section 5.3) we present the discussions of the calculated results on structural, electronic and magnetic properties of the compounds, studied here. The summarized main results is presented at the end.

5.2 Calculational Details

Both Mn_2RhSi and Co_2RhSi have Hg_2CuTi type structure as their ground state while CoRhMnSi has LiMgPdSn structure in the ground state. Denoting the $3d$ transition metal elements X occupying $4a(0,0,0)$ and $4c(1/4,1/4,1/4)$ sites in Hg_2CuTi structures as X_I and X_{II} respectively, we see that CoRhMnSi can be obtained by replacing Mn_I (Co_{II}) by Co (Mn) in Mn_2RhSi (Co_2RhSi). In this work, we systematically vary the concentration of Mn_I and Co_{II} (Co and Mn) in Mn_2RhSi and Co_2RhSi respectively to study the emergence of half-metallicity in $(Mn_{1-x}Co_x)RhMnSi$ and $CoRh(Co_{1-x}Mn_x)Si$ where $x = 0, 0.25, 0.50, 0.75$ and 1. We model these two systems by cosidering the 16 atom conventional cubic cell. In this, each of the four sub-lattices has four positions. Systems with different compositions are modelled by filling up these positions. For example, $(Mn_{1-x}Co_x)RhMnSi$ with $x = 0.25$ can be modeled by filling up the positions corresponding to Rh, Mn_{II}, Si and by putting one Co and three Mn_I atoms in the positions corresponding to the sub-lattice of Mn_I.

Spin-polarized DFT based projector augmented wave (PAW) method as implemented in Vienna Ab-initio Simulation Package (VASP) [137–139] is thereafter used for electronic structure calculations. We have used Generalized Gradient Approximation (GGA) [172] as implemented by Perdew-Burke-Ernzerhof for exchange correlation functional in our calculations. The valance electron configurations considered are, Mn: $3p^6 4s^2 3d^5$, Co: $3d^8 4s^1$, Rh: $4p^6 5s^1 4d^8$. An energy cut-off of 450 eV and a Monkhorst-Pack [173] $6 \times 6 \times 6$ k-mesh is used for sampling the Brillouin zone for the calculations of determining the equilibrium structures. After relaxing the structures fully, for self-consistent calculations we used a $11 \times 11 \times 11$ k-mesh. A larger $15 \times 15 \times 15$ k-mesh was used for calculating densities of sates (DOS). We set the total energy and the force convergence criteria to 10^{-6} eV and 10^{-2}

Table 5.1: Calculated lattice constants, formation energies, total magnetic moments M_{total} and spin polarization P of $(Mn_{1-x}Co_x)RhMnSi$ compounds. x is the Co-content at Mn_I site.

Co-content (x)	Lattice constant(Å)	Formation energy ($eV/atom$)	M_{total} ($\mu_B/f.u.$)	P (%)
0.00	5.81	-0.25	3.00	100.00
0.25	5.82	-0.27	3.50	100.00
0.50	5.82	-0.30	4.00	100.00
0.75	5.82	-0.32	4.50	100.00
1.00	5.83	-0.35	5.00	100.00

eV/Årespectively.

To calculate the magnetic pair exchange parameters as well as Curie temperatures we have used multiple scattering Green function formalism as implemented in SPRKKR code[140] mapping the spin part of the Hamiltonian is mapped to a Heisenberg model as shown in chapter 2. Using the the formulation of Liechtenstein *et. al.*[163], the magnetic pair exchange parameters, $J_{ij}^{\mu\nu}$, are calculated from the energy differences due to infinitesimally small orientations of a pair of spins. An angular momentum cut-off $l_{max} = 3$ along with full potential spin polarized scaler relativistic Hamiltonian is used to calculate the energy differences by the SPRKKR code. We have used an uniform k-mesh of $28 \times 28 \times 28$ for Brillouin zone integration. The Green's functions were calculated for 48 complex energy points distributed on a semicircular contour. For the self-consistence cycles, the energy convergence criterion was set to 10^{-6} Ry .

5.3 Results and Discussions

5.3.1 Structural Properties

We optimized the ground state structure in each case by relaxing the atoms in the 16 atoms supercells, and obtained lattice constants and formation energies. The results are presented in Tables 5.1 and 5.2. Total magnetic moments M_{total} and spin polarization (P%) are also given. The formation energies were calculated using the following equation.

$$E_f = E_{Compound} - \sum_{i=0}^{4} x_i E_i(element) \tag{5.1}$$

Table 5.2: Calculated lattice constants, formation energies, total magnetic moments M_{total} and spin polarization P of $CoRh(Co_{1-x}Mn_x)Si$ compounds. x is the Mn-content at Co_{II} site.

Co-content (x)	Lattice constant(Å)	Formation energy ($eV/atom$)	M_{total} ($\mu_B/f.u.$)	P (%)
0.00	5.76	-0.33	3.29	71.00
0.25	5.78	-0.34	3.74	52.00
0.50	5.80	-0.34	4.15	30.00
0.75	5.81	-0.35	4.57	28.00
1.00	5.83	-0.35	5.00	100.00

Here, $E_{Compound}$ represents the total energy of the unit-cell, $E_i(element)$ is the energy per atom of bulk Mn, Co, Rh or Si. The number of atoms present in a unit-cell for the element i, is given by x_i. We find that replacing Mn_I atoms in $(Mn_{1-x}Co_x)RhMnSi$ by Co atoms does not change the lattice constant significantly as we go from Mn_2RhSi ($x = 0$) to CoRhMnSi ($x = 1$) by replacing Mn_I with Co atoms continuously. On the other hand, there is a non-negligible and almost linear increase in the lattice constant as the Mn-content increases in $CoRh(Co_{1-x}Mn_x)Si$ system. The negative formation energy per atom in all cases implies that these compounds can form and further investigation for these compounds are worth a shot.

5.3.2 Electronic Structure

We have discussed earlier that for magnetic Heusler compounds, with magnetic components being $3d$ transition metals, the hybridization of the transition metal elements and the relative position of the Fermi level in minority spin channel with respect to position of bonding and non-bonding states would explain the origin of the half-metallic gaps [7, 59, 61, 64]. The same idea was found to be suitable in understanding the electronic structures of Mn_2RhSi, Co_2RhSi and CoRhMnSi [168, 228]. In this sub-section, we discuss the changes in the electronic structures of $(Mn_{1-x}Co_x)RhMnSi$ and $CoRh(Co_{1-x}Mn_x)Si$ with changes in x in order to understand how half-metallicity evolves with substitutions. In Fig 5.1 and Fig 5.2 spin polarized total and atom projected densities of states for two series, $(Mn_{1-x}Co_x)RhMnSi$ and $CoRh(Co_{1-x}Mn_x)Si$ are shown respectively, where $x = 0, 0.25, 0.50, 0.75$ and 1.

From Fig 5.1 we find that the gaps at the minority spin channels are flanked by

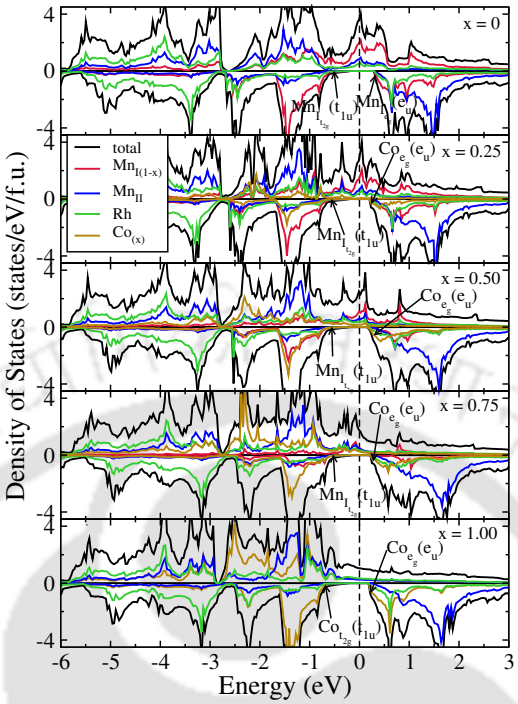

Figure 5.1: Spin polarized total and atom-projected densities of states for $(Mn_{1-x}Co_x)RhMnSi$ compounds.

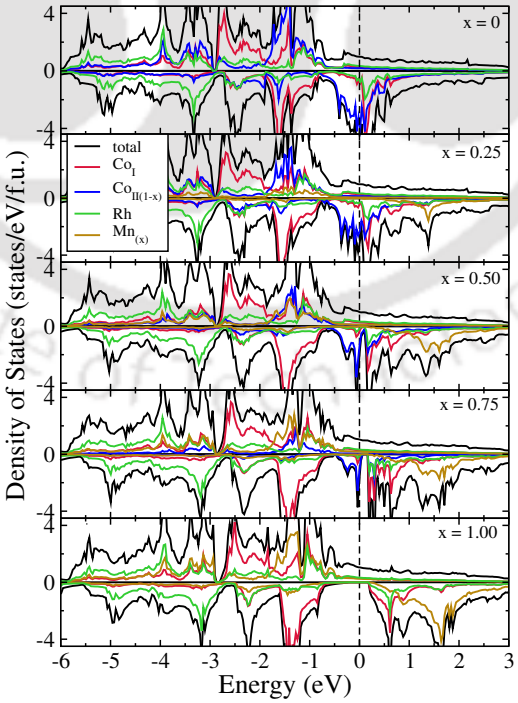

Figure 5.2: Spin polarized total and atom-projected densities of states for $CoRh(Co_{1-x}Mn_x)Si$ compounds.

the states from the atoms (Mn_I and Co) at $4a$ site. In case of $x = 0$ we see that the gap is due to the separation between the non-bonding t_{2g}/t_{1u} states below the Fermi energy and e_g/e_u states above the Fermi energy coming mainly from Mn_I. Mn_{II} spin down states are mostly in the unoccupied part and farther away from Fermi level so that they do not affect the features near the half-metallic gap. With introduction of Co replacing Mn_I, these features hardly change. The Co states are positioned extremely close to the Mn_I states affecting the position of the bottom of the conduction band only slightly. Thus, we found that substitution of the Co atoms at Mn_I sites in Mn_2RhSi does not change the minority spin densities of states significantly, leaving the direct band gap at the Γ point unchanged. The spin-resolved electronic band structures of these systems along the high symmetry direction in Brillouin zone are shown in the Fig. 5.3 to Fig. 5.6 to compare our findings from the total densities of states.

The situation is very different in case of $CoRh(Co_{1-x}Mn_x)Si$, as seen in Fig. 5.2. Unlike Mn_2RhSi where Mn_{II} spin down band was nearly empty with Mn_I spin down states being localised, both Co_I and Co_{II} spin down states are fairly delocalised and hybridize substantially. The substituting Mn atoms, on the other hand, occupy mostly the spin up band. The unoccupied part of the spin down band, away from the Fermi level, is spanned by the Mn states. As a result, a half-metallic gap does not open as long as there are Co_{II} atoms. With increasing x, the Co_{II} spin down bands, however, become narrow with a small gap opening near Fermi level, presumably because of the weakening of hybridization of the transition metal atoms. When Mn replaces Co_{II} completely, the states at the Fermi level completely disappear, giving rise to the half-metallic gap.

The evolution of the spin down electronic structure with x in these two cases, thus, imply that the extent of localisation, the degree of hybridization and the position of the d states are responsible for emergence and sustenance of half-metallicity in the systems under consideration. Taking cue from this, the site dependence of half-metallic or near half-metallic behaviour can be understood for the following parent-daughter families mentioned in chapter 4 : Mn_2TcSi - CoTcMnSi - Co_2TcSi and Mn_2RuSi - CoRuMnSi - Co_2RuSi. In case of the former, Mn_2TcSi Co_2TcSi and CoTcMnSi have spin polarizations of 87%, 22% and 100% respectively while in case of the later Mn_2RuSi, CoRuMnSi and Co_2RuSi have spin polarization of 91%, 97% and 65%. Upon examining the electronic structures of these compounds (chapters 3 and 4), one can see clear resemblance to the Mn_2RhSi - CoRhMnSi - Co2RhSi combination investigated here. The analysis of Fig. 5.1 and 5.2, thus, provide insights

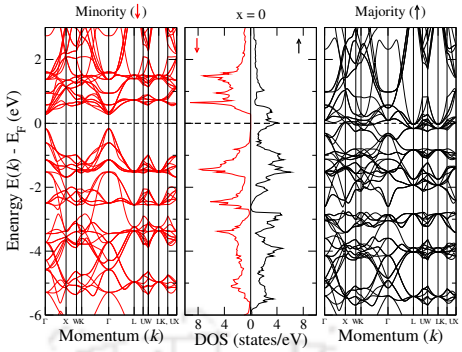

Figure 5.3: Spin-resolved band structure and density of states for $(Mn_{1-x}Co_x)RhMnSi$ where $x = 0$

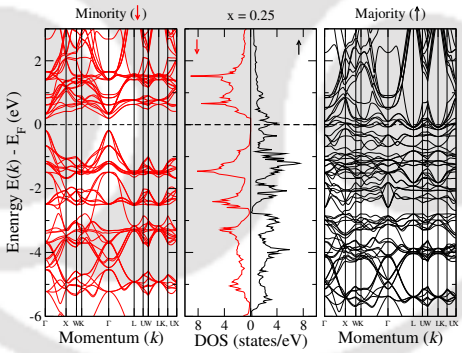

Figure 5.4: Spin-resolved band structure and density of states for $(Mn_{1-x}Co_x)RhMnSi$ where $x = 0.25$

which are not confined to the present study only.

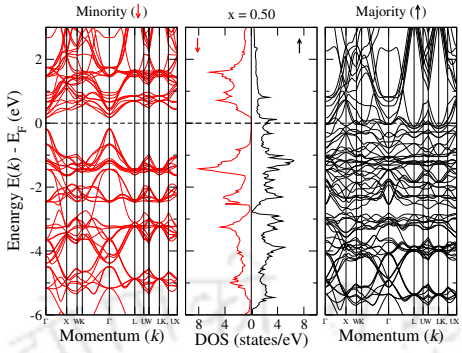

Figure 5.5: Spin-resolved band structure and density of states for $(Mn_{1-x}Co_x)RhMnSi$ where $x = 0.50$

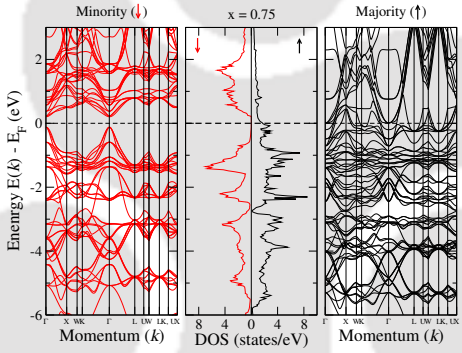

Figure 5.6: Spin-resolved band structure and density of states for $(Mn_{1-x}Co_x)RhMnSi$ where $x = 0.75$

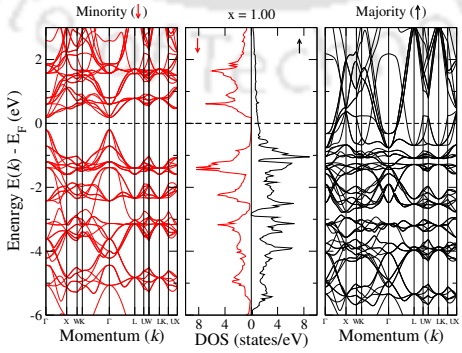

Figure 5.7: Spin-resolved band structure and density of states for $(Mn_{1-x}Co_x)RhMnSi$ where $x = 1$

5.3.3 Variations in the magnetic moments

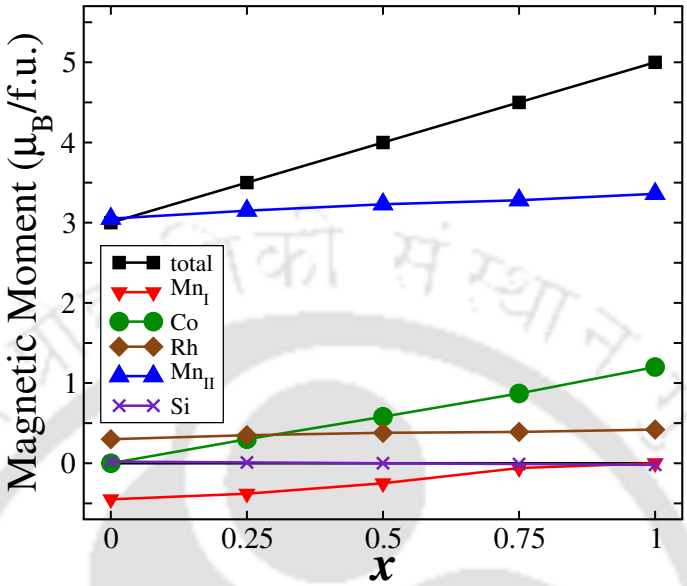

Figure 5.8: The variations of the total and atom resolved spin magnetic moments of Mn_I, Co, Rh, Mn_{II} and Si in $(Mn_{1-x}Co_x)RhMnSi$.

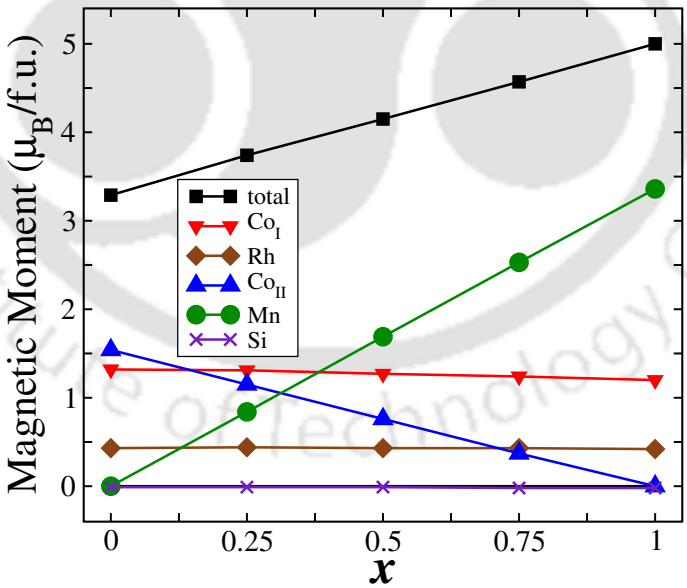

Figure 5.9: The variations of the total and atom resolved spin magnetic moments of Co_I, Rh, Co_{II}, Mn and Si in $CoRh(Co_{1-x}Mn_x)Si$.

The Slater-Pauling (SP) rules are necessary conditions for half-metallicity in Heusler compounds. As discussed in previous chapters, an integer value of the total magnetic moment is the signature of a potential half-metal. However, in the present case, we

find that $(Mn_{1-x}Co_x)$RhMnSi compounds are half-metals for all x but the magnetic moments for compounds with $x = 0.25$ and $x = 0.75$ are non-integers (Table 5.1). We found that the variations in the total magnetic moment can be mapped into a SP equation relation in this case,

$$M = |N_V - 24| \tag{5.2}$$

where $N_V = \sum_{i=1}^{4} N_i$, N_i is the average number of valance electrons at the sublattice i. This suggest that the SP rule is valid even in case of half-metals with non-integer magnetic moments, as was suggested earlier [68].

In Figures 5.8 and 5.9 we show the variations in the total and site-specific magnetic moments for $(Mn_{1-x}Co_x)$RhMnSi and CoRh$(Co_{1-x}Mn_x)$Si respectively. For the former, we find that moment of Mn_{II} remains near constant with a value close to 3 μ_B. This is in confirmation with the electronic structure where irrespective of the composition, the spin up band of Mn_{II} is almost full while the spin down band is almost empty. The weak hybridization of the Mn_{II} states with states from other atoms in the spin up band explains the little variation of its moment with x. With the introduction of Co, the total moment increases due to increasing moment of Co. The moment of Mn_I was quite quenched in Mn_2RhSi. With increase in Co content, its moment further quenches.

From Fig. 5.9, we find that the total moment in CoRh$(Co_{1-x}Mn_x)$Si also increases with x. However, unlike the other system, here the variations in the moment are aided by rapidly increasing moment of Mn and subsequent reduction in the moment of Co_{II}. This behaviour, can be easily understood from the variations in the electronic structure with x. Th Mn being substituted at the octahedral site fills the spin up states completely leaving the spin down states near empty. The Co_{II} states, on the other hand, dwindle as more Mn is incorporated in the system, thus reducing its moment gradually.

5.3.4 Magnetic Exchange interactions and Curie temperature

Variations of estimated Curie temperatures and inter atomic effective exchange coupling constants (J_{eff}) with x are shown in Fig. 5.10 and 5.11 respectively. From Fig. 5.10 we find that $(Mn_{1-x}Co_x)$RhMnSi compounds have relatively low Curie temperatures compared to CoRh$(Co_{1-x}Mn_x)$Si. This is due to the substantial anti-

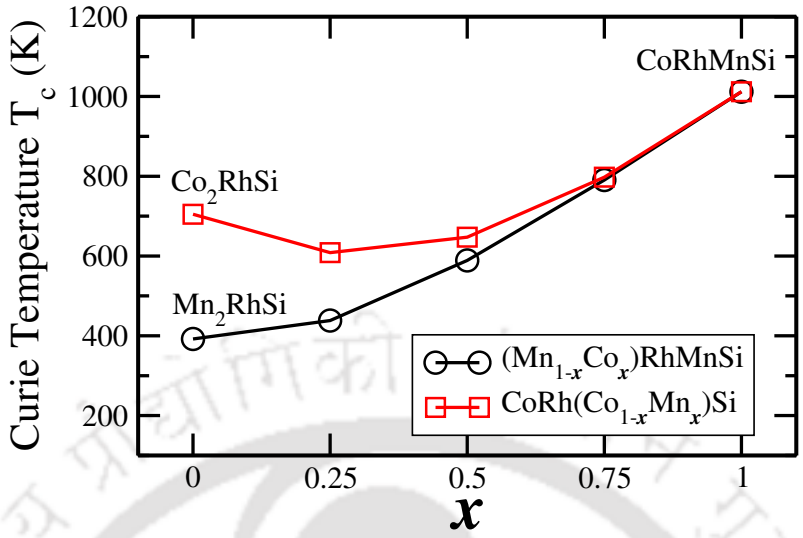

Figure 5.10: Variations of the Curie temperatures of $(Mn_{1-x}Co_x)RhMnSi$ and $CoRh(Co_{1-x}Mn_x)Si$ compounds.

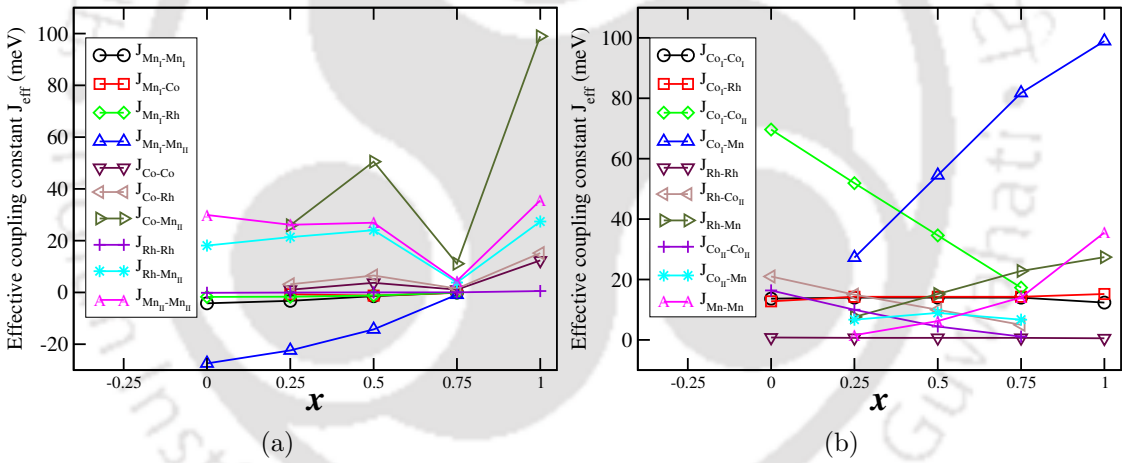

Figure 5.11: Effective exchange interactions for different x (**a**) $(Mn_{1-x}Co_x)RhMnSi$ and (**b**) $CoRh(Co_{1-x}Mn_x)Si$ compounds.

ferromagnetic Mn_I-Mn_{II} exchange coupling in $(Mn_{1-x}Co_x)RhMnSi$ that somewhat balances the ferromagnetic interactions. From Fig. 5.11.(a) and (b) we find that J_{eff} for nearest neighbour atoms are larger compared to those of the others: Mn_I-Mn_{II}, Co-Mn_{II} and Rh-Mn_{II} are dominant in Fig. 5.11.(a) and Co_I-Co_{II}, Co_I-Mn and Rh-Co_{II} are dominant in Fig. 5.11.(b). In case of $(Mn_{1-x}Co_x)RhMnSi$ compounds, as we go from $x = 0$ to 1 the Mn_I-Mn_{II}, Rh-Mn_{II} and Co-Mn_{II} J_{eff} values keep increasing with x. The variations in Curie temperatures follows the same trend, reaching to its highest value for $x = 1$. It is to be noted that very strong ferromagnetic Co-Mn_{II} interaction supersedes the antiferromagnetic Mn_I-Mn_{II} interactions and is primarily

responsible for increase in T_c with x. In case of $CoRh(Co_{1-x}Mn_x)Si$ compounds the variations of J_{eff} values for Co_I-Mn and Co_I-Co_{II} with respect to x resemble the variations of atom resolved spin magnetic moments of Mn and Co_{II} respectively as shown in Fig. 5.9. As we go from $x = 0$ to 1 the Mn content in the systems keep increasing as well as the total moment along with an increase in effective exchange coupling constant values for nearest neighbour Co_I-Mn interaction. On the other hand with decreased Co content J_{eff} for Co_I-Co_{II} nearest neighbour interaction is reduced significantly. This is reflected in the decrease in Curie temperature while going from $x = 0$ to 0.25. For $x = 0.50$ the contributions from Co_I-Co_{II} and Co_I-Mn are near identical reflecting in the near constant value of T_c between $x = 0.25$ and $x = 0.50$. Since the Co_I-Mn interaction is very high in case of $x = 0.75$ Curie temperature is also higher compared to $x = 0.50$ case. As one reaches $x = 1$, the Co-Mn interaction is the largest one, so is the Curie temperature.

5.4 Conclusions

In this chapter we have explored in detail the electronic and magnetic properties of the two sets of substitutionally disordered compounds, $(Mn_{1-x}Co_x)RhMnSi$ and $CoRh(Co_{1-x}Mn_x)Si$ where $x = 0, 0.25, 0.50, 0.75$ and 1, employing first-principles electronic structure calculations. Our focus was to systematically investigate the emergence of half-metallic behaviour in the daughter compound upon substitution in the parents, one of which is not a half-metal. In case of $(Mn_{1-x}Co_x)RhMnSi$ compounds the half-metallicity is intact as it was in parent Mn_2RhSi where as in case of $CoRh(Co_{1-x}Mn_x)Si$ compounds half-metallicity is observed only upon replacing the Co completely with Mn at the site of substitution. Analysing the electronic structures we find that the positions of the transition metal constituents energy states with respect to Fermi level and subsequent hybridizations are responsible for half-metallic behaviour being dependent on site-specific substitution. We find that the total magnetic moment of $(Mn_{1-x}Co_x)RhMnSi$ compounds, can easily be mapped onto a linear equation like that of celebrated SP-equation by considering the non integer site occupancies in these compounds, demonstrating that the integer moment is not always a necessary condition for half-metallicity in substitutionally disordered Heuslers.

In conclusion, we find that if we substitute Co at Mn_I site in Mn_2RhSi the structural and electronic properties of the system are hardly susceptible to the changes in the composition. Only the Curie temperature and the total spin magnetic moment

undergo changes due to the changes in the total valance electrons and magnetic exchange interactions as a result of Co substitution. In contrast if we substitute Mn at Co_{II} site in Co_2RhSi the electronic structure changes gradually, a gap starts opening near the Fermi level and half-metallicity shows up when all Co at the 4*c* site are replaced with Mn. Upon comparison with the parent-daughter combinations where the daughters are either half-metals or "near" half-metals while both parents are not, we find clear resemblances in their electronic structures. We, thus, infer that at least for Co-Mn based quaternary daughter compounds where the other transition metal constituent is one of the members of the 4*d* series, more half-metals with substantial Curie temperature can be obtained by selective substitution in the ternary parent compounds. These findings provide the necessary motivations for experimentalists to explore these materials in a systematic way.

Chapter 6

Conclusions and scopes for future work

6.1 Conclusions

In this thesis, we systematically explored the structural, electronic and magnetic properties of ternary and quaternary Heusler compounds with $3d$ and $4d$ transition metals using first principle electronic structure calculations. Apart from identifying a few new materials for spintronics applications we investigated the impacts of presence of both $3d$ and $4d$ transition metal constituents together, and their origin, on the structural, electronic and magnetic properties of series of ternary and quaternary compounds. Moreover, we did a comparative analysis of these compounds with more familiar family where all magnetic elements are from $3d$ series to understand the relative roles of $3d$ and $4d$ elements on their electronic properties like half-metallic behaviour. We conclude that the microscopic origin of features like half-metallicity, a very much sensitive and material specific property, can be explained in a more general way irrespective of the character of the valence electrons of the magnetic constituents. The aspect of site-dependence of substitution affecting the half-metallic behaviour is also addressed. A possibility to find predictors that can help to visualise possible new half-metals or materials with high spin polarizations, useful for various applications, is another important outcome of this work.

In the first chapter, the concepts relevant to the investigated ternary and quaternary Heusler compounds for spintronics applications were described. Depending on the site occupancies of different constituent transition metals of these compounds, the origin of half-metallicity is discussed using a generalised hybridisations picture.

A brief review of ternary and quaternary Heusler compounds is provided, leading to the indication of unexplored direction in this regard. We also provide the justifications behind choosing the specific series of Heusler compounds for the work presented in this thesis.

The theoretical methods used in this thesis are discussed in chapter 2. Along with a brief introduction, different implementations of Density Functional Theory (DFT), the backbone of modern first-principle electronic structure based methods, are presented. Approaches used to calculate finite temperature magnetic properties are then discussed.

In the next chapter we have performed a comprehensive study of structural, electronic and magnetic properties of 54 ternary compounds with the chemical formula $X_2X'Z$ where X = Mn, Fe and Co, X′ = 4*d* transition metal atoms ranging from Y to Ag and Z = Al and Si. We found seven half-metals Mn_2NbAl, Mn_2ZrSi, Mn_2RhSi, Co_2ZrAl, Co_2NbAl, Co_2YSi and Co_2ZrSi from the six ternary series investigated. We also found five "near half-metals" with spin polarization greater than 90% and a pseudo-gap near the Fermi level which might be tuned such that the gap falls at the Fermi level, inducing half-metallicity in these compounds. We found that the hybridisation picture used to explain the origin of half-metallicity in the ternary Heusler compounds with all 3*d* transition metal elements as magnetic components is also valid for the compounds where both 3*d* and 4*d* elements are present. This leads to a more general framework in explaining the origin of half-metallicity in Heusler $X_2X'Z$ compounds with X′ being either a 3*d* or a 4*d* electrons. A comparative analysis of our results with $X_2X'Z$ compounds where X′ is a 3*d* element, shows that if the number of valance electrons (N_V) are same, the electronic properties are more or less alike if a 3*d* element is replaced by a 4*d* one as long as both the compounds have same ground state crystal structures. Our study indicates that N_V can be a good predictor in searching new half-metals as the relative positions of X and X′ states near the Fermi level determines the half-metallicity in these compounds. We also concluded that the trends in the Curie temperature T_C could be understood with the trends in dominant exchange interactions of the nearest neighbour atoms irrespective of the structure types of the compounds.

In the following chapter, we extend our work on ternary Heuslers to quaternary Heuslers. We systematically explore the CoX′Y′Z series, where X′ is a transition

metal atom from the 4*d* series, Y′ is either Mn or Fe, strong magnet with unfilled 3*d* electrons in its outer shell and Z = Al, Si. Out of 36 quqternary Heusler compounds only three compounds (CoTcMnSi, CoRhMnSi and CoZrFeSi) from CoX′Y′Si series and two compounds (CoYMnAl and CoRuMnAl) from CoX′Y′Al series are found to be half-metallic ferromagnets. However we identified few other compounds like CoYMnSi, CoNbMnSi, CoRuMnSi, CoNbFeSi, CoZrMnAl, CoRuMnAl and CoMoFeAl as "nearly" half-metals with a gap near the Fermi level. The neighbourhood of the magnetic atoms which is dependent upon the crystal structure type is found to be responsible for the trends in electronic structures and magnetic properties of these compounds. Accordingly we find that the strongest exchange interactions between Co and Y′ are responsible for the trends in the Curie temperature showing that the Curie temperature for the compounds where Y′ and Co are in nearest neighbour position is higher compared to the compounds with other structure type. We also show that total number valance electrons (N_V) can be a good predictor to indicate useful Co-based Heusler compounds with high Curie temperature, as in our study we find compounds with $N_V = 29$ are having the highest Curie temperature and in general have high values of Curie temperature when N_V is in the range of 28-30. We find that this trend is similar to that of Co_2-based ternary alloys. Apart from the prediction of new half-metallic magnets for spintronics applications this work provides a better outlook to understand the physics of half-metallic quaternary Heuslers. Our results on comparative analysis between two series with different Z elements show that the Z element plays a minor yet significant role in affecting the half-metallicity, as long as the N_V and structure type remain same for two compounds in comparison. This is due to the fact that the *d* bands are pulled more towards the lower energies by the deep lying Si states as compared to the Al states which in turn changes the position of the 3*d* states near the Fermi level. The comparison between the isoelectronic quaternary (CoX′Y′Z) pairs with X′ as a 3*d* element in one case, and a 4*d* in the other, while keeping all other constituents same, shows that the half-metallic property is not guaranteed unless the structure types are same. This leads us to conclude that N_V and the structure types together can be predictors of half-metallicity in quaternary compounds irrespective of the X′ element. This fact is also verified by the generalised scheme of hybridisations between the transition metal atoms, which is valid across all the quaternary series. Another important finding of this work is that half-metallicity is not transferrable from two suitable parent ternary Heusler compounds to a daughter quaternary Heusler compound. This paves the way for addressing the issue of emergence of half-metallic behaviour through substitution at

select sites.

In chapter 5 we have investigated the effect of site dependent substitution on half-metallic behaviour in Heusler compounds. As a case study we have chosen Mn_2RhSi, Co_2RhSi and CoRhMnSi and explored the structural, electronic and magnetic properties of the two series, $(Mn_{1-x}Co_x)RhMnSi$ and $CoRh(Co_{1-x}Mn_x)Si$ where $x = 0, 0.25, 0.50, 0.75$ and 1.00. We find that if Co is substituted at tetrahedral Mn sites, the structural and electronic properties of the systems remain unchanged with Co content while a increase in Curie temperature and total spin magnetic moment are observed. Thus, as we go from Mn_2RhSi to CoRhMnSi the half-metallicity is found to be intact for different Co concentrations (x). However no such thing is observed as we go from Co_2RhSi to CoRhMnSi by gradually substituting Mn at octahedral Co sites of Co_2RhSi until the octahedral Co is completely replaced. We conclude that this is related to the extent of localisation of the states associated with magnetic components with $3d$ electrons and the positions of their bands with respect to the Fermi levels. In case of $(Mn_{1-x}Co_x)RhMnSi$ system where half-metallicity is insensitive to x, we also find a relation like the celebrated Slater-Pauling relation connecting magnetic moment and the number of valance electrons in case of later being non-integer. The work in this chapter, therefore, sheds significant light onto the relations between site dependent substitution and half-metallic behaviour and predicts $Mn_{(2-x)}Co_xRhSi$ as half metals with high Curie temperature.

6.2 Scopes for future work

The work presented in this thesis can be extended in various directions. In actual experiments, the systems are grown on semiconductor substrates. Thus, one of the possible extension of the present work can be to investigate the sustainability of half-metallic behaviour upon growing the bulk materials on semiconductor substrates.

One issue intricately connected to the growth of the systems experimentally is tetragonalization of the compounds. This is particularly relevant for Mn-based compounds. Therefore, one direction of the extension of the present work can be towards investigation of sustenance of half-metallic behaviour upon tetragonalization.

In this work we have considered ideal site occupancies for all the systems. How-

ever, during experimental synthesis there are possibilities of atomic swaps or creation of vacancies. The half-metallic behaviour should be checked against such possibilities. This will be the direction of another possible extension.

Finally, we have obtained a number of "nearly half-metals" with high spin polarization from the series under the investigation. We have proposed that these can be converted to half-metals by tuning the position of the Fermi level. This can be achieved either by applying pressure or by alloying with suitable elements. A quest towards new additions to the family of half-metals can be carried out along this line.

Bibliography

[1] C. Felser and A. Hirohata, *Heusler Alloys*, Springer, 2015.

[2] P. J. Webster, *The magnetic and chemical structures of the Heusler alloys.*, PhD thesis, University of Sheffield, 1968.

[3] M. Katsnelson, V. Y. Irkhin, L. Chioncel, A. Lichtenstein, and R. A. de Groot, Reviews of Modern Physics **80**, 315 (2008).

[4] J. Coey, M. Venkatesan, and M. Bari, Half-metallic ferromagnets, in *High Magnetic Fields*, pages 377–396, Springer, 2002.

[5] I. Galanakis, P. H. Dederichs, and N. Papanikolaou, Phys. Rev. B **66**, 134428 (2002).

[6] J. Pons, E. Cesari, C. Seguí, F. Masdeu, and R. Santamarta, Materials Science and Engineering: A **481**, 57 (2008).

[7] I. Galanakis, P. H. Dederichs, and N. Papanikolaou, Phys. Rev. B **66**, 174429 (2002).

[8] A. Planes, L. Maosa, and M. Acet, J. Phys.: Condens. Matter **21**, 233201 (2009).

[9] D. Do, M.-S. Lee, and S. D. Mahanti, Phys. Rev. B **84**, 125104 (2011).

[10] A. J. Bradley and J. Rodgers, Proc. R. Soc. Lond. A **144**, 340 (1934).

[11] T. Graf, S. S. Parkin, and C. Felser, IEEE Transactions on Magnetics **47**, 367 (2011).

[12] P. Webster and K. Ziebeck, Landolt-börnsteingroup iii condensed matter vol 19c, 1988.

[13] R. De Groot, F. Mueller, P. Van Engen, and K. Buschow, Physical Review Letters **50**, 2024 (1983).

[14] M. Pušelj and Z. Ban, Croatica Chemica Acta **41**, 79 (1969).

[15] H. Pauly, A. Weiss, and H. Witte, Z METALLKUNDE **59**, 47 (1968).

[16] X. Dai, G. Liu, L. Chen, J. Chen, and G. Wu, Solid state communications **140**, 533 (2006).

[17] V. Surikov, V. Zhordochkin, and T. Y. Astakhova, Hyperfine Interactions **59**, 469 (1990).

[18] N. Lakshmi, A. Pandey, and K. Venugopalan, Bulletin of Materials Science **25**, 309 (2002).

[19] U. Eberz, Z. Naturforsch. B **35**, 1341 (1980).

[20] J. Drews, U. Eberz, and H.-U. Schuster, Journal of the Less Common Metals **116**, 271 (1986).

[21] G. Bacon and J. Plant, Journal of Physics F: Metal Physics **1**, 524 (1971).

[22] P. Kharel, Y. Huh, N. Al-Aqtash, V. Shah, R. F. Sabirianov, R. Skomski, and D. J. Sellmyer, J. Phys.: Condens. Matter **26**, 126001 (2014).
[23] H. Kurt, K. Rode, H. Tokuc, P. Stamenov, M. Venkatesan, and J. Coey, Appl. Phys. Lett. **101**, 232402 (2012).
[24] T. Gasi, A. K. Nayak, J. Winterlik, V. Ksenofontov, P. Adler, M. Nicklas, and C. Felser, Appl. Phys. Lett. **102**, 202402 (2013).
[25] Z. Liu, Y. Zhang, H. Zhang, X. Zhang, and X. Ma, Appl. Phys. Lett. **109** (2016).
[26] P. Webster and K. Ziebeck, Part **2**, 75 (1988).
[27] G. Johnston and E. Hall, Journal of Physics and Chemistry of Solids **29**, 193 (1968).
[28] B. Balke, G. H. Fecher, J. Winterlik, and C. Felser, Applied physics letters **90**, 152504 (2007).
[29] M. E. Jamer et al., Physical Review Applied **7**, 064036 (2017).
[30] C. Felser and G. H. Fecher, *Spintronics: from materials to devices*, Springer Science & Business Media, 2013.
[31] S. Murakami, N. Nagaosa, and S.-C. Zhang, Science **301**, 1348 (2003).
[32] E. Saitoh, M. Ueda, H. Miyajima, and G. Tatara, Appl. Phys. Lett. **88**, 182509 (2006).
[33] I. Žutić, J. Fabian, and S. Das Sarma, Rev. Mod. Phys. **76**, 323 (2004).
[34] W. J. Gallagher, J. H. Kaufman, S. S. P. Parkin, and R. E. Scheuerlein, Magnetic memory array using magnetic tunnel junction devices in the memory cells, 1997, US Patent 5,640,343.
[35] K. Sin, S. Funada, H. C. Hiner, and X. Shi, Spin-dependent tunneling sensor suitable for a magnetic memory, 2002, US Patent 6,418,048.
[36] C. D. Mee and E. D. Daniel, *Magnetic recording; Vol. II: computer data storage*, McGraw-Hill, Inc., 1988.
[37] R. Coleman and A. Isin, J. Appl. Phys. **37**, 1028 (1966).
[38] M. N. Baibich et al., Phys. Rev. Lett. **61**, 2472 (1988).
[39] R. von Helmolt, J. Wecker, B. Holzapfel, L. Schultz, and K. Samwer, Phys. Rev. Lett. **71**, 2331 (1993).
[40] M. Johnson and R. H. Silsbee, Physical Review Letters **55**, 1790 (1985).
[41] P. Grünberg, Phys. Rev. Lett. **57**, 2442 (1986).
[42] T. Miyazaki and N. Tezuka, J. Magn. Magn. Mater. **139**, L231 (1995).
[43] J. S. Moodera, L. R. Kinder, T. M. Wong, and R. Meservey, Phys. Rev. Lett. **74**, 3273 (1995).
[44] J. Åkerman, Science **308**, 508 (2005).
[45] S. Bhatti, R. Sbiaa, A. Hirohata, H. Ohno, S. Fukami, and S. Piramanayagam, Materials Today **20**, 530 (2017).
[46] J.-M. Hu, Z. Li, L.-Q. Chen, and C.-W. Nan, Nature communications **2**, 553 (2011).
[47] J. C. Sankey, Y.-T. Cui, J. Z. Sun, J. C. Slonczewski, R. A. Buhrman, and D. C. Ralph, Nature Physics **4**, 67 (2008).
[48] D. C. Ralph and M. D. Stiles, J. Magn. Magn. Mater. **320**, 1190 (2008).
[49] C. Felser, G. H. Fecher, and B. Balke, Angewandte Chemie International Edition

46, 668 (2007).
[50] J. Kübler, A. William, and C. Sommers, Physical Review B **28**, 1745 (1983).
[51] S. Ishida, S. Fujii, S. Kashiwagi, and S. Asano, Journal of the Physical Society of Japan **64**.
[52] M. M. Rahman, M. Kisaku, T. Kishi, D. Matsunaka, W. Dino, H. Nakanishi, and H. Kasai, Journal of Physics: Condensed Matter **16**, S5755 (2004).
[53] R. Soulen Jr, Science **282**, 85 (1998).
[54] A. Stroppa, S. Picozzi, A. Continenza, and A. Freeman, Physical review B **68**, 155203 (2003).
[55] H. Akai, Physical Review Letters **81**, 3002 (1998).
[56] H. Akinaga, T. Manago, and M. Shirai, Japanese Journal of Applied Physics **39**, L1118 (2000).
[57] J. C. Slater, Phys. Rev. **49**, 537 (1936).
[58] L. Pauling, Phys. Rev. **54**, 899 (1938).
[59] S. Skaftouros, K. Özdoğan, E. Şaşıoğlu, and I. Galanakis, Phys. Rev. B **87**, 024420 (2013).
[60] I. Galanakis, *Theory of Heusler and Full-Heusler Compounds*, pages 3–36, Springer International Publishing, Cham, 2016.
[61] K. Özdoğan, E. Şaşıoğlu, and I. Galanakis, J. Appl. Phys. **113**, 193903 (2013).
[62] B. Nanda and I. Dasgupta, Journal of Physics: Condensed Matter **15**, 7307 (2003).
[63] G. Z. Xu, E. K. Liu, Y. Du, G. J. Li, G. D. Liu, W. H. Wang, and G. H. Wu, Europhys. Lett. **102**, 17007 (2013).
[64] L. Bouckaert, Phys. Rev. **50**, 58 (1936).
[65] J. Kübler, Physica B+ C **127**, 257 (1984).
[66] L. Wollmann, S. Chadov, J. Kübler, and C. Felser, Phys. Rev. B **90**, 214420 (2014).
[67] J. Ma et al., Phys. Rev. B **98**, 094410 (2018).
[68] G. H. Fecher, H. C. Kandpal, S. Wurmehl, C. Felser, and G. Schönhense, Journal of applied physics **99**, 08J106 (2006).
[69] S. V. Faleev, Y. Ferrante, J. Jeong, M. G. Samant, B. Jones, and S. S. Parkin, Physical Review B **95**, 045140 (2017).
[70] M. Gilleßen and R. Dronskowski, Journal of computational chemistry **31**, 612 (2010).
[71] K. Özdoğan, E. Şaşıoğlu, and I. Galanakis, Journal of applied physics **103**, 023503 (2008).
[72] P. Neibecker, M. E. Gruner, X. Xu, R. Kainuma, W. Petry, R. Pentcheva, and M. Leitner, Physical Review B **96**, 165131 (2017).
[73] S. Skaftouros, K. Özdoğan, E. Şaşıoğlu, and I. Galanakis, Applied Physics Letters **102**, 022402 (2013).
[74] G. Gao, L. Hu, K. Yao, B. Luo, and N. Liu, J. Alloys Compd. **551**, 539 (2013).
[75] S. Wurmehl, G. H. Fecher, H. C. Kandpal, V. Ksenofontov, C. Felser, and H.-J. Lin, Applied physics letters **88**, 032503 (2006).
[76] T. Graf, C. Felser, and S. S. Parkin, Prog. Solid State Chem. **39**, 1 (2011).
[77] R. Weht and W. E. Pickett, Physical Review B **60**, 13006 (1999).

[78] E. Şaşioglu, L. Sandratskii, and P. Bruno, Journal of Physics: Condensed Matter **17**, 995 (2005).
[79] T. Gasi et al., Physical Review B **87**, 064411 (2013).
[80] J. C. Slonczewski, Journal of Magnetism and Magnetic Materials **159**, L1 (1996).
[81] X. Wang, Physical review letters **100**, 156404 (2008).
[82] X.-L. Wang, S. X. Dou, and C. Zhang, NPG Asia Materials **2**, 31 (2010).
[83] S. Ouardi, G. H. Fecher, C. Felser, and J. Kübler, Phys. Rev. Lett. **110**, 100401 (2013).
[84] P. J. Webster, K. R. A. Ziebeck, S. L. Town, and M. S. Peak, Phil. Maga. B **49**, 295 (1984).
[85] G. Liu et al., Appl. Phys. Lett. **87**, 262504 (2005).
[86] G. D. Liu et al., Phys. Rev. B **74**, 054435 (2006).
[87] S. Barman and A. Chakrabarti, Phys. Rev. B **77**, 176401 (2008).
[88] S. Singh et al., Phys. Rev. Lett. **109**, 246601 (2012).
[89] S. Singh, S. Esakki Muthu, A. Senyshyn, P. Rajput, E. Suard, S. Arumugam, and S. Barman, Appl. Phys. Lett. **104**, 051905 (2014).
[90] F. Wu, S. Mizukami, D. Watanabe, H. Naganuma, M. Oogane, Y. Ando, and T. Miyazaki, Applied Physics Letters **94**, 122503 (2009).
[91] J. Winterlik, B. Balke, G. H. Fecher, C. Felser, M. C. Alves, F. Bernardi, and J. Morais, Physical Review B **77**, 054406 (2008).
[92] K. Rode et al., Phys. Rev. B **87**, 184429 (2013).
[93] H. Kurt, K. Rode, M. Venkatesan, P. Stamenov, and J. M. D. Coey, Physical Review B **83**, 020405 (2011).
[94] A. K. Nayak et al., Nature materials **14**, 679 (2015).
[95] M. Meinert, J.-M. Schmalhorst, C. Klewe, G. Reiss, E. Arenholz, T. Böhnert, and K. Nielsch, Phys. Rev. B **84**, 132405 (2011).
[96] Y. Zhang, G. Li, E. Liu, J. Chen, W. Wang, F. Meng, and G. Wu, Physica B: Condensed Matter **454**, 1 (2014).
[97] A. Chakrabarti and S. Barman, Appl. Phys. Lett. **94**, 161908 (2009).
[98] S. Paul and S. Ghosh, J. Phys.: Condens. Matter **23**, 206003 (2011).
[99] S. Paul and S. Ghosh, J. Appl. Phys. **110**, 063523 (2011).
[100] S. Paul, A. Kundu, B. Sanyal, and S. Ghosh, J. Appl. Phys. **116**, 133903 (2014).
[101] P. Klaer, B. Balke, V. Alijani, J. Winterlik, G. H. Fecher, C. Felser, and H. J. Elmers, Phys. Rev. B **84**, 144413 (2011).
[102] T. Block, J. Solid State Chem. **176**, 646 (2003).
[103] H. C. Kandpal, G. H. Fecher, and C. Felser, Journal of Physics D: Applied Physics **40**, 1507 (2007).
[104] S. Picozzi, A. Continenza, and A. J. Freeman, Physical Review B **69**, 094423 (2004).
[105] S. Wurmehl, G. H. Fecher, H. C. Kandpal, V. Ksenofontov, C. Felser, H.-J. Lin, and J. Morais, Phys. Rev. B **72**, 184434 (2005).
[106] T. Marukame, T. Ishikawa, S. Hakamata, K.-i. Matsuda, T. Uemura, and M. Yamamoto, Applied physics letters **90**, 012508 (2007).

[107] N. Tezuka, N. Ikeda, S. Sugimoto, and K. Inomata, Applied physics letters **89**, 252508 (2006).
[108] P. Brown, K.-U. Neumann, P. Webster, and K. Ziebeck, Journal of Physics: Condensed Matter **12**, 1827 (2000).
[109] S. Ishida, S. Akazawa, Y. Kubo, and J. Ishida, Journal of Physics F: Metal Physics **12**, 1111 (1982).
[110] J. Kübler, G. H. Fecher, and C. Felser, Phys. Rev. B **76**, 024414 (2007).
[111] M. Gilleßen and R. Dronskowski, Journal of computational chemistry **30**, 1290 (2009).
[112] C. Sterwerf et al., Journal of Applied Physics **120**, 083904 (2016).
[113] Y. Nishino, Development of thermoelectric materials based on fe2val heusler compound for energy harvesting applications, in *IOP Conference Series: Materials Science and Engineering*, volume 18, page 142001, IOP Publishing, 2011.
[114] B. Xu, X. Li, G. Yu, J. Zhang, S. Ma, Y. Wang, and L. Yi, Journal of Alloys and Compounds **565**, 22 (2013).
[115] Z. Liu et al., Applied Physics Letters **86**, 182507 (2005).
[116] L. Bainsla et al., Phys. Rev. B **91**, 104408 (2015).
[117] L. Bainsla et al., Phys. Rev. B **92**, 045201 (2015).
[118] L. Bainsla et al., J. Magn. Magn. Mater. **394**, 82 (2015).
[119] X. Dai, G. Liu, G. H. Fecher, C. Felser, Y. Li, and H. Liu, J. Appl. Phys. **105**, 07E901 (2009).
[120] P. Hohenberg and W. Kohn, Phys. Rev. **136**, B864 (1964).
[121] W. Kohn and L. J. Sham, Phys. Rev. **140**, A1133 (1965).
[122] R. M. Martin, *Electronic structure: basic theory and practical methods*, Cambridge university press, United Kindom, 2004.
[123] J. Korringa, Physica **13**, 392 (1947).
[124] W. Kohn and N. Rostoker, Phys. Rev. **94**, 1111 (1954).
[125] D. J. Singh and L. Nordstrom, *Planewaves, Pseudopotentials, and the LAPW method*, Springer Science & Business Media, 2006.
[126] P. Blaha, K. Schwarz, P. Sorantin, and S. Trickey, Computer Physics Communications **59**, 399 (1990).
[127] J. C. Slater, Phys. Rev. **51**, 846 (1937).
[128] J. Slater, Advances in quantum chemistry **1**, 35 (1964).
[129] J. Kubler, K.-H. Hock, J. Sticht, and A. Williams, Journal of Physics F: Metal Physics **18**, 469 (1988).
[130] L. Sandratskii, Advances in Physics **47**, 91 (1998).
[131] L. Nordström and D. J. Singh, Phys. Rev. Lett. **76**, 4420 (1996).
[132] D. Hobbs, G. Kresse, and J. Hafner, Phys. Rev. B **62**, 11556 (2000).
[133] S. Y. Savrasov, Phys. Rev. B **54**, 16470 (1996).
[134] S. Baroni, S. De Gironcoli, A. Dal Corso, and P. Giannozzi, Reviews of Modern Physics **73**, 515 (2001).
[135] I. Turek, V. Drchal, J. Kudrnovskỳ, M. Sob, and P. Weinberger, *Electronic structure*

of disordered alloys, surfaces and interfaces, Springer Science & Business Media, 2013.
[136] R. McCormack and D. De Fontaine, Phy. Rev. B **54**, 9746 (1996).
[137] P. E. Blöchl, Phys. Rev. B **50**, 17953 (1994).
[138] G. Kresse and J. Furthmüller, Phys. Rev. B **54**, 11169 (1996).
[139] G. Kresse and D. Joubert, Phys. Rev. B **59**, 1758 (1999).
[140] H. Ebert, D. Koedderitzsch, and J. Minar, Rep. Prog. Phys. **74**, 096501 (2011).
[141] M. Born and R. Oppenheimer, Annalen der Physik **389**, 457 (1927).
[142] W. Kohn, Reviews of Modern Physics **71**, 1253 (1999).
[143] L. H. Thomas, The calculation of atomic fields, in *Mathematical Proceedings of the Cambridge Philosophical Society*, volume 23, pages 542–548, Cambridge University Press, 1927.
[144] E. Fermi, Rend. Accad. Naz. Lincei **6**, 32 (1927).
[145] D. R. Hartree, The wave mechanics of an atom with a non-coulomb central field. part i. theory and methods, in *Mathematical Proceedings of the Cambridge Philosophical Society*, volume 24, pages 89–110, Cambridge University Press, 1928.
[146] V. Fock, Zeitschrift für Physik A Hadrons and Nuclei **61**, 126 (1930).
[147] F. Giustino, *Materials modelling using density functional theory: properties and predictions*, Oxford University Press, 2014.
[148] J. P. Perdew, P. Ziesche, and H. Eschrig, *Electronic structure of solids 91*, volume 11, Akademie Verlag, Berlin, 1991.
[149] J. P. Perdew, K. Burke, and M. Ernzerhof, Physical review letters **77**, 3865 (1996).
[150] J. P. Perdew and W. Yue, Phys. Rev. B **33**, 8800 (1986).
[151] J. P. Perdew and Y. Wang, Phys. Rev. B **45**, 13244 (1992).
[152] D. Vanderbilt, Phys. Rev. B **41**, 7892 (1990).
[153] K. Laasonen, R. Car, C. Lee, and D. Vanderbilt, Phys. Rev. B **43**, 6796 (1991).
[154] K. Laasonen, A. Pasquarello, R. Car, C. Lee, and D. Vanderbilt, Phys. Rev. B **47**, 10142 (1993).
[155] T. Loucks, *Augmented plane wave method*, Benjamin, New York, 1967.
[156] G. Kresse and J. Hafner, Phys. Rev. B **47**, 558 (1993).
[157] G. Kresse and J. Hafner, Phys. Rev. B **49**, 14251 (1994).
[158] S. Cottenier, Instituut voor Kern-en Stralingsfysica, KU Leuven, Belgium **4**, 41 (2002).
[159] G. Kresse et al., *Vienna ab-initio simulation package (VASP)*, Vienna University, Vienna, Austria, 2001.
[160] A. R. Thieß, *Development and application of a massively parallel KKR Green function method for large scale systems*, Forschungszentrum Jülich, 2013.
[161] R. Zeller, Journal of Physics C: Solid State Physics **20**, 2347 (1987).
[162] H. Ebert et al., *The Munich SPR-KKR package, version 6.3*, University of Munich, Munich, Germany, 2012.
[163] A. Liechtenstein, M. Katsnelson, V. Antropov, and V. Gubanov, J. Magn. Magn. Mater. **67**, 65 (1987).

[164] M. Methfessel and J. Kubler, Journal of Physics F: Metal Physics **12**, 141 (1982).
[165] E. Şaşıoğlu, L. M. Sandratskii, and P. Bruno, Phys. Rev. B **70**, 024427 (2004).
[166] E. Şaşıoğlu, L. M. Sandratskii, P. Bruno, and I. Galanakis, Phys. Rev. B **72**, 184415 (2005).
[167] V. V. Sokolovskiy, V. D. Buchelnikov, M. A. Zagrebin, P. Entel, S. Sahoo, and M. Ogura, Phys. Rev. B **86**, 134418 (2012).
[168] S. Ghosh and S. Ghosh, arXiv preprint arXiv:1812.02856 (2018).
[169] Y. Han, A. Bouhemadou, R. Khenata, Z. Cheng, T. Yang, and X. Wang, Journal of Magnetism and Magnetic Materials **471**, 49 (2019).
[170] Y. Han, M. Wu, M. Kuang, T. Yang, X. Chen, and X. Wang, Results in Physics **11**, 1134 (2018).
[171] Y. Han, Z. Chen, M. Kuang, Z. Liu, X. Wang, and X. Wang, Results in Physics **12**, 435 (2019).
[172] J. P. Perdew, K. Burke, and M. Ernzerhof, Phys. Rev. Lett. **77**, 3865 (1996).
[173] M. Methfessel and A. T. Paxton, Phys. Rev. B **40**, 3616 (1989).
[174] N. Kervan, S. Kervan, O. Canko, M. Atiş, and F. Taşkın, Journal of Superconductivity and Novel Magnetism **29**, 187 (2016).
[175] B. Hamad, Journal of Materials Science **51**, 10887 (2016).
[176] A. Abada, K. Amara, S. Hiadsi, and B. Amrani, Journal of Magnetism and Magnetic Materials **388**, 59 (2015).
[177] P. D. Patel, S. B. Pillai, S. M. Shinde, S. D. Gupta, and P. K. Jha, Physica B: Condensed Matter **550**, 376 (2018).
[178] J.-Y. Jong, J. Zhu, M.-G. Jon, Y. Zhou, J. Kim, and J. Yan, Journal of Alloys and Compounds **693**, 462 (2017).
[179] V. Alijani, J. Winterlik, G. H. Fecher, S. S. Naghavi, and C. Felser, Phys. Rev. B **83**, 184428 (2011).
[180] Enamullah, Y. Venkateswara, S. Gupta, M. R. Varma, P. Singh, K. G. Suresh, and A. Alam, Phys. Rev. B **92**, 224413 (2015).
[181] S. Berri, D. Maouche, M. Ibrir, and F. Zerarga, J. Magn. Magn. Mater. **354**, 65 (2014).
[182] Q. Gao, H.-H. Xie, L. Li, G. Lei, J.-B. Deng, and X.-R. Hu, Superlattices Microstruct. **85**, 536 (2015).
[183] L. Xiong, L. Yi, and G. Gao, J. Magn. Magn. Mater. **360**, 98 (2014).
[184] S. Izadi and Z. Nourbakhsh, J. Supercond. Novel Magn. **24**, 825 (2011).
[185] M. Singh, H. S. Saini, J. Thakur, A. H. Reshak, and M. K. Kashyap, J. Alloys Compd. **580**, 201 (2013).
[186] G. Gökoğlu, Solid. State. Sciences. **14**, 1273 (2012).
[187] A. Kundu, S. Ghosh, R. Banerjee, S. Ghosh, and B. Sanyal, Scientific Reports **7**, 1803 (2017).
[188] H. Zenasni, H. Faraoun, and C. Esling, Journal of Magnetism and Magnetic Materials **333**, 162 (2013).

[189] C. Jiang, M. Venkatesan, and J. Coey, Solid state communications **118**, 513 (2001).
[190] K. zdogan, I. Galanakis, E. aioglu, and B. Akta, Journal of Physics: Condensed Matter **18**, 2905 (2006).
[191] K. Nagai et al., Physical Review B **97**, 035143 (2018).
[192] H. Luo et al., Journal of Magnetism and Magnetic Materials **320**, 421 (2008).
[193] G. Gao and K.-L. Yao, Applied Physics Letters **103**, 232409 (2013).
[194] Y. Ze-Jin, G. Qing-He, X. Heng-Na, S. Ju-Xiang, W. Xian-Wei, and X. Zhi-Jun, Scientific reports **7**, 16522 (2017).
[195] H. Luo et al., Journal of Applied Physics **103**, 083908 (2008).
[196] N. Xing, H. Li, J. Dong, R. Long, and C. Zhang, Computational Materials Science **42**, 600 (2008).
[197] H. Luo et al., Physica B: Condensed Matter **405**, 3092 (2010).
[198] S. Li, Z. Ren, X. Zhang, and C. Cao, Physica B: Condensed Matter **404**, 1965 (2009).
[199] N. Arıkan, A. İyigör, A. Candan, Ş. Uğur, Z. Charifi, H. Baaziz, and G. Uğur, Journal of materials science **49**, 4180 (2014).
[200] K. Brzakalik, Intermetallics **16**, 1053 (2008).
[201] E. Shreder, A. Svyazhin, and S. Streltsov, Phys. Met. Metallogr **100**, S5 (2005).
[202] K. Buschow and P. Van Engen, Journal of Magnetism and Magnetic Materials **25**, 90 (1981).
[203] N. Arıkan, A. İyigör, A. Candan, Ş. Uğur, Z. Charifi, H. Baaziz, and G. Uğur, Journal of materials science **49**, 4180 (2014).
[204] T. Graf, J. Barth, B. Balke, S. Populoh, A. Weidenkaff, and C. Felser, Scripta Materialia **63**, 925 (2010).
[205] H. Khosravi, A. Boochani, G. Rasolian, S. Solaymani, and S. Naderi, International Journal of Modern Physics B **31**, 1750109 (2017).
[206] T. Kanomata et al., Physical Review B **82**, 144415 (2010).
[207] M. Zhang et al., Journal of magnetism and magnetic materials **277**, 130 (2004).
[208] Y. Kudryavtsev et al., Physical Review B **77**, 195104 (2008).
[209] P. Webster, Journal of Physics and Chemistry of Solids **32**, 1221 (1971).
[210] Z. Pezeshki-Nejad, A. Ramazani, S. Alikhanzadeh-Arani, M. Almasi-Kashi, and M. Salavati-Niasari, Journal of Magnetism and Magnetic Materials **412**, 243 (2016).
[211] H. Luo, Y. Xin, B. Liu, F. Meng, H. Liu, E. Liu, and G. Wu, Journal of Alloys and Compounds **665**, 180 (2016).
[212]
[213] Q.-L. Fang, J.-M. Zhang, X.-M. Zhao, K.-W. Xu, and V. Ji, Journal of Magnetism and Magnetic Materials **362**, 42 (2014).
[214] I. H. Bhat, S. Yousuf, T. M. Bhat, and D. C. Gupta, Journal of Magnetism and Magnetic Materials **395**, 81 (2015).
[215] X.-P. Wei, X.-R. Hu, S.-B. Chu, G.-Y. Mao, L.-B. Hu, T. Lei, and J.-B. Deng, Physica B: Condensed Matter **406**, 1139 (2011).
[216] S. Yabuuchi, M. Okamoto, A. Nishide, Y. Kurosaki, and J. Hayakawa, Applied

Physics Express **6**, 025504 (2013).
[217] M. Kawakami, S. Nishizaki, and T. Fujita, Journal of the Physical Society of Japan **64**, 4081 (1995).
[218] S. Yoshimura et al., Journal of Applied Physics **103**, 07D716 (2008).
[219] L. Zhang, E. Brück, O. Tegus, K. J. Buschow, and F. De Boer, Physica B: Condensed Matter **328**, 295 (2003).
[220] L. Bainsla, M. M. Raja, A. Nigam, B. C. S. Varaprasad, Y. Takahashi, K. Suresh, and K. Hono, Journal of Physics D: Applied Physics **48**, 125002 (2015).
[221] Y. Du et al., EPL (Europhysics Letters) **103**, 37011 (2013).
[222] D. C. Gupta, I. H. Bhat, and M. Chauhan, Structural and magnetic stability of fe 2 nisi, in *AIP Conference Proceedings*, volume 1591, pages 1501–1502, AIP, 2014.
[223] Y. Li, Journal of Shanghai Jiaotong University (Science) **22**, 530 (2017).
[224] D. P. Rai et al., Bulletin of Materials Science **34**, 1219 (2011).
[225] S. Wurmehl, G. H. Fecher, H. C. Kandpal, V. Ksenofontov, C. Felser, H.-J. Lin, and J. Morais, Physical Review B **72**, 184434 (2005).
[226] H. C. Kandpal, C. Felser, and G. H. Fecher, Journal of Magnetism and Magnetic Materials **310**, 1626 (2007).
[227] M. Zagrebin, V. Sokolovskiy, and V. Buchelnikov, Journal of Physics D: Applied Physics **49**, 355004 (2016).
[228]
[229] V. Alijani, O. Meshcheriakova, J. Winterlik, G. Kreiner, G. H. Fecher, and C. Felser, J. Appl. Phys. **113**, 063904 (2013).
[230] O. Meshcheriakova et al., Phys. Rev. Lett. **113**, 087203 (2014).
[231] V. Alijani, J. Winterlik, G. H. Fecher, S. S. Naghavi, S. Chadov, T. Gruhn, and C. Felser, J. Phys.: Condens. Matter **24**, 046001 (2012).
[232] I. Galanakis, K. Özdoğan, E. Şaşıoğlu, and S. Blügel, J. Appl. Phys. **116**, 033903 (2014).
[233] H.-H. Xie, Q. Gao, L. Li, G. Lei, G.-Y. Mao, X.-R. Hu, and J.-B. Deng, Comp. Mater. Sci. **103**, 52 (2015).
[234] K. Endo, T. Kanomata, H. Nishihara, and K. Ziebeck, J. Alloys Compd. **510**, 1 (2012).
[235] M. Benkabou et al., J. Alloys Compd. **647**, 276 (2015).
[236] L. Bainsla, M. M. Raja, A. Nigam, and K. Suresh, J. Alloys Compd. **651**, 631 (2015).
[237] J. Drews, U. Eberz, and H.-U. Schuster, J. Less-Common Met. **116**, 271 (1986).
[238] V. Alijani et al., Phys. Rev. B **84**, 224416 (2011).
[239] M. Rahmoune, A. Chahed, A. Amar, H. Rozale, A. Lakdja, O. Benhelal, and A. Sayede, Materials Science-Poland **34**, 905 (2016).
[240] M. A. Hossain, M. T. Rahman, M. Khatun, and E. Haque, Computational Condensed Matter **15**, 31 (2018).
[241] N. A. Koshi and R. John, Journal of Superconductivity and Novel Magnetism , 1

(2018).

[242] L. Bainsla and K. Suresh, Applied Physics Reviews **3**, 031101 (2016).

[243] M. Elahmar, H. Rached, D. Rached, S. Benalia, R. Khenata, Z. Biskri, and S. B. Omran, Materials Science-Poland **34**, 85 (2016).

List of Publications

Peer-reviewed journals

1. Ashis Kundu, **Srikrishna Ghosh**, Rudra Banerjee, Subhradip Ghosh, Biplab Sanyal, *New quaternary half-metallic ferromagnets with large Curie temperatures*, Scientific Reports **7**, 1803 (2017).*

2. **Srikrishna Ghosh**, Subhradip Ghosh, *Systematic understanding of half-metallicity of ternary compounds in Heusler and Inverse Heusler structures with 3d and 4d elements*, https://arxiv.org/pdf/1812.02856.pdf (Accepted in Physica Scripta).*

3. **Srikrishna Ghosh**, Subhradip Ghosh,*Half-metallicity in quaternary Heusler alloys with 3d and 4d elements: observations and insights from DFT calculations*, physica status solidi (b) **256**, 1900039 (2019).*

4. **Srikrishna Ghosh**, Subhradip Ghosh,*Site dependent substitution and half-metallic behaviour in Heusler compounds: a case study for Mn_2RhSi, Co_2RhSi and CoRhMnSi*, (Accepted in Computational Condensed Matter).*

Communicated/Unpublished

1. **Srikrishna Ghosh**, Subhradip Ghosh,*High spin polarization and compensated ferrimagnetism with very low net magnetization in Heusler alloy Mn_2TcAl*, (manuscript under preparation)

Publications marked with * are included in the thesis

Conference Proceedings

1. **Srikrishna Ghosh**, Ashis Kundu, Subhradip Ghosh, *First principles study of quaternary Heusler compounds CoXFeSi (X = 4d transition elements) for spintronics applications*, AIP Conference Proceeding **1832**, 090030 (2017).*

Schools/workshops/Conferences attended

1. Asia-Sweden meeting on *understanding functional material from lattice dynamics*, January 9-11 (2014), **IIT Guwagati**, Guwahati, Assam, India.

2. DST-SERC School on *Density Functional Theory and Beyond: Computational Materials Science and Materials Design*, November 24 - December 13, 2014, **Department of Physics, Faculty of Science, The M. S. University of Baroda**, Vadodara, Gujarat, India.

3. *Functional Materials for Today and Tomorrow*, October 28-30, 2015, **HHI Kolkata**, India.

4. *61st DAE-solid State Physics Symposium*, December 26-30, 2016, **KIIT University, Bhubaneswar**, Odisha, India.